Dynamic and turbulent premixed combustion using flamelet-generated manifold in openFOAM

Dynamic and turbulent premixed combustion using Flamelet-Generated Manifold in OpenFOAM

Alessio Fancello

ISBN: 978-90-8891-967-1

Printed at: Proefschriftmaken.nl, Uitgeverij BOXPress

A catalogue record is available from the Eindhoven University of Technology Library.

The present thesis is the result of the work performed within H_2**-IGCC**, co-funded by the European Union's 7th Framework Program for Research and Development, is based on the initiative outlined in the European Turbine Network's (ETN) Position Paper on Gas Turbine Fuel Flexibility (August 2007). In November 2009 the H_2**-IGCC** project kicked off with 24 partners from 10 countries with a total budget of 17,8 million euro. Successful dissemination and implementation of the project results will be an important step towards opening up the market for Integrated Gasification Combined Cycle (IGCC) with Carbon Capture and Storage (CCS) by 2020, by increasing gas turbine efficiency and fuel flexibility.

The cover picture, created by Valentina Fancello, represents an imaginary flame whose shape resembles the north-eastern side of the island of Sardinia (Italy).

Dynamic and turbulent premixed combustion using Flamelet-Generated Manifold in OpenFOAM

PROEFSCHRIFT

ter verkrijging van de graad van doctor aan de
Technische Universiteit Eindhoven, op gezag van de
Rector Magnificus, prof.dr.ir. C.J. van Duijn, voor een
commissie aangewezen door het College voor
Promoties in het openbaar te verdedigen
op woensdag 15 oktober 2014 om 16:00 uur

door

Alessio Fancello
geboren te Nuoro, Italië

Dit proefschrift is goedgekeurd door de promotoren en de samenstelling van de promotiecommissie is als volgt:

voorzitter:	prof.dr.ir. M.G.D. Geers
promotor:	prof.dr. L.P.H. de Goey
copromotor:	dr.ir. R.J.M. Bastiaans
leden:	prof.dr.ir. P.D. Anderson
	prof. M. Germano (Politecnico di Torino)
	prof. F. Pittaluga (Università degli Studi di Genova)
	dr. Lukasz Panek (Siemens AG)

ad Eleonora

Μῆνιν ἄειδε, θεά, Πηληιάδεω Ἀχιλῆος οὐλομένην, ἣ μυρί' Ἀχαιοῖς ἄλγε' ἔθηκε, πολλὰς δ' ἰφθίμους ψυχὰς Ἄϊδι προΐαψεν ἡρώων, αὐτοὺς δὲ ἑλώρια τεῦχε κύνεσσιν οἰωνοῖσί τε πᾶσι· Διὸς δ' ἐτελείετο βουλή· ἐξ οὗ δὴ τὰ πρῶτα διαστήτην ἐρίσαντε Ἀτρεΐδης τε ἄναξ ἀνδρῶν καὶ δῖος Ἀχιλλεύς. *Iliad* (Book 1, verses 1-7) - Homer

Summary

The interest towards gas turbine technology has grown significantly in the last years. Moreover, the aim of reducing pollution emissions in turbo-machinery combustion is considered of primary importance. Reaching these standards and trying to develop efficient combustion systems become then an important challenge and new burner configurations are required. In classical approaches such as experimental tests, the requirements are highly demanding, since operating these setups is very expensive and can be potential dangerous.

The European H2-IGCC project has started by the end of 2009 with the objective to provide and demonstrate technical solutions for highly efficient and reliable gas turbines in the next generation of Integrated Gasification Combined Cycle (IGCC) plants. In this project, the main goal is to find a working model for the design and the enhancement of a gas turbine combustion process. The important issues in the combustion modeling are stability and fuel flexibility which demand to use a compressible reactive CFD solver while handling the hydrogen addition in the fuel. In order to do that, a compressible code is utilized. Due to oscillation modes related to this code, special interest to pressure boundary conditions is given. One of the aspects of this research is the use of an open source code such as OpenFOAM ® for which the implementation of the combustion model needs a strong effort.

The Flamelet Generated Manifold (FGM) technique is a particular reduced combustion model. Its main idea is to treat the combustion process by solving a small amount of the partial differential transport equations, in addition to the conservation ones: this new mathematical configuration becomes an answer to the problem of the huge computational effort required for the solution of the whole reactive system. In fact, the equations for all species are then replaced by the equations of a small number of controlling variables. Other species are stored in a database. The creation of this database, also known as manifold, in the FGM technique, is achieved by using the solution of the one dimensional flamelet equation. These flamelets are produced

with the detailed chemistry code CHEM1D. All thermal properties, such as density, diffusivity, temperature, are stored in the manifold.

A laminar approach is first used to show the FGM performance and a simple 2D geometry test case called *flame in a box* is used as a validation case. Stationary solutions are already present in literature performed with a stationary incompressible solver. There is no previous work with transient effects and this aspect needs to be considered as an important starting point of this research. Due to these reasons, a *dynamic flame in a box* has been introduced in this study, in order to take into account all the transient aspects of this test case. A few interesting unsteady phenomena have been observed in this study and the important message which can be read from this analysis is that initial conditions strongly affect the combustion process. The study has been done by using an adiabatic system and also including heat loss by adding the enthalpy equation as an extra controlling variable.

After the laminar combustion application, turbulent combustion is studied. A β-PDF approach for turbulent flows can be assumed as a reasonable choice for the probability distribution of the sub-grid chemical terms. An algebraic model for the variance is used. The variance of the progress variable becomes then an extra controlling variable of the FGM system.

Two different combustor configurations are presented in the following work. The applications have been performed together with some industrial partners. First, a *single jet flame* configuration, for which PIV and RAMAN are provided by DLR, is introduced and LES calculations are presented and compared with experimental data. Afterwards, a *sudden expansion flow* configuration is studied by using both RANS and LES approaches and including heat loss effects in turbulent combustion. Results show a good comparison with respect to experimental data and a significant improvement compared to previous work results.

Summarizing, both laminar and turbulent combustion with FGM approach are presented by using OpenFOAM ® . The combustion method has resulted in significant savings in calculation times, with respect to application of a detailed chemistry approach. Moreover, the code shows satisfactory validations of previous work and experimental data, resulting in a promising tool for future developments.

Contents

Chapter 1

Introduction

"φλογιστόν"
"phlogiston (lit. burning up). The earliest theory of combustion"

J.J. Becher, 1667

1.1 Turbulent combustion and gas turbines

Combustion energy is mainly used to generate heat and power [Law,2006]. The power generation can also be performed by many alternative sources, such as nuclear, wind and hydroelectric ones. On the other hand, the energy obtained by the burning of fossil fuel still gives a large fraction of the total energy supply. Some examples of energy applications in the combustion field are domestic heating, spark-ignition and compression-ignition engines, industrial furnaces and gas turbines. In energy generation, gas turbine power plants are ones of the main power suppliers in industrial combustion and deserve special interest. Figure 1.1 illustrates the inside of a Siemens AG stationary gas turbine.

Gas turbines are generally operated in the premixed combustion regime, where fuel and oxidizer are already mixed before the combustion takes place. An important aspect to consider in gas turbine combustion is the presence of turbulence in the flow. In recent years, [Peters,2000] the unresolved problems of turbulent combustion have inspired many researchers and this makes the topic probably one of the most significant unresolved problem in classical physics. In order to solve most of the engineering problems related to combustion, turbulence models

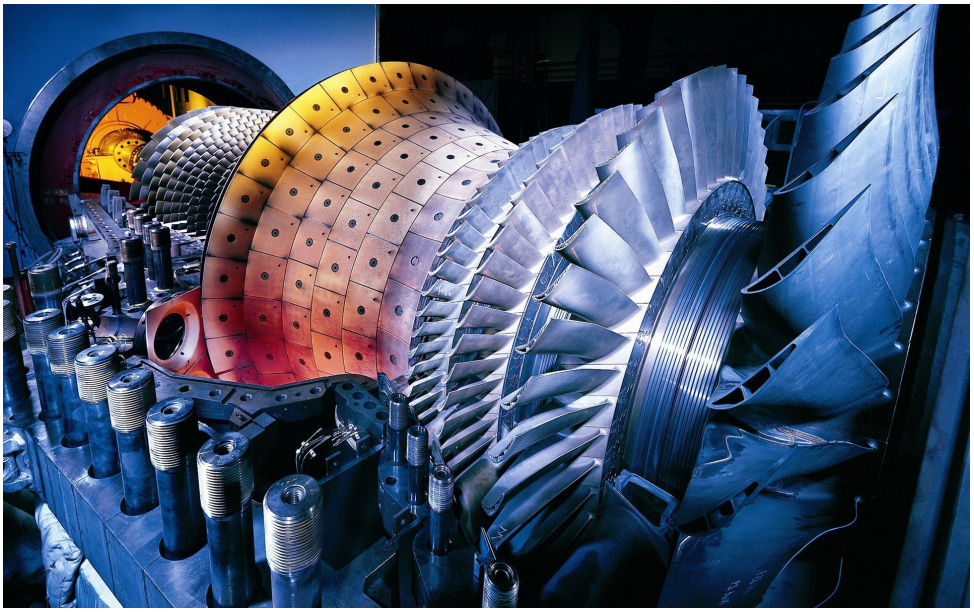

Figure 1.1: A stationary gas turbine (Courtesy of Siemens AG).

have to be introduced. However, this introduction implies some closure problems, making the solution sometimes quite empirical. In cold flows, turbulence modeling has shown to be successful. In view of this, such models are important building blocks in the modeling of reacting flow phenomena. Moreover, the wide range of chemical scales involved in the combustion reaction, the radiation aspects and the multiphase problems increase the overall problem complexity. The interaction between turbulence and combustion needs a particular focus [Bray-Swaminathan,2011]. In particular, a statistical analysis of the fluctuating variables has to be considered. Basically, the statistical properties depend on the small scales in the turbulent flow, which are generally lost due the averaging procedures to model these phenomena. The principle of Damköhler states that there are two limiting situations which can be described: if the length and time scales of the chemical reactions are small in comparison with the smallest scales of the turbulent flows, then combustion should be restricted to the so called thin, laminar-like reaction zones. Turbulence distorts these zones, which are therefore stretched, resulting in a change of the mean reaction rate and heat release. The second situation occurs if chemical length and time scales are large compared to the biggest scales of turbulence. In this case the structure of the reaction zone is expected to be more randomly distributed. In this thesis we mainly focus on the first situation of laminar flamelets as this mainly occurs in gas turbine.

1.2 Numerical approach for the modeling of turbulent combustion

Although the capacity of modern computing power has significantly increased during the last few decades, the simulation of combustion with detailed chemistry is implausible in practical

devices [vanOijen,2000], considering the enormous CPU power required for the numerical simulations. In complex reaction mechanisms, the number of species and reactions can result in the order of hundreds and thousands respectively. For each species involved, a partial differential equation (PDE) has to be solved. Furthermore, the overall PDE system becomes very stiff. The need of chemistry reduction methods has been always a priority in the modeling environment in order to decrease the computational cost. This needs to be done without losing the accuracy standard.

In specialized literature a few chemistry reduction methods are available [Lam-Goussis,1991] [Poinsot-Veynante,2005] [Maas-Pope,1992]. In general, reduction techniques are based on the idea that a combustion system shows a large number of these species in a quasi-steady state or partial equilibrium. With this assumption, the corresponding differential equation of each such species can be replaced by an algebraic one, resulting finally in a reduction in computation cost. The Flamelet Generated Manifold (FGM) technique [deGoey-TenThijeBoonkkamp,1997] [deGoey-TenThijeBoonkkamp,1999] [vanOijen,2000] is a reduction method based on the assumption that the full composition space can be described in terms of a reduced number of variables while a large number of species are assumed to be in steady state. Moreover, FGM takes also into account the important aspects of convection and diffusion which occur in the system.

FGM is based on the *flamelet approach* [Peters,2000], which states that a multidimensional flame can be considered as a set of many one-dimensional flames called flamelets. This principle implies that the path in composition space followed by a multidimensional flame can be considered close to the path observed in a one-dimensional flame. The flamelets are computed with a detailed chemistry code and then converted from physical space to composition space. A database of quantities of interest is built and expressed as a function of the so-called controlling variables Y_i, using the solution of a flamelet calculation. This database is called the *manifold*. In this manifold, the physical and chemical properties of the flamelet are stored. During the application of the manifold in a combustion CFD problem, conservation equations for a premixed flame are adapted in terms of these controlling variables. Typical controlling variables are, for example, the reaction progress variable and the enthalpy. The calculation of the Navier-Stokes equations and the controlling variable equations are performed. During this calculation, key variables such as chemical source term, temperature, and diffusivity are tabulated on the manifold. To summarize, the multidimensional flame is calculated by tabulating the chemistry of a series of one-dimensional flames.

In the last decades, the approach to solve the turbulent Navier Stokes equations numerically has become a very highly demanding challenge. For a cold flow, the problem related with Direct Numerical Simulations (DNS) of turbulent flows is relatively simple [Germano,2000]. There is a set of equations, which describes the evolution in time of velocity, pressure, temperature fields of a moving fluid subjected to boundary conditions. Due to nonlinear terms, the memory of the past is rapidly lost and the predictability of this flow is limited to short intervals of time.

As a consequence of this, the numerical solution becomes challenging and requires a high-order accuracy. As already mentioned, the coupling of turbulence and combustion involves a wide range of scales. Furthermore, when applying a DNS approach, all scales down to the Kolmogorov scale should be resolved. Unfortunately, this is still impossible for realistic combustion engineering configurations such as gas turbines. Hence, this approach can be applied only to very simple configurations. Consequently, turbulence models are therefore required. Some methods have been proposed to produce directly the statistical quantities. These methods are based on the Reynolds Averaged Navier-Stokes equations (RANS) and rely on models that are currently applied to complex geometries such as airplanes, but they are not universal. The large Eddy Simulation (LES) of turbulent flow is located between these limiting formulations and shares the problems of both. What is important in this approach, is the introduction of a new scale, the grid length. LES is a multiscale approach and requires some modeling technique in order to reproduce the effect of the unresolved scales on the resolved ones. One of the main ingredients in the LES computation, the sub-grid modeling, has to be studied. In recent years, a dynamic modeling procedure has been introduced [Germano-Piomelli,1991]. The application of this modeling method needs particular attention switching from incompressible to compressible flows, from non-reacting to reacting flows.

RANS and LES techniques can also be applied in conjunction with FGM for turbulent reacting flows. A Probability Density Function (PDF) method with presumed PDF configuration has been introduced to provide a suitable description of the sub-grid chemical terms [Kaul,2011]. In this context, the variance of each progress variable becomes an extra controlling variable of the FGM system. Two methods to include the variances in the equation system are considered here: [CardosoDeSouza,2011] [Kaul,2009] [Knudsen,2012] the first one with an extra transport equation and the second one with an algebraic model.

1.3 Outline of this thesis

This thesis work is related to the H_2 - *IGCC* European project promoted under the supervision of the European Turbine Network (ETN). The overall objective of this project is to provide and demonstrate technical solutions which will allow the use of state-of-the-art highly efficient, reliable gas turbines in the next generation of Integrated Gasification Combined Cycle (IGCC) power plants. The project has started in November 2009 and has ended in May 2014.

In this thesis, a modeling approach related to turbulent combustion for gas turbine application is presented. The FGM technique is applied in the numerical calculations. In order to reach this goal, a CFD code known as OpenFOAM ® [OpenFOAM-URL] is used. OpenFOAM ® is an open source code which has been modified and adapted for the FGM application. This implementation is first validated by performing a laminar combustion analysis on a two-dimensional flame geometry known as *flame in a box* [vanOijen,2000]. During this configuration analysis, a dynamic approach has been used, since no previous work was available in literature. Few

dynamic phenomena, which have occurred during the calculations of this flame, have been described and outlined. Moreover, the use of a compressible solver in this application forced particular attention to the pressure boundary conditions.

Secondly, an application of the approach to turbulent combustion has been carried out. Two industrial combustor configurations have been used for the numerical simulations. A *jet flame*, of which experimental data have been provided by DLR German Aerospace Center [DLR], has been studied in collaboration with **Siemens AG** (Germany). Moreover, a *sudden expansion flow* configuration is studied [Banhawy,1983], by means of the RANS and LES approach, in collaboration with **CFD Engineering** (Italy). New aspects in this work are the LES approach applied for this second test case and the inclusion of heat loss by the cooling of the wall. The results show a significant improvement in comparison with experimental data, with respect to previous published work on this subject. A description of recirculation zone bubble, cross profiles and flame length estimations are also presented to show the different effects in modeling approaches.

Chapter 2

Theoretical background for reacting flows

" Ἡ φύσις οὐδὲν ποιεῖ ἅλματα"
"The nature does not make jumps"
Principle of natural philosophy, attributed to Aristoteles

2.1 The conservation equations

Flames and other combustion processes can be classified as chemically reacting flows, which are governed by a particular set of *conservation equations* describing the flow, the chemical species mass fractions and the energy. Conservation equations for reacting flows are presented in this Chapter. In general, conservation equations are divided into the Navier-Stokes equations typically used in the non-reacting cases and the extra equations which contribute to the reacting aspects of the flow. A full and detailed derivation of these equations can be found in references [Peters,2000],[Poinsot-Veynante,2005] and [Williams,1958].

Mass conservation is described by the continuity equation:

$$\frac{\partial \rho}{\partial t} + \nabla \cdot (\rho \mathbf{u}) = 0, \tag{2.1}$$

with ρ the mass density of the mixture, $\mathbf{u}$ the three dimensional flow velocity vector and t the time.

Conservation of momentum is described by:

$$\frac{\partial(\rho\mathbf{u})}{\partial t} + \nabla\cdot(\rho\mathbf{u}\mathbf{u}) = -\nabla p + \rho\mathbf{g} - \nabla\cdot\boldsymbol{\tau}, \tag{2.2}$$

where p is the hydrostatic pressure, $\mathbf{g}$ the gravitational acceleration and $\boldsymbol{\tau}$ the stress tensor. In Equation 2.2 no other volumetric forces rather than gravity are considered.

Energy conservation can be expressed in several ways. For convenience, this equation is written in terms of specific enthalpy h:

$$\frac{\partial(\rho h)}{\partial t} + \nabla\cdot(\rho\mathbf{u}h) = -\nabla\cdot\mathbf{q} - \boldsymbol{\tau} : (\nabla\mathbf{u}) + \frac{\mathrm{D}p}{\mathrm{D}t}, \tag{2.3}$$

with $\mathbf{q}$ being the heat flux vector. The second and third term of the right-hand side of Equation represent the enthalpy production due to viscous effects and pressure variations. Moreover, no volumetric heat source is assumed. The mass fraction Y_i is defined as the ratio between the mass density of species i over the mass density of the whole mixture: $Y_i = \rho_i/\rho$. In fact, for the total number of species N_s the mixture density reads: $\rho = \sum_{i=1}^{N_s}\rho_i$. In order to consider the conservation for the chemical species, a transport equation for the species mass reads

$$\frac{\partial\rho_i}{\partial t} + \nabla\cdot(\rho_i\mathbf{u}_i) = \dot{\omega}_i, \tag{2.4}$$

with ρ_i being the mass density of the i-species, $\mathbf{u}_i$ the velocity of species i and $\dot{\omega}_i$ the chemical source term of the i-species. The source term represents the formation or consumption due to chemical reactions. Velocity of species $\mathbf{u}_i$ can be split in $\mathbf{u}_i = \mathbf{u} + \mathbf{U}_i$, with $\mathbf{U}_i$ the diffusion velocity of species i and $\mathbf{u}$ the convective velocity. By using the diffusion velocity $\mathbf{U}_i$ and mass fraction Y_i, Equation 2.4 can be written as:

$$\frac{\partial(\rho Y_i)}{\partial t} + \nabla\cdot(\rho\mathbf{u}Y_i) + \nabla\cdot(\rho\mathbf{U_i}Y_i) = \dot{\omega}_i. \tag{2.5}$$

In addition to Equations 2.1, 2.2, 2.3, 2.5, two state equations are introduced: the thermal and caloric equations of state.

The thermal equation of state gives a relationship between pressure, density, temperature and the species mass fractions. It is commonly assumed, in most combustion problems, that species behave like an ideal gas. Considering the partial pressure p_i, related to the i-species, the thermal equation reads:

$$p_i = n_i R^0 T, \tag{2.6}$$

with n_i the molar concentration of species i, T the temperature of the mixture and R^0 the universal constant of gases. According to Dalton's law, the sum of partial pressures p_i is equal to the pressure of the whole mixture p. Furthermore, the molar concentration for the species i can be expressed as:

$$n_i = nX_i = nY_i\frac{\bar{M}}{M_i} = \rho\frac{Y_i}{M_i}, \tag{2.7}$$

with X_i is the species mole fraction and $\bar{M}$ is the average molar mass, defined as

$$\bar{M} = \frac{1}{\sum_{i=1}^{N_s}\frac{Y_i}{M_i}}. \tag{2.8}$$

Thus, it is possible to express the total pressure as function of the other quantities:

$$p = \sum_{i=1}^{N_s} p_i = \sum_{i=1}^{N_s} \rho R^0 T\frac{Y_i}{M_i}. \tag{2.9}$$

The caloric equation of states is related to the enthalpy h. Also enthalpy is referred to as the sum of the i-species enthalpies h_i:

$$h = \sum_{i=1}^{N_s} Y_i h_i, \quad \text{with} \quad h_i = h_i^{\text{ref}} + \int_{T^{\text{ref}}}^{T} c_{p,i}(T)\mathrm{d}T. \tag{2.10}$$

The quantity $c_{p,i}$ is the specific heat of species i at constant pressure. The enthalpy of species i can be considered as the sum of enthalpy of formation h_i^{ref} at temperature T^{ref} and a sensible part, i.e. the integral part of Equation (2.10). Generally, $c_{p,i}$ can be tabulated in polynomial form [Kee,1986] as follows:

$$\frac{c_{p,i}}{R^0} = \sum_{n=1}^{5} b_{ni}T^{n-1}. \tag{2.11}$$

The specific heat of the mixture is the average specific heat of all species weighted with the corresponding species mass fractions:

$$c_p = \sum_{i=1}^{N_s} Y_i c_{p,i}. \tag{2.12}$$

Summarizing, a system of N_s + 6 equations has been presented. In this system, the evolutions of N_s species and the variables ρ, $\mathbf{u}$, T, p and Y_i are represented.

The solution of the conservation equations requires models for certain quantities. Using the assumption that the fluid behaves like a Newtonian fluid, the viscous stress tensor $\boldsymbol{\tau}$ can be expressed by using the Stokes' assumption [Law,2006] as

$$\boldsymbol{\tau} = \mu \left(\nabla \mathbf{u} + (\nabla \mathbf{u})^T - \frac{2}{3}(\nabla \cdot \mathbf{u}) \mathscr{I} \right), \tag{2.13}$$

where μ is the dynamic viscosity of the mixture.

The diffusion velocity field $\mathbf{U}_i$ is obtained by solving the Stefan-Maxwell equation [Bird,1960]:

$$\nabla X_i = \sum_{j=1}^{N_s} \frac{X_i X_j}{D_{ij}} (\mathbf{U}_j - \mathbf{U}_i), \tag{2.14}$$

by neglecting Soret and Dufour effects [Hirschfelder,1964], since they probably do not have significant effects on the diffusion velocity. In Equation 2.14, D_{ij} is the binary mass diffusion coefficient of species i into species j. However, the solution of Equation (2.14) is quite difficult from a computational point of view. A simplified approach is often used and consists of applying Fick's law. This law states that the diffusion of each species in the mixture can be expressed as

$$\mathbf{U}_i = -\frac{D_{\text{im}}}{Y_i} \nabla Y_i, \tag{2.15}$$

where D_{im} is the mixture-averaged diffusion coefficient.

The heat flux in Equation 2.3 can be modeled by using an expression that contains the heat transport due to conduction and mass diffusion [Williams,1985]:

$$\mathbf{q} = -\lambda \nabla T + \rho \sum_{i=1}^{N_s} \mathbf{U}_i Y_i h_i, \tag{2.16}$$

with λ the thermal conductivity of the mixture. Considering Equations (2.10), (2.12) and (2.15), the heat flux can be rewritten as:

$$\mathbf{q} = -\frac{\lambda}{c_p} \nabla h - \frac{\lambda}{c_p} \sum_{i=1}^{N_s} \left(\frac{1}{Le_i} - 1 \right) h_i \nabla Y_i, \tag{2.17}$$

where Le_i is the Lewis number of i-species i. The Lewis number is a number that describes the ratio between thermal diffusivity ($\lambda / c_p \rho$) to the species mass diffusivity (D_{im}):

$$Le_i = \frac{\lambda}{\rho D_{\mathrm{im}} c_p}. \tag{2.18}$$

When the Lewis number is not equal to one, species and heat are redistributed in the flame zone and, locally, there will be more mass or more heat. The phenomenon associated with this is known as *preferential diffusion*.

Thermal conductivity and the dynamic viscosity are also modeled to reduce computational costs [Smooke-Giovangigli,1991]:

$$\lambda / c_p = 2.58 \cdot 10^{-5} (T/298\mathrm{K})^{0.69}, \tag{2.19}$$

and

$$\mu / c_p = 1.67 \cdot 10^{-8} (T/298\mathrm{K})^{0.51}. \tag{2.20}$$

In general, the mixture averaged dynamic viscosity and conductivity depends on temperature and composition of the mixture in a complex way. The models proposed in Equations (2.19) and (2.20) are obtained by fitting the results of methane-air flame simulations with more complex models [VanOijen,2002-thesis]. The models presented above are valid if the conditions are comparable to the fitted simulations, i.e. fuel and air with an abundant quantity of nitrogen. In that case, the stoichiometric ratio does not have a large influence on the model coefficients.

The dynamic viscosity can also be modeled by using a formula proposed by Wilke [Wilke,1950]:

$$\mu = \sum_{i=1}^{N_s} \frac{Y_i \mu_i}{M_i \left(\sum_{j=1}^{N_s} \frac{Y_j \Phi_{ij}}{M_{ij}} \right)}, \tag{2.21}$$

with Φ defined as:

$$\Phi_{ij} = \frac{1}{\sqrt{8}} \left(1 + \frac{M_i}{M_j} \right)^{-1/2} \cdot \left[1 + \left(\frac{\mu_i}{\mu_j} \right)^{1/2} \left(\frac{M_j}{M_i} \right)^{1/4} \right]^2. \tag{2.22}$$

Equation 2.21 is based on a mixture-averaged approach.

Also thermal conductivity can be expressed with a mixture-averaged approach formula, proposed by Kee et al. [Kee,2003]:

$$\lambda = \frac{1}{2}\left[M \sum_{i=1}^{N_s} \frac{Y_i \lambda_i}{M_i} + \left(\frac{1}{\left(M \sum_{i=1}^{N_s} \frac{Y_i \lambda_i}{M_i} \right)} \right) \right]. \tag{2.23}$$

Introducing the heat flux vector expression into the equation for enthalpy and species, gives the following expression:

$$\begin{aligned} \frac{\partial \rho h}{\partial t} + \nabla \cdot (\rho \mathbf{u} h) = \nabla \cdot \left(\frac{\lambda}{c_p} \nabla h \right) + \nabla \cdot \left(\frac{\lambda}{c_p} \sum_{i=1}^{N_s} (\frac{1}{Le_i} - 1) h_i \nabla Y_i \right) \\ + \rho \mathbf{u} \cdot \mathbf{g} + \boldsymbol{\tau} : (\nabla \mathbf{u}) + \frac{\mathrm{d}p}{\mathrm{d}t}, \end{aligned} \tag{2.24}$$

and

$$\frac{\partial (\rho Y_i)}{\partial t} + \nabla \cdot (\rho \mathbf{u} Y_i) = \nabla \cdot \left(\frac{\lambda}{Le_i c_p} \nabla Y_i \right) + \dot{\omega}_i. \tag{2.25}$$

In the expressions 2.24 and 2.25, Lewis effects appear clearly.

2.2 Combustion chemistry and mechanisms

When combustion occurs, exothermal chemical reactions appear and the fuel is oxidized. Depending on the combustion phenomena, a source of ignition might be required and the flame should produce enough heat to keep burning. In a combustion process a large number of elementary chemical steps are present. In the beginning, the fuel breaks up into smaller molecules, in a chain process. Intermediate structures appear and, at the end, these structures react to form different product molecules. Keeping track on this large amount of chemical reactions is not trivial. Sometimes, only the global reaction is presented in the analysis and intermediate species are not considered. If for instance a very basic example of methane-air combustion is considered, the global reaction reads:

$$CH_4 + 2O_2 \rightarrow CO_2 + 2H_2O. \tag{2.26}$$

The presence of nitrogen, which is in the air mixture, has been neglected, considering that it is not involved in the basic reaction.

As mentioned before, the global reaction consists of a large set of many elementary reactions which can be described as:

$$\sum_{i=1}^{N_s} \nu_{li}^{'} \mathscr{A}_i \leftrightharpoons \sum_{i=1}^{N_s} \nu_{li}^{''} \mathscr{A}_i \quad \text{for} \quad l = 1, ..., N_r, \tag{2.27}$$

with $\nu_{li}^{'}$ and $\nu_{li}^{''}$ the molar stoichiometric coefficients of species i in reaction l, N_r the number of reactions, N_s the number of species and $\mathscr{A}_i$ the chemical symbol for species i. In a detailed description of such combustion process it is important to take into account the chemical kinetics of the whole set of these elementary reactions. The nature of chemical source term of species i, indicating the mass of species i produced per unit volume per unit time, depends basically on all reactions in which the i-species are involved:

$$\dot{\omega}_i = M_i \sum_{l=1}^{N_r} (\nu_{li}^{''} - \nu_{li}^{'}) \mathscr{Q}_l, \tag{2.28}$$

where $\dot{\omega}_i$ represents the chemical source term of species i, M_i the molar mass of species i and $\mathscr{Q}_l$ the reaction rate for elementary reaction l. This last quantity can be written as:

$$\mathscr{Q}_l = k_l^f \prod_{i=1}^{N_s} [\mathscr{A}_i]^{\nu_{li}^{'}} - k_l^b \prod_{i=1}^{N_s} [\mathscr{A}_i]^{\nu_{li}^{''}}. \tag{2.29}$$

This expression shows that the total reaction rate depends on a formation reaction rate, the first term on the right hand side, while the consumption reaction rate appears as the second term on the right hand side. The rate of formation and consumption depends basically on some reaction rate constants, the molar concentration and the stoichiometric coefficients. The term $[\mathscr{A}_i] = \rho Y_i / M_i$ represents the molar concentration of species $\mathscr{A}_i$ and k is the reaction rate coefficient and superscripts f and b refer to forward (going from left to right in Equation (2.27)) and backward (from right to left in Equation (2.27)) reactions, respectively. The reaction rate k (either regarding a forward or backward reaction), is often written in an Arrhenius form [Warnatz,1996] [Williams,1985]:

$$k = A_c T^{\beta} \exp\left(\frac{-E_a}{R^0 T}\right), \tag{2.30}$$

with A_c the pre-exponential constant, β the temperature exponent, E_a the activation energy and R^0 is the universal gas constant. The backward reaction rates, k_l^b, can be computed from the forward rates and the equilibrium constants $\mathscr{K}_{c_l} = k_l^f / k_l^b$. The equilibrium constants are well defined by thermodynamic properties. There are tables in which data such as A_c, β, E_a, from a collection of elementary reactions, are stored in the so-called *reaction mechanisms*. Comprehensive reaction mechanisms, which are also often called kinetic schemes, have been developed by several research groups [Smooke-Giovangigli,1991] [Smith,1999] [Goswami,2014].

Regarding the choice of the mechanisms for the present work, further details are given in later Chapters.

A comprehensive description of conservation equations, equations of state, together with some models have been presented. Moreover, a combustion chemistry introduction has been given, but still a model for the chemical source term is required. This will be the topic of the next Chapter.

Chapter 3

Flamelet-Generated Manifolds

"Τὸ σὸν γὰρ ἄνθος, παντέχνου πυρὸς σέλας, θνητοῖσι κλέψας ὤπασεν."
"For thine own blossom of all forging fire, he stole and gave to mortals"

Prometheus donated the *fire* to humans - from
"Prometheus Unbound" - Aeschylus

3.1 Introduction

In the previous Chapter, conservation equations for reacting flows have been given and described. As already mentioned, the chemical source term creates a coupling between these equations, which therefore result in a very stiff and difficult system to solve. The stiffness comes from the disparity of time scales associated with the chemical processes. All reactions together involve processes with a large range of time scale in the chemical source term [Maas-Pope,1992]. Consequently, calculation with detailed chemistry is restricted to simple geometries. In this Chapter, a model on how to simplify the combustion system is presented.

To reduce computational costs, the chemical reaction model can be simplified. Considering a combustion process, several chemical processes involved in the reaction have time scales that are smaller than the flow time scales, resulting in a fast subset of chemical reactions. By decoupling these processes, the system of equations becomes less stiff, resulting on an improvement in computational efficiency. The methods that adopt this assumption of fast chemistry are

known as *reduction methods*. For the fast chemistry process, a *quasi-steady state* assumption is used: the assumption states that, for a certain species, the chemical reactions balance reads

$$\dot{\omega}_i = M_i \sum_{j=1}^{N_{sr}} r_{ij} \nu_{ij} = 0. \tag{3.1}$$

By imposing the assumption of equation 3.1, the conservation equation for species i can be replaced, in a stationary case, by the following one:

$$\dot{\omega}_i = 0. \tag{3.2}$$

A number of reduction methods have been proposed [Maas-Pope,1992] [Peters,1991] [Lam-Goussis,1991] . Each of these methods identifies the fast chemical processes in a different manner. The main difficulty in these methods is how to identify the steady state species. In order to do this, a deep insight of the chemical kinetics is required. One of the most known reduction methods, Intrinsic Low Dimensional Manifold (ILDM) [Maas-Pope,1992], considers the fast chemical processes by a local eigenvalue analysis of the chemical source term. However, it remains still complicated, especially in case of higher hydrocarbon fuels applied to premixed flames [vanOijen,2000]. Furthermore, the assumption of steady state used in most reduction methods is valid only in higher temperature regions, where chemistry is dominant. Therefore, in the lower temperature regions this assumption is not valid anymore. In fact, in these regions, convection and diffusion are dominant and thus cannot be neglected. Van Oijen [vanOijen,2000] proposed an improved method which incorporates the effects of convection and diffusion related to the colder region of the flame. This method is based on the flamelet assumption [Peters,1991] for which a multi dimensional flame can be considered as a set of one-dimensional (1D) flames called *flamelets*. This implies that the path followed in composition space by a multidimensional flame is close to the path observed in a 1D flame. Moreover, the chemical compositions in the flamelets are used to construct the *manifold* describing how steady-state species depend on the progress variable. This method is known as the Flamelet-Generated Manifold (FGM) technique.

3.2 FGM: the flamelet equations

The Flamelet-Generated Manifolds technique is briefly reviewed here. A detailed description can be found in [VanOijen,2002-thesis].

A premixed flame [deGoey-TenThijeBoonkkamp,1997] [deGoey-TenThijeBoonkkamp,1999] [vanOijen,2000] is defined as the region in space, where a scalar variable $\mathscr{Y}$ assumes the value between $\mathscr{Y}_u = 0$ in the unburnt gases and $\mathscr{Y}_b = 1$ in the burnt gases. The variable $\mathscr{Y}$ can be any

linear combination of species mass fractions, which obeys to the rule $\nabla\mathscr{Y} \neq 0$. A flame surface is defined as an iso-surface of $\mathscr{Y}$, meaning a surface at which $\mathscr{Y}(x,t) = \text{const}$. The motion of this surface is given by:

$$\frac{d\mathscr{Y}}{dt} := \frac{\partial\mathscr{Y}}{\partial t} + \mathbf{u}_f \cdot \nabla\mathscr{Y} = 0. \tag{3.3}$$

This implies that a point on a flame surface remains on this surface for all times t. The local velocity of a flame surface $\mathbf{u}_f$ is derived by a balance between the local fluid velocity $\mathbf{u}$ and the local burning velocity s_L:

$$\mathbf{u}_f = \mathbf{u} + s_L\mathbf{n}. \tag{3.4}$$

The burning velocity is the velocity at which the flame surface propagates normal to itself and relative to the flow in the unburnt mixture. The local normal vector $\mathbf{n}$ is determined from the scalar field $\mathscr{Y}$:

$$\mathbf{n} = -\frac{\nabla\mathscr{Y}}{|\nabla\mathscr{Y}|}. \tag{3.5}$$

.

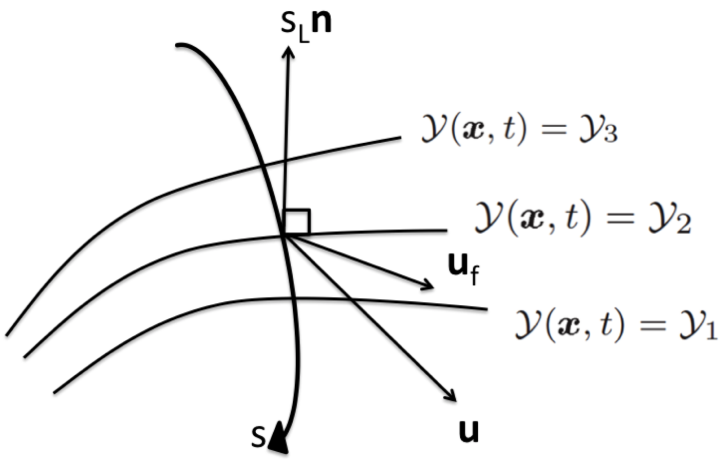

Figure 3.1: Flamelet adapted in the iso-surfaces of $\mathscr{Y}$.

In Figure [3.1], a scheme of the flamelet adapted to the iso-surfaces $\mathscr{Y}$ is shown. As presented in [VanOijen,2002-thesis], equation 3.3 can be written in another form:

$$\frac{\partial\mathscr{Y}}{\partial t} + \mathbf{u} \cdot \nabla\mathscr{Y} = s_L|\nabla\mathscr{Y}|. \tag{3.6}$$

Equation 3.6 describes the motion of all flames surfaces by knowing $\mathbf{u}$ and s_L.

According to [Williams,1958], the stretch rate of a flame is defined as the fractional rate of change of a flame surface element A:

$$K_A = \frac{1}{A}\frac{dA}{dt}. \tag{3.7}$$

Since this definition of stretch can be applied only to flames where the thickness δ is considered infinitely thin, De Goey et al. [deGoey-TenThijeBoonkkamp,1997] proposed a mass-based stretch, which can be applied also to finite thickness flames. Considering that the mass rate of change $M(t)$ is defined as

$$M(t) = \int_{V(t)} \rho dV, \tag{3.8}$$

with $V(t)$ the infinitesimal volume in the flame, moving with velocity $\mathbf{u}_f$, the mass-based stretch rate equation then reads:

$$K = \frac{1}{M}\frac{dM}{dt}. \tag{3.9}$$

By applying Reynolds' transport theorem to equation 3.8, an expression for the scalar quantity K is then proposed [VanOijen,2002-thesis]:

$$\rho K = \frac{\partial \rho}{\partial t} + \nabla \cdot (\rho \mathbf{u_f}). \tag{3.10}$$

The continuity equation in terms of K then becomes:

$$\nabla \cdot (\rho s_L n) = \rho K, \tag{3.11}$$

where the values ρK includes all the distortions from the typical 1D behavior. The conservation equation for a scalar $\mathscr{Y}$ reads:

$$\frac{\partial(\rho\mathscr{Y})}{\partial t} + \nabla \cdot (\rho \mathbf{u}\mathscr{Y}) - \nabla \cdot \left(\frac{\lambda}{Le_{\mathscr{Y}} c_p} \nabla \mathscr{Y} \right) - \dot{\omega}_{\mathscr{Y}} = 0, \tag{3.12}$$

where $Le_{\mathscr{Y}}$ and $\dot{\omega}_{\mathscr{Y}}$ depend on different parameters of the flame [VanOijen,2002-thesis].

The following quantities are now introduced: the mass burning rate $m = \rho s_L$ can be considered as the consumption of mass over time along a certain surface; the arc-length s (as shown in

Figure 3.1) is considered perpendicular to the flame surfaces; finally, σ is the measure for the flame surface area through which transport takes place. With these new quantities, equation 3.12 can be written in a so-called quasi-1D form [VanOijen,2002-thesis]:

$$\frac{\partial(\sigma m\mathscr{Y})}{\partial s} - \frac{\partial}{\partial s}\left(\sigma\frac{\lambda}{Le_{\mathscr{Y}}c_p}\frac{\partial\mathscr{Y}}{\partial s}\right) - \dot{\omega}_{\mathscr{Y}} = -\sigma\rho K\mathscr{Y}. \tag{3.13}$$

If κ is the curvature of the flame surface, a relation between κ and σ reads: $\kappa = -\frac{1}{\sigma}\frac{\partial\sigma}{\partial s}$.

Given the above relations, the flamelet equations are written in the following form: [VanOijen,2002-thesis]

$$\frac{\partial m}{\partial s} = \rho K + \kappa m, \tag{3.14}$$

$$\frac{\partial F_i}{\partial s} - \dot{\omega}_i = -\rho K Y_i + \kappa F_i + Q_i, \tag{3.15}$$

$$\frac{\partial F_h}{\partial s} = -\rho K h + \kappa F_h + Q_h, \tag{3.16}$$

where the fluxes are given by $F_i = mY_i - \frac{\lambda}{Le_i c_p}\frac{\partial Y_i}{\partial s}$, $F_h = mh - \frac{\lambda}{cp}\frac{\partial h}{\partial s} - \frac{\lambda}{c_p}\sum_{i=1}^{Ns}\left(\frac{1}{Le_i} - 1\right)h_i\frac{\partial Y_i}{\partial s}$.

The set given by equations 3.14, 3.15 and 3.16 describes the internal structure of the flame front in terms of $Y_i(s)$, $h_i(s)$ and m for a flamelet with stretch field $K(s)$ and a curvature $\kappa(s)$. The terms Q_i and Q_h in equation 3.6 describe the transport along the flame surfaces, which arises because the iso-surfaces of the variables Y_i and h generally do not coincide with iso-surfaces of the $\mathscr{Y}$ [VanOijen,2002-thesis]. All perturbations proportional to K and κ from the 1D flat flame behavior are taken into account in the right-hand side of the flamelet equations.

The Karlovitz number Ka, which is the dimensionless stretch rate and measures the perturbations induced on the flame, reads:

$$Ka = \frac{K\delta_f}{s_L} \ll 1, \tag{3.17}$$

If $Ka \ll 1$ the flames are weakly distorted and turbulence does not affect the flame structure, i.e. the situation is close to laminar.

Curvature effects are also negligible if the curvature radius $R = \frac{1}{k}$ of the flame is much larger than the thickness.

$$|k^{-1}| \gg \delta_f. \tag{3.18}$$

By neglecting all perturbation terms, setting $K = \kappa = 0$, the set of 1D equations reads now [VanOijen,2002-thesis]:

$$\frac{\partial m}{\partial s} = 0, \tag{3.19}$$

$$\frac{\partial F_i}{\partial s} = \dot{\omega}_i \quad \Leftrightarrow \quad \frac{\partial}{\partial s}\left(mY_i - \frac{\lambda}{Le_i c_p}\frac{\partial Y_i}{\partial s}\right) = \dot{\omega}_i, \tag{3.20}$$

$$\frac{\partial F_h}{\partial s} = 0 \quad \Leftrightarrow \quad \frac{\partial}{\partial s}\left(mh - \frac{\lambda}{cp}\frac{\partial h}{\partial s} - \frac{\lambda}{c_p}\sum_{i=1}^{Ns}\left(\frac{1}{Le_i} - 1\right)h_i\frac{\partial Y_i}{\partial s}\right) = 0. \tag{3.21}$$

These equations describe the structure of an undistorted planar flame. The balance equations between convection, diffusion and reaction can be considered as a steady state relation, which forms the basis for the creation of the manifold.

3.3 1D manifold

The set of equations 3.19-3.21 is solved by treating the system as an adiabatic, freely-propagating, premixed and flat flame [VanOijen,2002-thesis], for which the following boundary conditions are used.

For the unburnt u side, Dirichlet boundary conditions are introduced:

$$Y_i(s \to -\infty) = Y_{i,-\infty}, \qquad h(s \to -\infty) = h_{-\infty}, \tag{3.22}$$

while for the burnt b side, a homogeneous Neumann type is utilized:

$$\frac{dY_i}{ds}(s \to \infty) = 0, \qquad \frac{dh}{ds}(s \to \infty) = 0. \tag{3.23}$$

In this system, the mass burning rate m is an eigenvalue of the problem. The solution of the system of the equations 3.19-3.21 is a one-dimensional curve in the composition space and it is determined by its starting points $(Y_{i,-\infty}, h_{-\infty})$ and ends in the equilibrium point $(Y_{i,\infty}, h_\infty)$. The 1D curve in composition space is basically a flamelet starting at the point that represents the unburnt mixture and represents the so-called 1D manifold. Figure 3.2 shows the source term parametrized by the progress variable. The fuel used in this example is pure methane CH_4. The equivalence ratio of this mixture, which represents the deviation of the mixture with respect to the stoichiometric condition, is set to $\phi = 0.9$. Progress variable selection is also an important

step in the manifold creation: in this case, one progress variable is chosen and this is O_2. The progress variable is generally scaled by using $Y_{O_2,-\infty}$ and $Y_{O_2,\text{eq}}$ which are, respectively, the mass fractions at initial condition and at equilibrium condition. The progress variable is then defined as:

$$\mathscr{Y} = \frac{Y_{O_2} - Y_{O_2,-\infty}}{Y_{O_2,\text{eq}} - Y_{O_2,-\infty}}. \tag{3.24}$$

In Chapter 4, a more complete description regarding the choice of progress variable is outlined.

A one-dimensional manifold (1D-FGM) is related to the fact that one variable $\mathscr{Y}$ is used to fully describe the chemical composition state. In this explanation, the variable is the reaction progress variable. It is a common procedure, in the FGM implementation, to refer to the variable considered, i.e. the progress variable, as *controlling variable*. When an extra dimension is considered, an extra controlling variable is then introduced. For each controlling variable considered, an extra differential equation is added to the calculation during combustion CFD. By doing this, an extra degree of freedom is therefore introduced. Once the manifold is created, this is coupled with a multi-dimensional combustion computation, i.e. a CFD tool that solves the transport equations and the controlling variable equations. Before describing the coupling of the manifold with the CFD tool, a description on how to add an extra dimension to the manifold is given in the following Section.

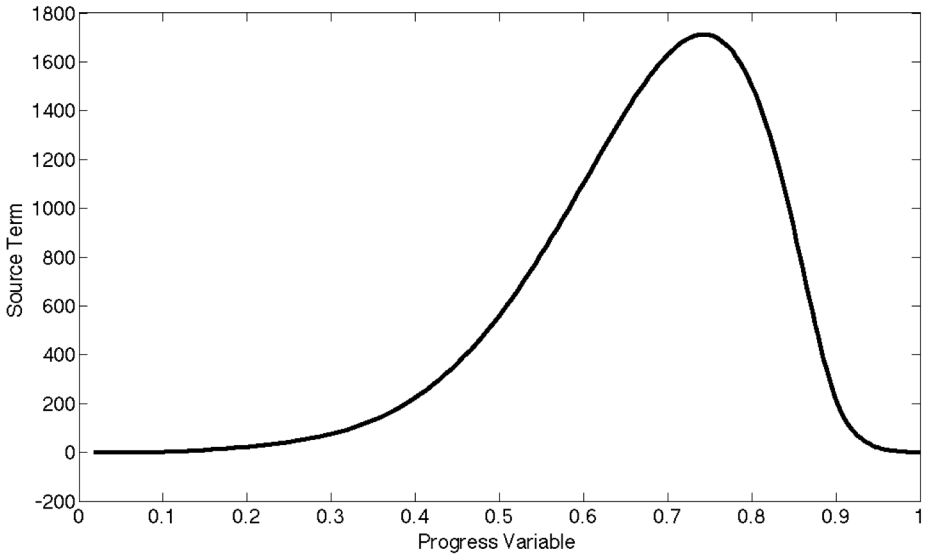

Figure 3.2: Chemical source term $\dot{\omega}_{\mathscr{Y}}$ as function of progress variable $\mathscr{Y}_{O_2}$. Fuel: CH_4 with $\phi = 0.9$.

3.4 Extension to higher FGM dimensions

In the previous description of the 1D-FGM, only the progress variable is changing, while some other quantities such as enthalpy is conserved. Hence, if enthalpy is conserved, no heat loss is taken into account and thus the system is considered fully adiabatic. However, in problems such as burner-stabilized flames, the stabilization of a flame is subjected to heat loss, cooling of the wall and radiation effects. These phenomena can be taken into account by assuming that the system is no more adiabatic, but it is subject to enthalpy changes. In order to include the heat loss effect, enthalpy is therefore considered the extra controlling variable.

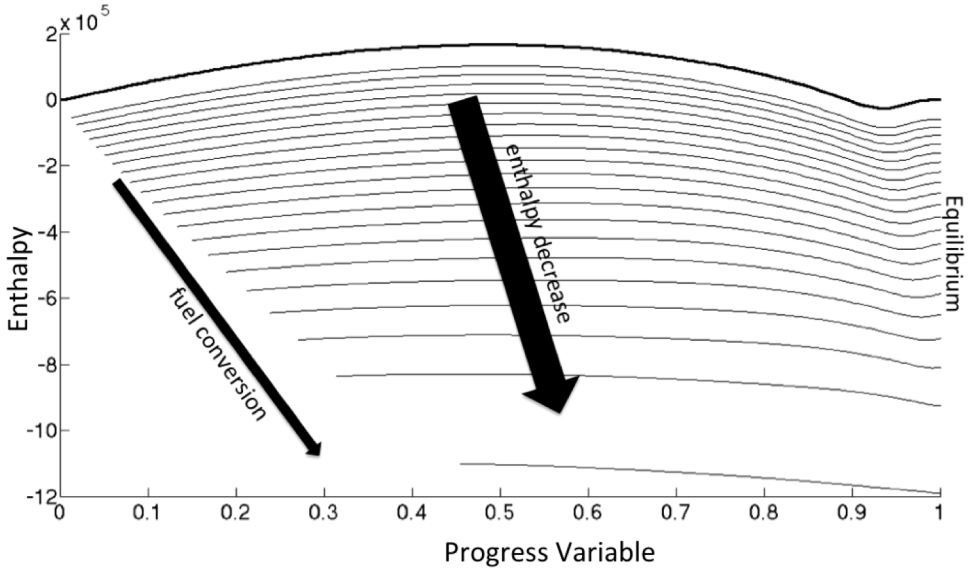

Figure 3.3: Projection of different flamelets for different values of h, Pure methane, $\phi = 0.9$, Progress variable $\mathscr{Y}_{O_2}$ - Lewis constant transport approach.

In order to create a 2D manifold, a series of flamelets with enthalpy variation is computed by starting from the adiabatic flame and lowering $h_{-\infty}$ until the lower enthalpy level. The enthalpy of the flamelet can be changed in many ways [vanOijen,2000], for instance by decreasing, for each flamelet, the mass burning rate m or by decreasing the unburnt temperature T_u.

The first (adiabatic) flamelet is computed with a relatively high temperature, such as for example $T_{-\infty,\max} = 390K$.

The following flamelets are computed with decreasing temperature steps. Each computed flamelet becomes the starting solution for the new one. When reaching a temperature value which is not more realistic, such as for example $T_{-\infty,\max} = 240K$, another method to derive the lower enthalpy is used. The other method consists in lowering the enthalpy by converting the initial fuel into products. By using a methane mixture with $\phi = 0.9$ as an example, the conversion of fuel into products is done by converting a fraction of fuel CH_4 with O_2 into the CO_2 and H_2O. This process is iterated until the T_b is too low that the flame extinguishes.

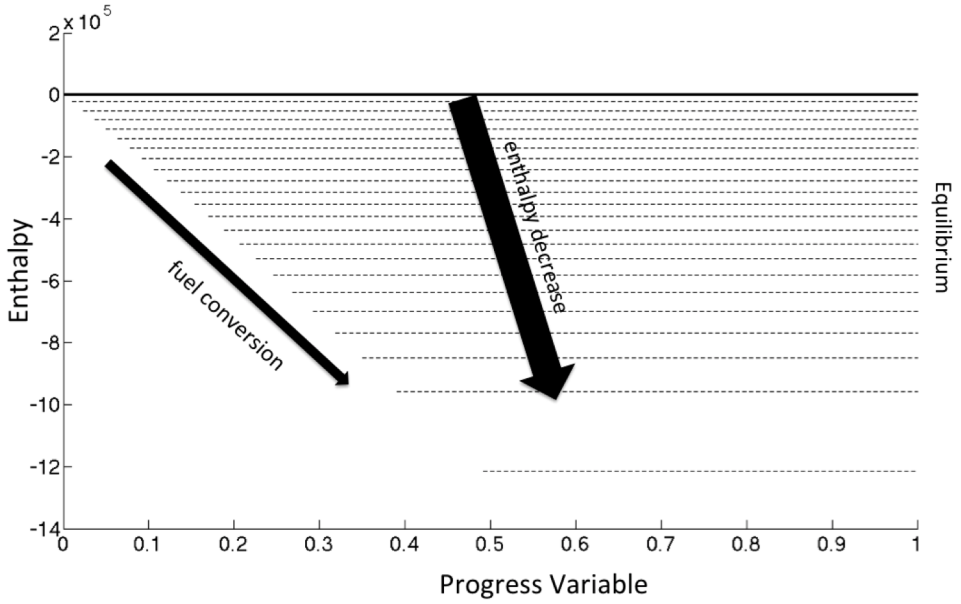

Figure 3.4: Projection of different flamelets for different values of h, Pure methane, $\phi = 0.9$, Progress variable $\mathscr{Y}_{O_2}$ - $Le = 1$ transport approach.

In Figure 3.3, the series of flamelet computed with different enthalpies are presented by using the example explained above. Due to the conservation of enthalpy in the flamelet equations, the initial and the equilibrium values of enthalpy are coincident for each flamelet. Preferential diffusion effects can be seen in the enthalpy behavior: although the enthalpy, along the flamelet, is conserved, since the enthalpy at the unburnt side is equal to the one at equilibrium condition, locally the values are higher and lower. In case preferential diffusion is not taken into account in creating the flamelets, i.e. for $Le = 1$, the flamelets would be completely straight, since no local enthalpy change along the flamelet would occur, as shown in Figure 3.4.

The procedure proposed for the creation of a 2D-FGM system can be extended similarly to higher dimensions. In general, for a typical premixed system, the controlling variables involved in the system are $N_{\text{cv}} = N_{\text{PV}} + N_{\text{add}}$ with N_{cv} the total number of controlling variables, N_{PV} the number of progress variables taken into account and N_{add} the additional controlling variables like enthalpy, pressure and element mass fraction to be included in the FGM system. However, the number of additional controlling variables is generally small for most applications [vanOijen,2000]. The detailed chemistry code used to compute the flamelets is an in-house code known as CHEM1D [CHEM1D-URL]. In later Chapters, a more detailed description on how this code performs the calculations is given.

Chapter 4

A dynamic flame in a box

"Γιά το καρφί έχασε το πέταλο."
Lit. "If you don't take care of small problems, they eventually get bigger."

old greek proverb

Part of this work is described in *Towards numerical simulation of turbulent hydrogen combustion in OpenFOAM* published in AIP proceedings 2013 [Fancello,2013].

4.1 Introduction

In Chapter 3 it has been mentioned that the set of flamelet Equations is solved by treating the system as a one-dimensional adiabatic premixed flame. Its solution is referred to as a flamelet, which generates a 1D curve in the composition space parameterized by the curvilinear coordinate *s*. Furthermore, the 1D manifold is simply described by the flamelet, starting from the point that represents the unburnt mixture and ending at the equilibrium point [vanOijen,2000]. Thereby, the manifold connects these two points in composition space. Similarly, a 2D manifold can be constructed from a set of flamelets with e.g. different enthalpy levels, starting at different points on a 1D curve in composition space.

In the current Chapter, an application of FGM with a combustion solver is presented. A *flame in a box* geometry is used as a test case. Although prior studies extensively exploited stationary aspects on this configuration [VanOijen,2002-thesis] [Donini,2014], the author is not

aware of any study that has examined the dynamic aspects. Hence, this work adds new insights on dynamic phenomena, which are fundamental in transient combustion. Their importance emerges from their effects on the stability of the flame [Law,2006]. Instabilities can affect the expected stationary solution, in such a way that a stationary pattern might not be achieved [Poinsot-Veynante,2005]. Figure 4.1 shows a scheme for the presented test case.

To achieve this aim, an open source code known as OpenFOAM ® is employed for the CFD calculations. Although this software does not have a *user-friendly* interface if compared to other CFD codes, it provides high quality results within an open source environment [Park,2013] [Nilsson,2008] [Chen,2014]. An ILDM [Maas-Pope,1992] approach with extension to FGM application has been already implemented in the OpenFOAM ® environment [Kroger,2010], but this code was not available for testing. Thus, a new implementation has been performed, by using the standard OpenFOAM ® code as a starting point. This implementation is explained in the next Sections of this Chapter.

4.1.1 Stability and stabilization of the flame

Two main aspects have to be considered in a dynamic approach when simulating a flame: flame stability and flame stabilization. Flame stability is highly desirable in gas turbine engines and industrial furnaces [Law,2006] [Williams,1985]. Flame instabilities arise as unsteady motions of the flame, invoked by different mechanisms. For instance, aspects such as gravity might influence the stability of many combustion processes, particularly due to buoyant convection which affects transport of thermal energy and reactants to and from the chemical reaction zones [Law,1994] [Ronney,1998].

The principle of flame stabilization [Law,2006] is to provide a condition through which the flame is able to have sufficient capableness to adjust its location, orientation and configuration, along a non-uniform and temporally varying flow field, so it finally becomes steady.

In the present work, some phenomena regarding these two aspects above mentioned are presented and discussed.

4.1.2 Outlook of the Chapter

The present work is organized as follows: the first part shows an implementation of a 1D-FGM system, while the second part presents the extension of the work to a 2D-FGM. In particular, this Chapter is based on the following steps:

- Description of the test case boundary conditions.
- Implementation of the one-dimensional manifold (1D-FGM), by using an incompressible

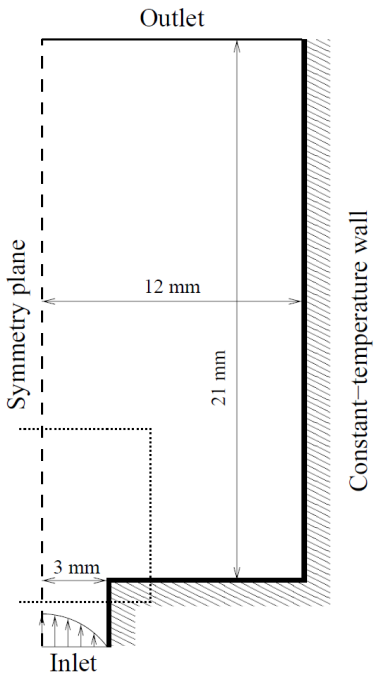

Figure 4.1: Flame in a box geometry (from [vanOijen,2000]).

flow approach. This is performed by adding a transport reactive scalar equation with a source term given by an analytical distribution.

- Tabulation of a realistic manifold database for a reactive scalar transport equation. This manifold is obtained by a flamelet calculation (through CHEM1D).

- 1D-FGM implementation to a compressible solver.

- Implementation of a 2D manifold (2D-FGM) with addition of heat loss effects.

- Presentation of problems related to oscillations and instabilities of the flame and proposal for a subsequent solution.

- Validation with known steady solution [vanOijen,2000].

- Description of transient phenomena in the test case configuration, important for stabilization of the flame.

- Concluding remarks.

4.2 1D manifold: the progress variable $\mathscr{Y}$

4.2.1 Parameters and Boundary Conditions for 1D FGM case

Since the progress variable is defined as a measure of the status of the combustion process, it is often used to define the unburnt value as $\mathscr{Y}_u = 0$ and the burnt one as $\mathscr{Y}_b = 1$. The choice of progress variable has been done by using the same approach as described in Chapter 2. While using methane as fuel, the mass fraction of oxygen is a proper choice for $\mathscr{Y}$, due to its monotonic behavior.

The first step for a 1D-FGM approach calculation consists of the addition of a transport equation for the $\mathscr{Y}$ scalar in the CFD solver. Considering a simple incompressible ($\rho = const$) transient laminar solver, the equation for the scalar $\mathscr{Y}$ reads:

$$\frac{\partial \mathscr{Y}}{\partial t} + \nabla \cdot (\mathbf{u}\mathscr{Y}) = D \cdot \nabla^2 \mathscr{Y} + \dot{\omega}_{\mathscr{Y}}, \tag{4.1}$$

where D is the diffusion coefficient for the $\mathscr{Y}$ scalar and $\dot{\omega}_{\mathscr{Y}}$ the chemical source term. In this case the enthalpy is constant and thus we are considering adiabatic conditions.

Boundary conditions (B.C.) and few parameters, which are used in the CFD simulations of 1D-FGM, are listed as follows:

- Diffusion coefficient $D = 2 \cdot 10^{-5}\ m^2/s$.
- Grid size: uniform standard width $\Delta x = 4 \cdot 10^{-5}\ m$.
- Inlet B.C. :
  - Velocity $\mathbf{u}_{\text{inlet}}$: parabolic profile with max value of $1\ m/s$,
  - Progress variable $\mathscr{Y}_{\text{inlet}} = 0$.
- Outlet B.C. :
  - Velocity $\mathbf{u}_{\text{outlet}}$: zero gradient ,
  - Progress variable $\mathscr{Y}_{\text{outlet}}$: zero gradient .

The scalar $\mathscr{Y}$ is initialized as a *planar flame* near the inlet $\mathscr{Y}_0 = \mathscr{Y}(t = 0)$ by using a tanh profile resulting in a gradient initialization from 0 to 1 expressed by:

$$\mathscr{Y}_0 = \frac{\frac{\tanh(y - y_0)}{\delta} + 1}{2}, \tag{4.2}$$

where

- $y_0 = 0.001$ is the initial position in vertical direction,
- $\delta = 0.0005$ the flame thickness,
- y the coordinate in streamwise direction.

Figure 4.2 shows the initialization of scalar $\mathscr{Y}$ as presented in Equation 4.2.

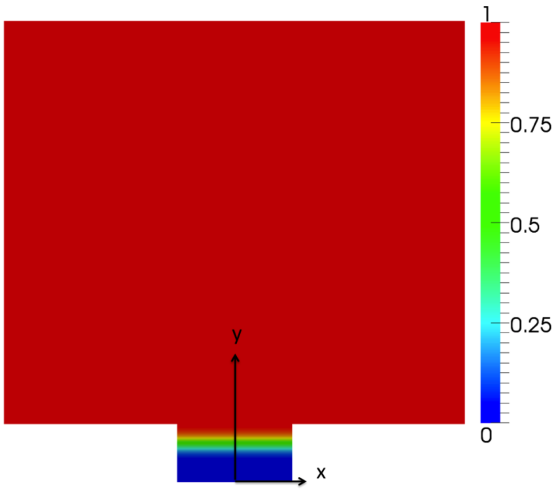

Figure 4.2: Initial Conditions for the scalar field $\mathscr{Y}_0$ as presented in Equation (4.2).

4.2.2 Source term $\dot{\omega}_{\mathscr{Y}}$ modeled with analytical function and incompressible solver

With regards to Equation 4.1, the chemical source term $\dot{\omega}_{\mathscr{Y}}$ is unclosed and has to be modeled. This term $\dot{\omega}_{\mathscr{Y}}$ represents the consumption of the progress variable $\mathscr{Y}$. An example of $\dot{\omega}_{\mathscr{Y}}$ as function of $\mathscr{Y}$ is presented in Figure 3.2. The following analytical formula for $\dot{\omega}_{\mathscr{Y}}$ is adopted for proposing a model with similar behavior:

$$\dot{\omega}_{\mathscr{Y}}(\mathscr{Y}) = A \cdot [\mathscr{Y} \cdot (1 - \mathscr{Y})]^2, \tag{4.3}$$

Equation 4.3 has been chosen to represent the behavior of the source term $\dot{\omega}_{\mathscr{Y}}$, in a qualitative way, compared to the manifold presented in Figure 3.2. In Equation 4.3, A represents the magnitude of the source term. In order to have a value of $\dot{\omega}_{\mathscr{Y}}$ which can be compared with the one given in Figure 3.2, the value presented for A is chosen to be 25000. The behavior of the source term as function of progress variable is illustrated in Figure 4.3.

Mathematical modeling of the source term is very convenient to explain the physical mechanism which occurs during the flame propagation. After an initial transient, the result emerging from this calculation is shown in Figure 4.4. The scalar $\mathscr{Y}$, which represents the flame, is transported in the domain and has stabilized in the lower side of the inlet with a particular shape, given basically by the parabolic profile of the inlet velocity and the propagation speed. The flame tip height is related to the magnitude of the source term in the scalar equation. Consequently, as the source term is higher, the flame tip is shorter. This effect can be explained as follows: when the burning velocity s_L and the flow velocity $\mathbf{u}$ are balanced, the flame is stabilized at a certain height. Since the flame propagates from the burnt to the unburnt side, a stronger source term would result in higher contribution given by the burning velocity with respect to the flow velocity and, therefore, the flame tip height would become lower, compared to the one shown in Figure 4.4.

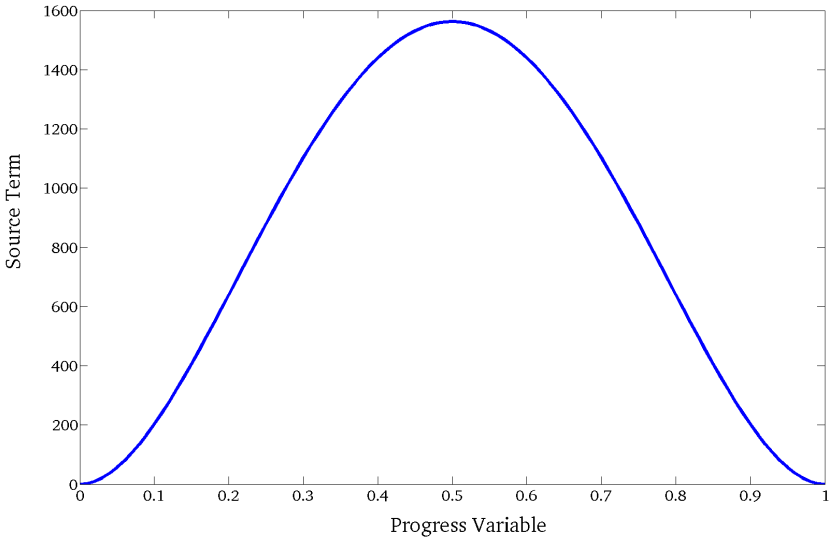

Figure 4.3: Source term as function of progress variable modeled with analytical function given by Equation 4.3.

4.2.3 Creation of the manifold from CHEM1D

The solution presented in Figure 4.4 is not realistic because the chemical source term is not realistic. In order to include the contribution given by the realistic chemistry, a description on how to compute the one-dimensional flamelet with detailed chemistry is presented in this Section. The in-house code CHEM1D [Somers,1994] solves equations for flamelets including detailed models for chemistry and transport. For instance, the code is able to consider different configurations, such as freely propagating premixed flames, counterflow (diffusion) flames, burner stabilized flames, spherical flames in open and closed domains. In CHEM1D, the conservation equations are discretized in 1D by using a second order finite volume approach, while time integration is performed with a second order backwards differencing scheme. Further informations

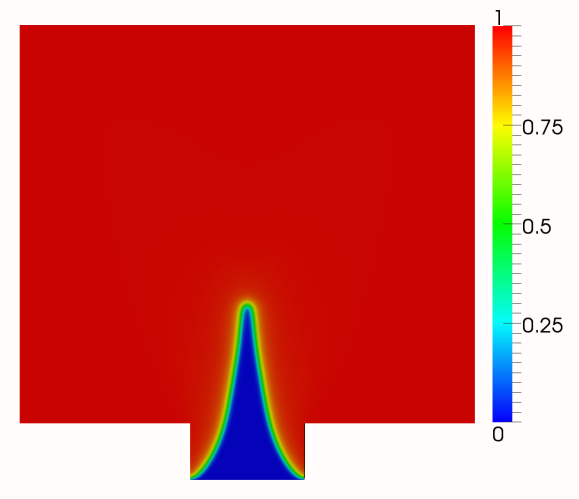

Figure 4.4: Progress variable solution with source term given by analytical function (as shown in Figure 4.3), after a transient of $t = 1\ s$.

about this detailed chemistry code can be found in [Somers,1994].

A simulation of a one-dimensional flame is based on a freely propagating flame calculation, under adiabatic conditions. The characteristics of this flamelet read:

- Gas composition : pure CH_4 in air .
- Equivalence ratio: $\phi = 0.9$.
- Transport method: constant Lewis approach. This transport model is used by imposing a fixed value of the Le number for each species. A particular case of a constant Le number is $Le = 1$, which is adopted here. Since the Le number of each species is generally different from unity, this assumption is a simplification of the real problem. This assumption is still reasonable for a gas such as methane, considering that its Le number is very close to unity.
- Type of flame: freely propagating flat flame .
- Unburnt temperature $T_u = 300\ K$.
- pressure: 1 bar .

The kinetic scheme, or mechanism, which is used in this computation is the GRI 3.0 mechanism [Smith,1999].

In Figure 4.5, the structure of a methane-air flow is shown in terms of different species involved in the reaction. Species are expressed in mass fraction [-].

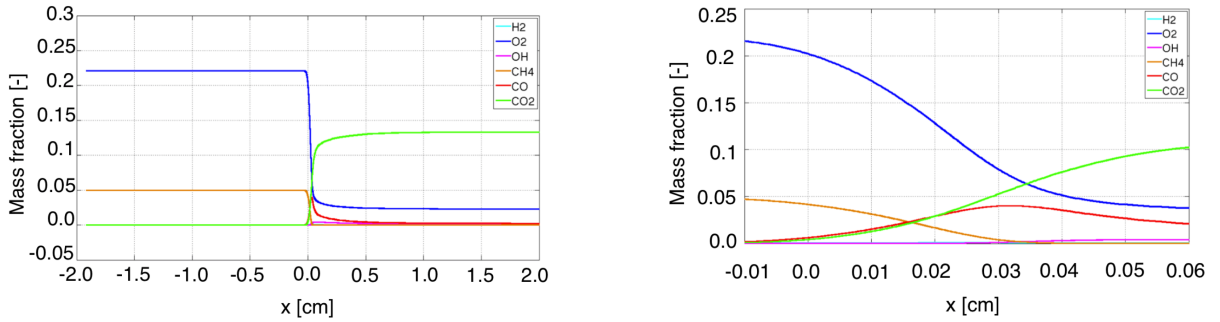

(a) Full domain

(b) Zoom of reaction zone

Figure 4.5: Combustion of Methane, $\phi = 0.9$, 1 *bar*. Different species in physical space.

As anticipated in Chapter 3, a manifold is computed by a transformation of coordinates. The transformation acts between the physical and the controlling variable space. O_2 is chosen as progress variable. In this way, the manifold is created by considering the flamelet properties as function of the progress variable $\mathscr{Y}_{O_2}$, scaled between 0 and 1. Typical key properties included in the manifold are: source term, temperature, density and diffusion coefficients. All these quantities are tabulated as function of the progress variable.

In this manifold, all the key properties are stored from the calculation performed by the detailed chemistry solver. In order to reduce the computational costs, c_p, λ and μ are modeled with respect to a mixture-averaged approach, already introduced in Chapter 2. In particular, the heat capacity is modeled with Equation 2.12, dynamic viscosity with Equation 2.21 and thermal conductivity with Equation 2.23. The source term $\dot{\omega}_{\mathscr{Y}-O_2}$ as function of progress variable $\mathscr{Y}_{O_2}$, as calculated with CHEM1D [Somers,1994], is presented in Figure 4.6.

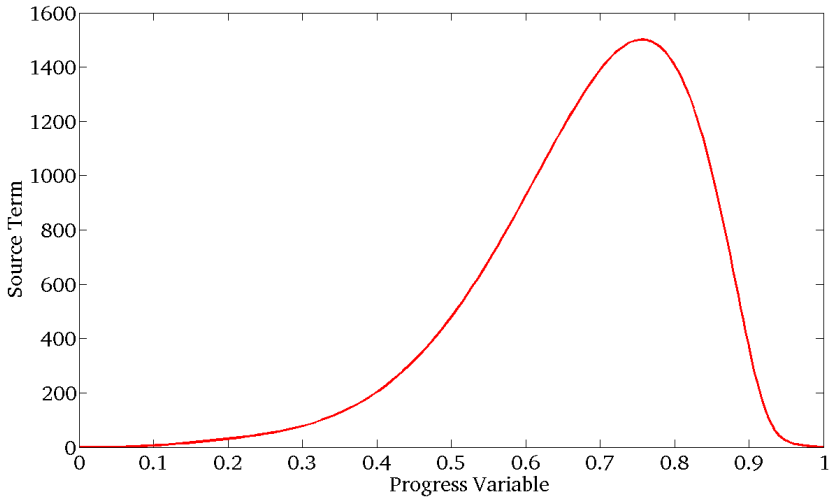

Figure 4.6: Source term $\dot{\omega}_{\mathscr{Y}-O_2}$ as function of scaled progress variable $\mathscr{Y}_{O_2}$ for a CH_4-air mixture, $\phi = 0.9$, GRI 3.0 mechanism, $Le = 1$ transport approach.

The manifold is used as an input for the multi-dimensional combustion solver. The CFD tool OpenFOAM ® is manipulated in order to look up the manifold values during the simulation runtime. As mentioned above, the different values in the manifold are written as function of the progress variable. Regarding this aspect, an interpolation between each look up value is performed, in order to take into account the discrete form of the database. In addition to the manifold parameters such as temperature and diffusivity, also minor species can be included in the manifold. In CH_4-air combustion, minor species typically considered are: NO_x, CO and OH.

A preliminary application of the realistic manifold in a CFD solver is presented in Appendix A.1. This CFD application in OpenFOAM ® is compared with a commercial software code. Regarding this preliminary results, Figure 4.7 shows the comparison of the steady solution obtained both with OpenFOAM ® and Comsol Multiphysics [Comsol-URL]. The comparison adopts the assumption of constant density in the flow: this has been used since the commercial software adopted for the comparison has the same approach of keeping the density as a constant value.

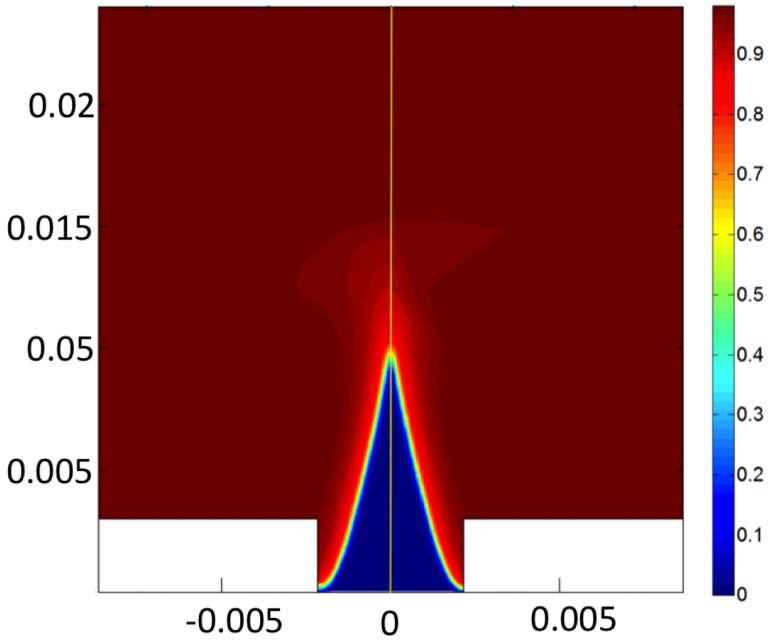

Figure 4.7: Comparison between Open FOAM (left) and Comsol (right) with a stabilized adiabatic flame after a time of 1 s.

4.2.4 A compressible solver for reacting flows

OpenFOAM ® provides a compressible solver for heating, ventilating, and air conditioning (HVAC) known as *rhoPimpleFoam*. This solver has been largely adopted for different applications [Pashami,2010] [Kumar,2011] [Rezaei,2013] [Xisto,2010]. A low Mach number setting is a singular limiting situation in compressible flows. As Mach number approaches zero,

compressible (density-based) flow solvers encounter severe deficiencies, both in efficiency and accuracy [Turkel,1997] [Turkel,1987] [vanLeer,1991].

The adopted solver, named *rhoPimpleFoam*, is based on the PIMPLE algorithm, which is a combination of PISO and SIMPLE algorithms [Ferziger-Peric,2002], [Anderson,1984]. In particular, the PISO (Pressure Implicit with Splitting of Operators) [Issa,1986] is an efficient method to solve the Navier-Stokes equations in unsteady problems. The SIMPLE (Semi-Implicit Method for Pressure-Linked Equations) [Patankar,1972] allows coupling the Navier-Stokes equations with an iterative procedure. More informations regarding this compressible solver can be found in Appendix A.2.

4.2.5 Solution of 1D-FGM with a compressible solver

In Figure 4.8, a stationary solution is presented, by using a modified version of *rhoPimpleFoam* solver. One important aspect in reacting flows regards the non-constant density across the flame front, since it changes due to the changing temperature. Together with density and temperature, also velocity fields and other parameters are subjected to a change across the flame front. These quantities are therefore coupled. These results describe a more realistic scenario, compared to those discussed in Figure 4.4. In Figure 4.8a, it can be observed how the velocity is coupled with the density: velocity in the inlet is subjected by the higher density. Once the density drops throughout the flame front the velocity is evidently subjected to this density variation and, as a result, it increases, as displayed in Figures 4.8a and 4.8c.

Summarizing, a 1D-FGM implementation has been presented by using the reaction progress variable as a controlling variable. The system considered is adiabatic since no heat loss effects are taken into account.

4.3 Inclusion of heat loss: the 2D-FGM manifold

4.3.1 The equations for the controlling variables

The inclusion of heat loss requires an extra equation for enthalpy. As anticipated in Chapter 3, a two dimensional manifold is created by using the 1D manifold and extending this curve by varying h in an extra dimension (Figure 3.3). In this case, the progress variable $\mathscr{Y}$ is computed for different values of enthalpy h. (The full procedure is explained in [vanOijen,2000], [VanOijen,2002-thesis].)

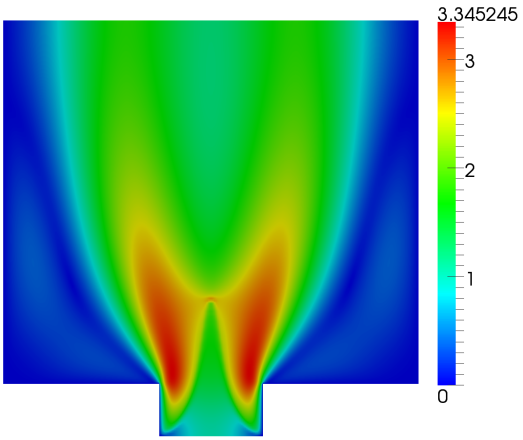

(a) Velocity magnitude

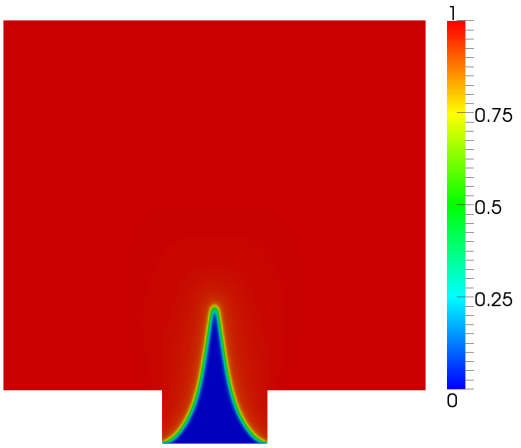

(b) Progress variable

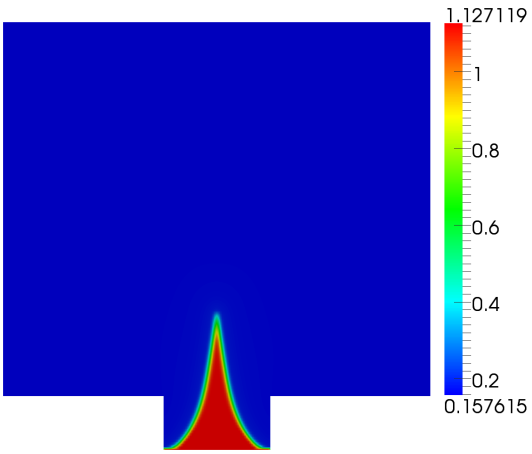

(c) Density

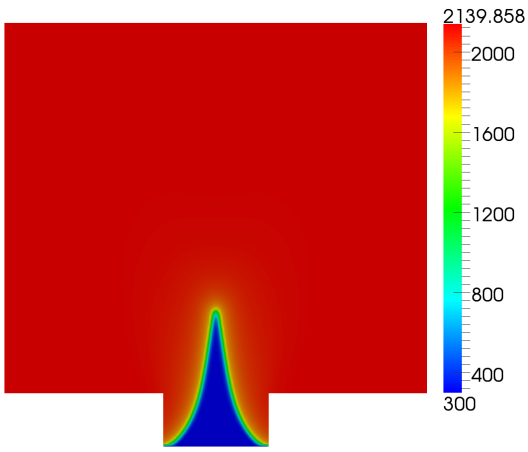

(d) Temperature

Figure 4.8: Compressible solver results for 1D-FGM calculation. Fuel: CH_4-air with $\phi = 0.9$, progress variable: $\mathscr{Y}_{O_2}$ after a time of 1 s.

The equations for the controlling variable $\mathscr{Y}$ and h read:

$$\frac{\partial}{\partial t}(\rho\mathscr{Y}) + \nabla\cdot(\rho\mathbf{u}\mathscr{Y}) - \nabla\cdot\left(\frac{1}{Le_{\mathscr{Y}}}\frac{\lambda}{c_p}\nabla\mathscr{Y}\right) = \dot{\omega}_{\mathscr{Y}}, \tag{4.4}$$

$$\frac{\partial}{\partial t}(\rho h) + \nabla\cdot(\rho\mathbf{u}h) - \nabla\cdot\left(\frac{\lambda}{c_p}\nabla h\right) = \nabla\cdot\mathscr{H}, \tag{4.5}$$

with $\mathscr{H} = \left[\frac{\lambda}{c_p}\sum_{i=1}^{N_s}\left(\frac{1}{Le_i}-1\right)h_i\nabla Y_i\right]$, being the enthalpy flux due to preferential diffusion.

By imposing $Le = 1$, preferential diffusion effects are not included and thus, Equations 4.4 and 4.5 reduce to:

$$\frac{\partial}{\partial t}(\rho\mathscr{Y}) + \nabla\cdot(\rho\mathbf{u}\mathscr{Y}) - \nabla\cdot\left(\frac{\lambda}{c_p}\nabla\mathscr{Y}\right) = \dot{\omega}_{\mathscr{Y}}, \tag{4.6}$$

$$\frac{\partial}{\partial t}(\rho h) + \nabla\cdot(\rho\mathbf{u}h) - \nabla\cdot\left(\frac{\lambda}{c_p}\nabla h\right) = 0. \tag{4.7}$$

4.3.2 CHEM1D computation to include heat loss and 2D-FGM

The different flamelets with different enthalpies can be computed in two different ways: [vanOijen,2000] (i) by using burner-stabilized flames and reducing m until this value becomes low enough that the flame extinguishes, and (ii) by using adiabatic flames and decreasing the unburnt temperature T_u. In this work, the first method is adopted. A series of flamelets under *burner-stabilized* condition are computed with decreasing the mass burning rate m, until this values reaches the limit value $m \to 0$. As a consequence, the enthalpy decreases. For convenience, the enthalpy value referred to as the adiabatic flame is set to 0 and, thus, the decreasing enthalpy levels have negative values. This computation is performed by creating a loop: each flamelet is calculated by using the one related to the upper level of enthalpy as starting solution. Afterwards, these flamelets are collected to create the manifold. This method is fully described in [Donini,2014]. The new 2D-FGM system can be expressed as a three-dimensional plot, in which the parameters, e.g. source term and temperature, are visualized as function of progress variable and enthalpy. An example of manifolds is presented in Figure 4.9. The enthalpy levels in Figure 4.9a are computed with a transport approach of $Le = 1$. As illustrated in Figure 4.9a, in a $Le = 1$ approach there are no preferential diffusion effects and thus the enthalpy lines are straight. A manifold with constant Lewis number approach is further presented in Appendix A.3.

This manifold includes few parameters which are read during the calculation in the tri-dimensional

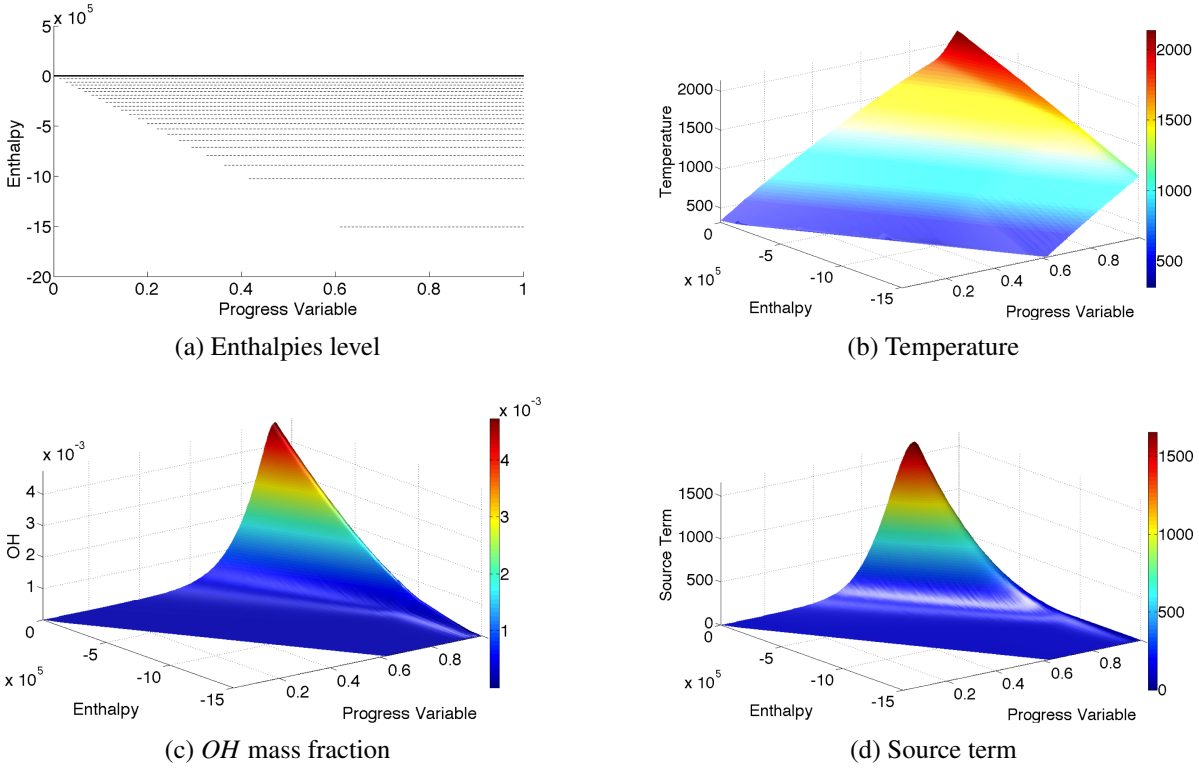

(a) Enthalpies level

(b) Temperature

(c) *OH* mass fraction

(d) Source term

Figure 4.9: Overview of different variables (h, T, Y_{OH} and $\dot{\omega}_{\mathscr{Y}}$) calculated from a 2D manifold. Fuel: methane-air with $\phi = 0.9$. Controlling variables: $\mathscr{Y}_{O_2}$ and h. Transport approach: $Le = 1$.

combustion calculation. The complete list of the values retrieved from the manifold is given in Table 4.1:

The CFD calculations with the 2D-FGM approach are performed by using the same compressible solver introduced for the 1D-FGM. In the case of 1D-FGM, only a stationary solution was presented through this solver; whereas in the case of 2D-FGM, the main focus regards transient aspects and stabilization of the flame. In van Oijen et al. [vanOijen,2000], a stationary solution was presented and this was achieved by using a stationary solver. Here, a transient solver is used and stable steady solutions are harder to find. In addition, a validation referring to [vanOijen,2000] is performed.

4.3.3 Boundary condition for 2D-FGM

Boundary conditions for progress variable and velocity, with respect to the 1D-FGM case calculations, remain the same. Pressure boundary conditions are given by imposing a fixed value of 101325 *Pa* in the outlet boundary, while imposing a zero gradient setting to the other boundaries (inlet and walls). As heat loss is taken into account, boundary conditions either for enthalpy or for temperature can be used. In this work, T boundary conditions are given (Table 4.2) .

Table 4.1: Manifold values retrieved by the CFD solver. $Le = 1$ approach.

MANIFOLD VALUES
Control variable 1: Enthalpy
Control variable 2: ($\mathscr{Y}_{O_2}$)
Source Term $\dot{\mathscr{Y}}_{O_2}$
CH_4 mass fraction
O_2 mass fraction
N_2 mass fraction
CO_2 mass fraction
H_2O mass fraction
OH mass fraction
CO mass fraction
NO mass fraction
Density
Thermal Conductivity
Heat capacity at constant pressure
Gas constant
Viscosity
Thermal diffusivity
Temperature

Table 4.2: Temperature boundary conditions.

Boundary	Temperature boundary condition type
inlet	fixed value (300 K)
walls	fixed value (300 K)
symmetry axis	symmetry type
outlet	zero gradient

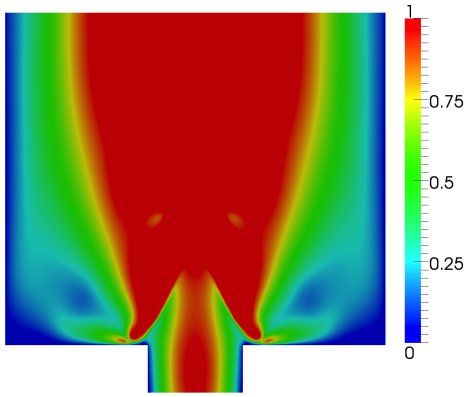

(a) Velocity

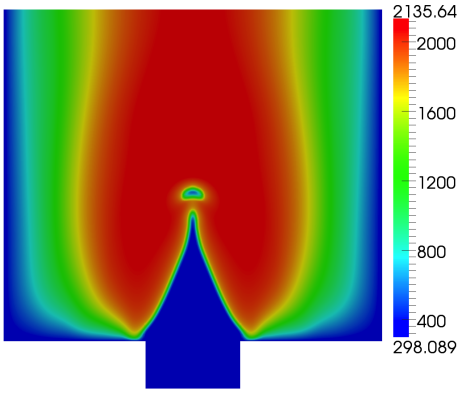

(b) Temperature

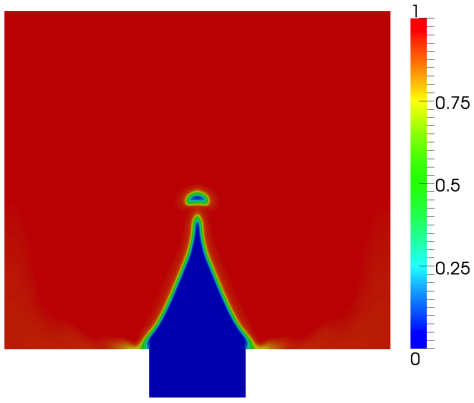

(c) Progress variable

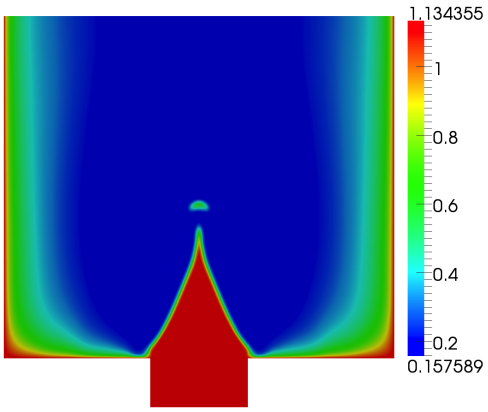

(d) Density

Figure 4.10: CFD Solution of 2D-FGM with $\mathscr{Y}_{O_2}$ and h as controlling variable. Transient period: $t = 1\ s$.

4.3.4 Preliminary results and comments

The solution of the 2D-FGM case is presented in Figure 4.10 after a transient time of 1 s. As evident from the results, the final solution is not stable and shows a bubbling behavior of the flame tip, which is recurring over time. In fact, no stationary solution is found. Another question that arises concerns the dependence of this unsteady behavior due to compressibility effects, boundary conditions or other settings. Few snapshots of the instabilities of this flame are presented in Figure 4.11. A few attempts have been made to get rid of the oscillations.

4.3.5 Error function method

A first attempt to solve the problem related to the instability in the flame tip consists of applying a smooth change in the velocity field given by an error function [Whittaker,1967], which has been set in the velocity field to ensure a smooth variation of the velocity profile, in order to avoid

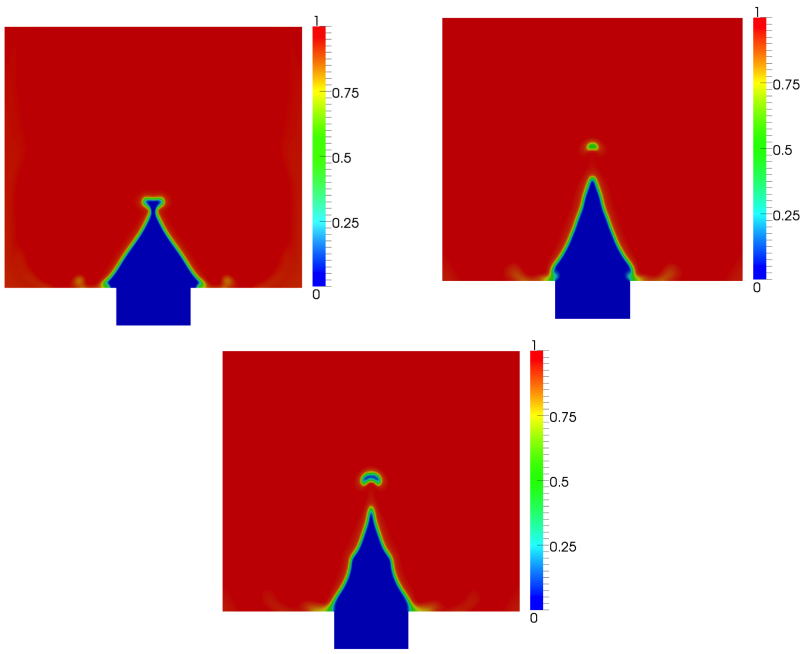

Figure 4.11: Examples of instability of the flame.

any abrupt change in the inlet, regarding the velocity from 0 to 1 m/s values. A mathematical formula for this error function is:

$$\mathscr{E}(t) = 1 + \frac{\left(erf\left(\frac{t-0.1}{0.025}\right)\right)}{2}, \tag{4.8}$$

with the relative plot in Figure 4.12.

4.3.6 Non-reflecting boundary conditions for pressure

A hypothesis has been posed in order to explain this unexpected behavior: the possibility that acoustic waves, captured in the domain during the starting time of calculation, can eventually affect the stability of the flame. So far, pressure boundary conditions in previous calculation have been set by imposing the atmospheric value of pressure in the outlet region. Nevertheless, in order to avoid reflected waves, a new set of boundary conditions, *non-reflecting* boundary conditions [Alpert,2002] are imposed at the outlet. The standard pressure boundary condition, imposed on the boundaries of an artificially truncated domain, results in the reflection of the outgoing waves. As a consequence, the interior domain would contain spurious wave reflections. Non-reflecting boundary conditions provide a special treatment to the domain boundaries to control these spurious wave reflections. Thereby, these boundary conditions *absorb* the outgoing pressure waves in order to avoid both continuous reflections of such perturbations along the domain and possible acoustic interaction with the flame.

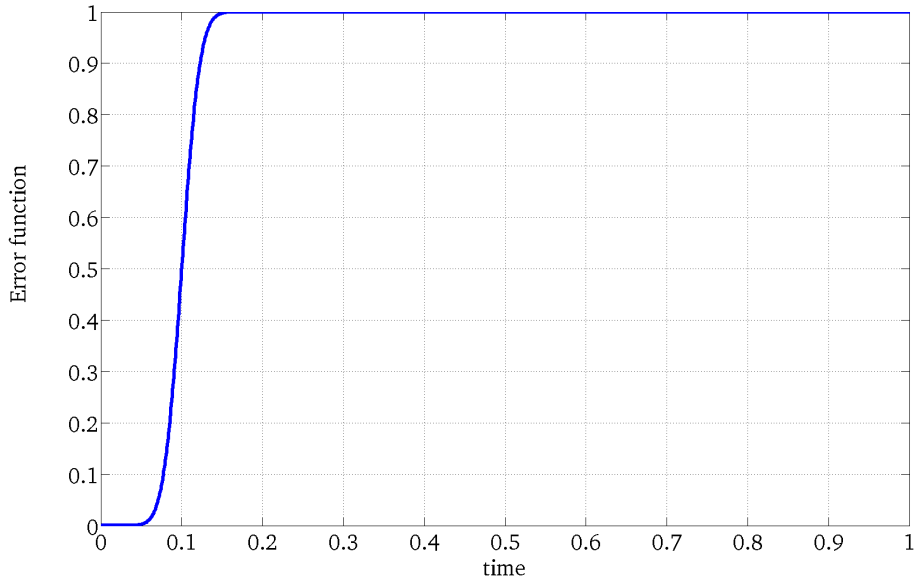

Figure 4.12: Error function given by Equation 4.8.

4.3.7 Stationary solution and discussion

By both applying the special boundary conditions for pressure and introducing an error function approach, a solution with no more bubbles in the flame tip has been finally obtained, as shown in Figures 4.13 and 4.14. An important aspect of heat loss effects is stabilization of the flame above the outlet tube, with respect to the adiabatic case, in which the flame was attached to the inlet. This is caused by the cooling of the wall, and thus conduction plays an important role in this new configuration. Cooling of the wall [Law,2006], [Peters,2000], [Poinsot-Veynante,2005] is crucial in combustion processes, since it ensures that the overall temperature in the combustion chamber is reduced as well as are the pollutants which are produced by the high temperature reactions. In fact, industry is currently very interested in considering heat loss calculations for their configurations. From the FGM point of view, the cooling of the wall is an important effect for the accounting of heat loss phenomena.

4.3.8 Validation of stationary solution

In van Oijen [VanOijen,2002-thesis], a validation between detailed chemistry and FGM was presented. This Section shows a comparison between the FGM simulations performed by van Oijen and the results presented in Figures 4.13 and 4.14. In Figure 4.15, comparisons of iso-contours of O_2 and T are presented. By considering Figure 4.15a, it is evident that the flame height on the left is slightly lower than the one on the right. The exact height of the flame tip is $8mm$ in [VanOijen,2002-thesis] while it is 7.7 mm in the present work. These results are consistent with the T iso-contours in Figure 4.15b, which shows also a similar difference. Despite these differences, the patterns are essentially the same. It should be noted

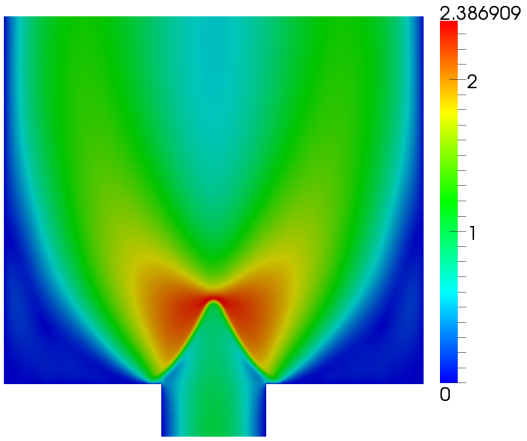

(a) Velocity

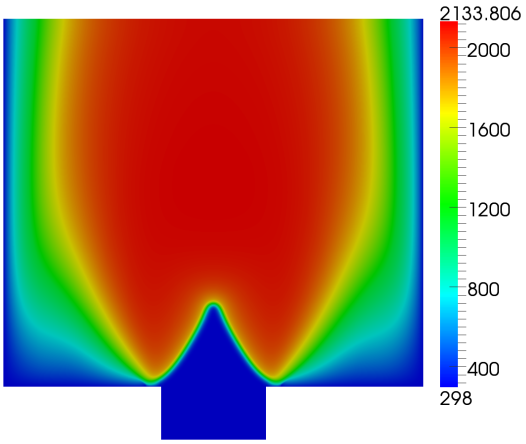

(b) Temperature

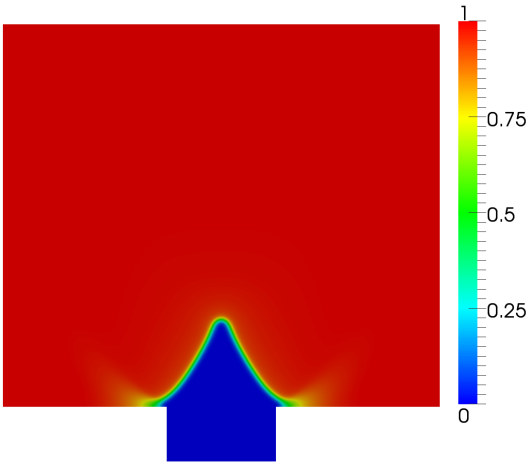

(c) Progress variable

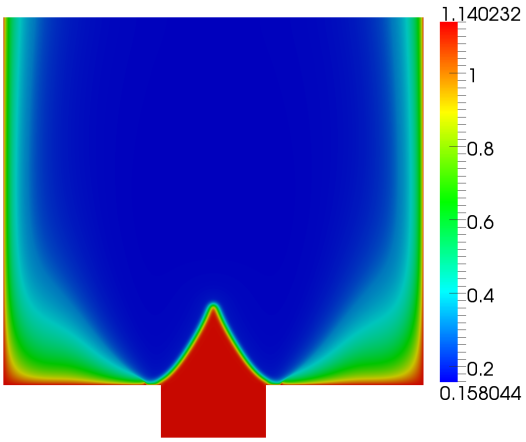

(d) Density

Figure 4.13: Stationary solution with heat loss, with $erf(t)$ function and non-reflecting boundary conditions. Fuel: CH_4, $\phi = 0.9$, controlling variables: $\mathscr{Y}_{O_2}$ and h. Contours of velocity, temperature, progress variable and density.

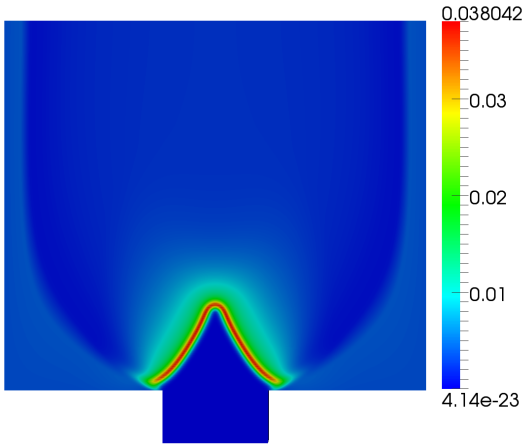

(a) CO mass fraction

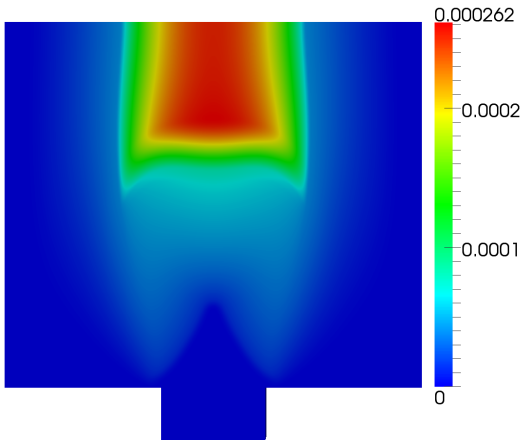

(b) NO mass fraction

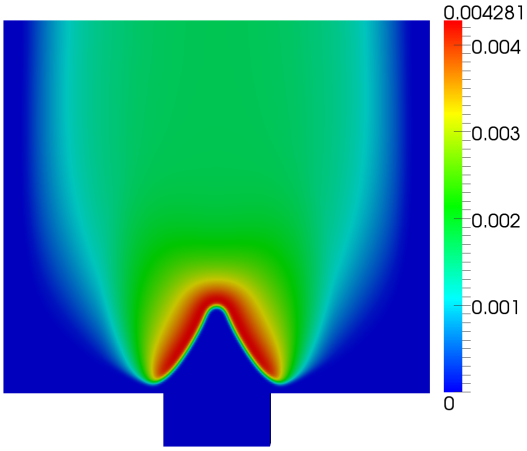

(c) OH mass fraction

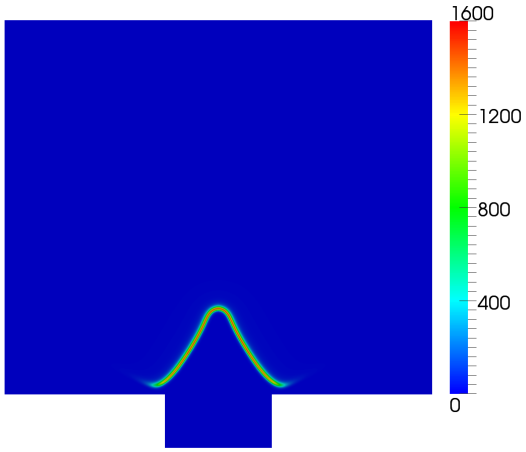

(d) Chemical source term $\dot{\mathscr{Y}}_{O_2}$

Figure 4.14: Stationary solution with heat loss, with $erf(t)$ function and non-reflecting boundary conditions. Fuel: CH_4, $\phi = 0.9$, controlling variables: $\mathscr{Y}_{O_2}$ and h. Minor species and chemical source term.

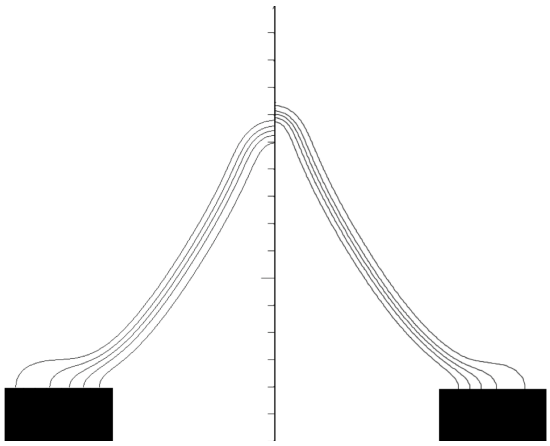

(a) O_2 contours. OpenFOAM ® results (left) and *van Oijen* [VanOijen,2002-thesis] (right)

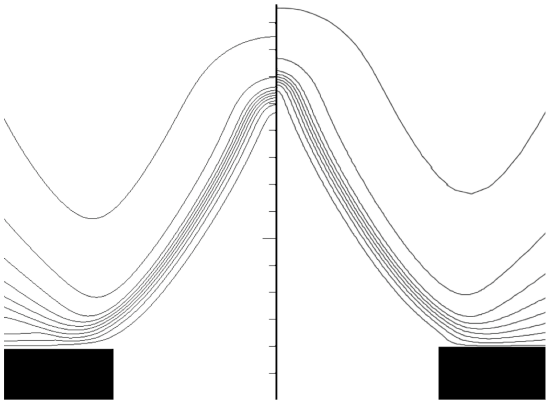

(b) T contours. OpenFOAM ® results (left) and *van Oijen* [VanOijen,2002-thesis] (right)

Figure 4.15: Flame in Box stationary result. Comparison between FGM results in OpenFOAM ® and FGM results from van Oijen [VanOijen,2002-thesis].

that the diffusion mechanisms used in the two different approaches are different. In fact, in [VanOijen,2002-thesis], preferential diffusion are taken into account, while in this work such effects are not considered. Moreover, in the current results the mechanism GRI 3.0 [Smith,1999] is adopted, while in van Oijen the Smooke mechanism [Smooke-Giovangigli,1991] is used.

4.3.9 Effects of initial conditions on flame stabilization

In transient flows, initial conditions may affect the final solution of the problem. In order to investigate this, a few simulations have been performed to show differences in behavior of the flame.

By using the $\mathscr{E}(erf(t))$ function presented in Figure 4.8, the delay at which the velocity field starts developing is typically 0.1 s. After this *delay*, the velocity field starts developing towards the parabolic profile with 1 m/s of maximum velocity.

Effects of changes in initial conditions for the progress variable $\mathscr{Y}_{O_2}$ can be investigated by choosing different positions of the flame front initialization along the y axis. Up to now, the progress variable has been initialized with a flat flame front position very close to the inlet. This initialization can be changed, to analyze how this flame front propagates and how the final solution is affected. An alternative initialization of this flame front is used as:

$$\mathscr{Y}_{O_2\,\text{initial}} = 0.5 \cdot (\tanh(\theta - (y - y_{\text{pos}})/r) + 1). \tag{4.9}$$

where y_{pos} is the position of the flame front, whereas the other parameters regard the thickness of the front and the gradient steepness.

During the simulations, the other fields such as temperature, density are consistent with the flame initialization. This means that they are also subjected to this gradient, given by the progress variable inside the domain. For example, in the unburnt zone the density is higher than in the burnt zone, thus the density has a gradient located at the same position where the progress variable is initialized.

While performing the simulations with two different initialization of the progress variable, two different phenomena have been captured during the transient of the flame. These phenomena are flashback and blowoff.

Flashback is presented first in Figure 4.16. The initialization of the progress variable is set to a planar flame at a distance of 8mm, along the y axis, from the inlet. The velocity boundary condition is imposed by using the error function $erf(t)$. Thus, during the first instants of the simulation this value is 0. Since there is no flow velocity, the flame flashes back. Anchoring of the flame might occur only when the gas speed u_g is balanced by the burning velocity s_u. Due to the absence of the balance in this configuration, the burning speed is higher than the gas speed. The flashback simulation is illustrated in Figure 4.16. The velocity at the inlet is zero as shown in Figure 4.16b. Once the simulation starts, velocity is subjected to the progress variable field initialization. In fact, since the progress variable field affects also temperature and density, the velocity fields shows the pattern evidenced in Figure 4.16d with an increase of velocity at the position of the flame front. Similarly, the flame starts to propagate from the top part of the domain towards the inlet zone, since there is no flow velocity which balances the burning velocity of the flame. Finally, the flame propagates towards the inlet and it flashes back, considering that the flow starts developing too late, once flame is already extinguished.

Opposite to flashback, blowoff may occur when the burning velocity is lower relative to the gas velocity. During this phenomenon, the flame is pushed further in the domain and it is transported out. This can happen, for example, when a flame front propagates from a long distance with respect to the inlet, as shown in Figure 4.17a. Velocity boundary conditions are imposed by using an $erf(t)$ function, thus, the velocity in the inlet is 0 at the starting time. The propagating flame crosses the entire domain, from top to the bottom, since there is no flow velocity coming from the inlet. The flame loses its power, due to the heat loss to the wall and the loss in propagating speed. Once reaching the inlet area, the flow velocity starts developing and impacts against the flame front which is completely blown off to the outlet. In fact, the burning velocity of the flame is not able to balance the flow velocity resulting from the inlet fast enough. Figure 4.17 shows the steps of this phenomenon. In Figure 4.17h, it is evident how the flow velocity which has entered the domain blows the flame completely away.

From the phenomena described, we conclude that a stationary solution with the transient solver cannot be reached under some particular initial conditions. The occurrence of extreme situations such as flashback and blowout, which depend on the flame initialization, requires further investigation from a dynamical point of view, whilst stationary condition of this configuration

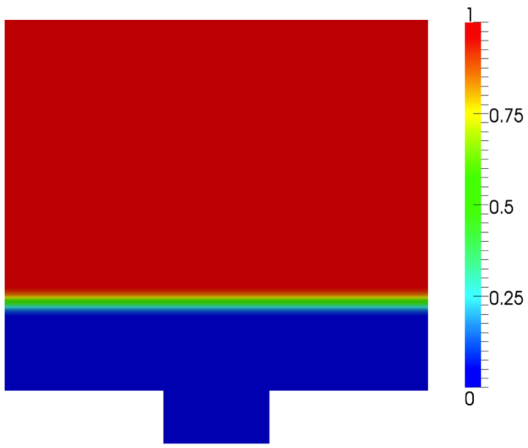

(a) progress variable at instant $t = 0$

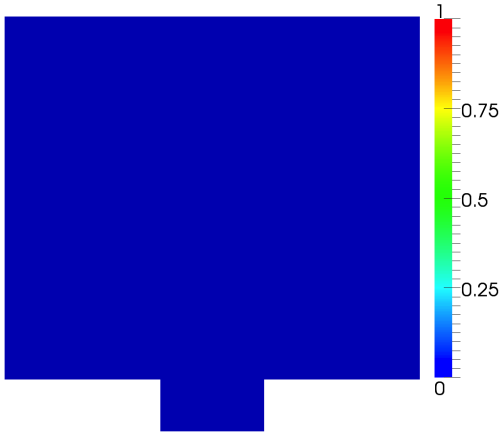

(b) velocity at instant $t = 0$

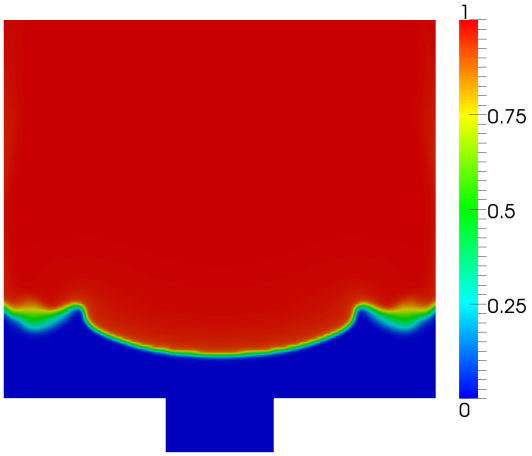

(c) progress variable at instant $t = 0.001$

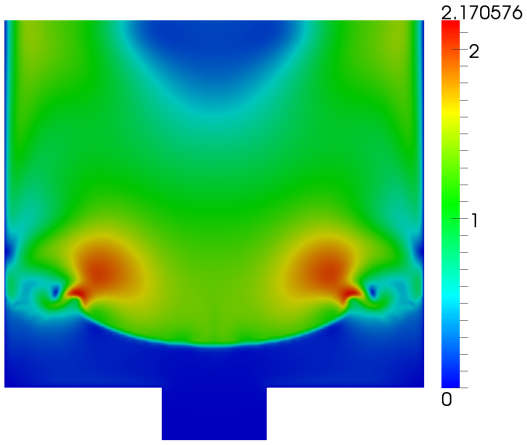

(d) velocity at instant $t = 0.001$

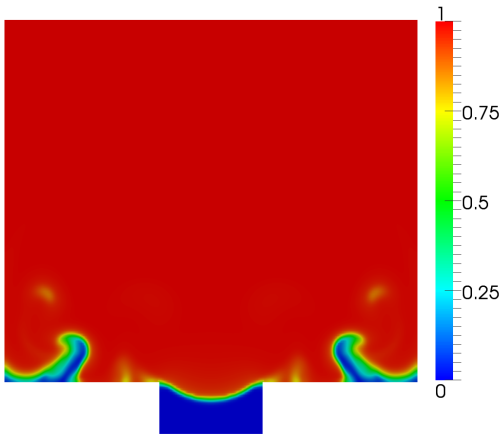

(e) progress variable at instant $t = 0.005$

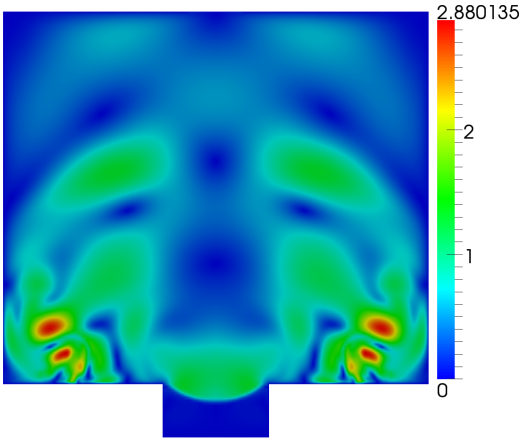

(f) velocity at instant $t = 0.005$

Figure 4.16: Flashback of the flame.

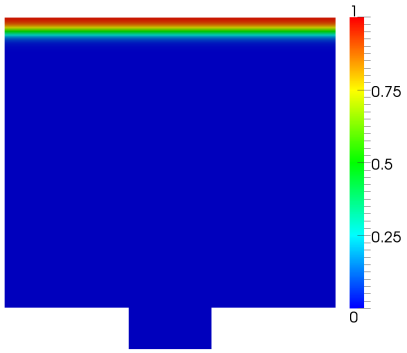

(a) progress variable at instant $t = 0$

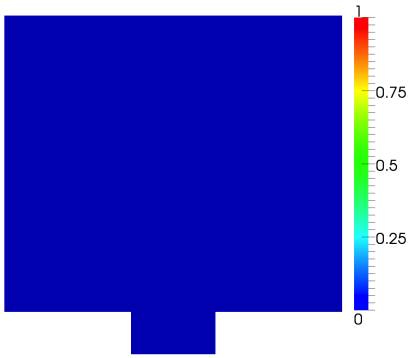

(b) velocity at instant $t = 0$

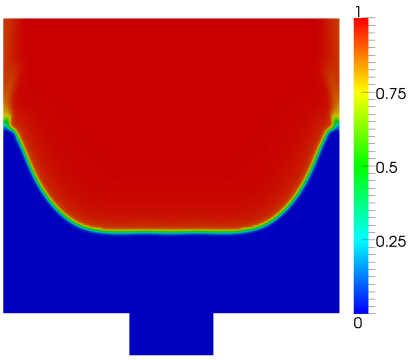

(c) progress variable at instant $t = 0.005$

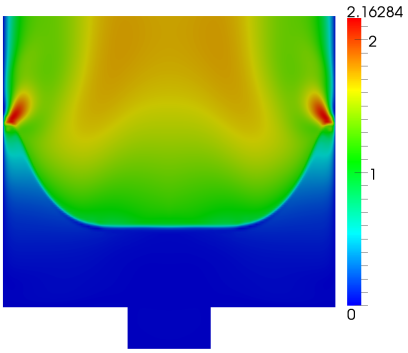

(d) velocity at instant $t = 0.005$

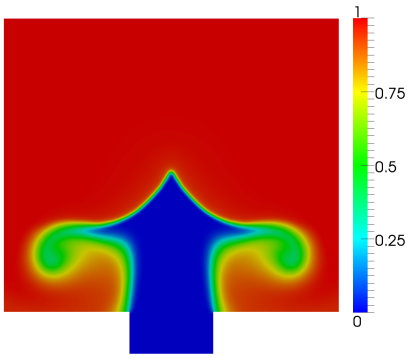

(e) progress variable at instant $t = 0.02$

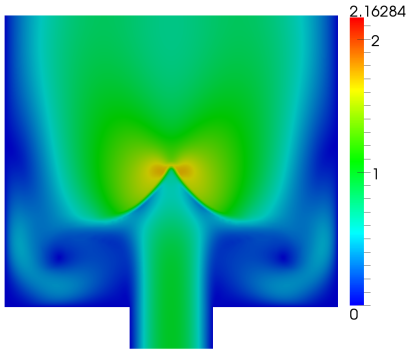

(f) velocity at instant $t = 0.02$

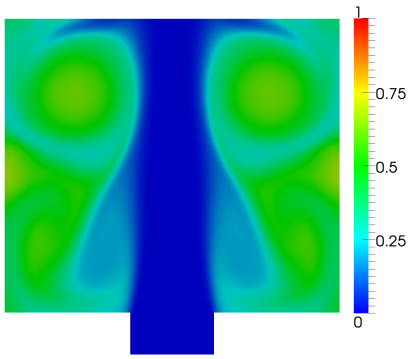

(g) progress variable at instant $t = 0.05$

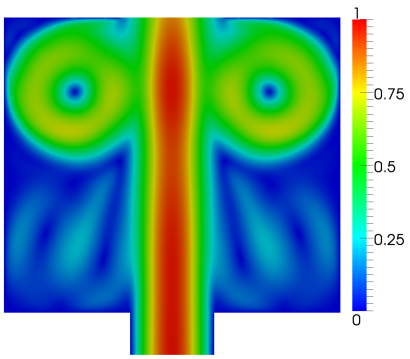

(h) velocity at instant $t = 0.05$

Figure 4.17: Blowoff of the flame.

can be reached under the circumstances that have been described.

4.4 Conclusions on laminar combustion

This Chapter has shown an implementation of laminar premixed combustion using the FGM technique. Heat loss effects have been compared with adiabatic conditions and differences have been discussed. Distinct solvers, incompressible and compressible, using a transient approach, have been presented within particular results concerning a two-dimensional configuration. Literature describes only stationary solutions regarding this configuration. A *dynamic* flame in a box test case has been analyzed. Stability problems can affect the solution due to improper boundary and initial conditions in compressible flows, resulting in oscillating phenomena in the flame tip. These problems have been solved by imposing non-reflecting boundary conditions for pressure. Therefore, a steady solution has been achieved and a validation with an existing stationary solution has been made. Initialization of the flame can affect the final solution and the stabilization of the flame leading to extreme phenomena such as flashback or blowoff. The achieved results are important to describe how to reach a stable and stationary solution.

Chapter 5

Turbulence modeling in combustion problems

"Γόρδιος δεσμός"
"Gordian knot"
A metaphor for an intractable problem solved by a bold stroke - attributed to Alexander the Great

5.1 Introduction to turbulence

Turbulent flows can be observed in everyday surroundings [Pope,2000] and in most of flow-related engineering problems [Law,2006], [Peters,2000], [Poinsot-Veynante,2005]. Buffeting of a strong wind, a rough stream in a river and smoke from a chimney are just few examples of turbulent flows. By observing for instance a waterfall, it is quite evident that the motion is unsteady, irregular and chaotic. On the other hand, the plume formed by a solid rocket motor shows several scales in the overall turbulent motion. An essential feature of turbulent flow is that the fluid velocity varies in both position and time. Moreover, turbulence has the ability to transport and mix fluid parcels much more rapidly as compared to a laminar flow. From the early experimental studies performed by Reynolds [Reynolds,1895] up to date, turbulence has remained one of the most attractive and, at the same time, unresolved problems in physics. The major motivation to study turbulent flows is mainly related to the fact that the majority of flows is turbulent. Evidently, the transport and mixing of mass, momentum and heat in flows are enhanced by turbulence.

Many different categorizations have been provided to describe turbulence aspects. A partic-

ular categorization is to distinguish between small scales and large scales of motion. In high Reynolds number flows, these scales are evidently separated. The turbulent cascade hypothesis proposed by Richardson [Richardson,1922] is connected with the idea that large eddies break up into smaller ones, step by step, until the smallest eddies, due to viscosity, disappear. Another aspect of this hypothesis is the inertial range invariance, which satisfies the Reynolds number independence, leading to the well-known universal power-law spectrum, the so-called $-5/3$ law, proposed by Kolmogorov, in the limit of infinite Reynolds number.

5.2 Interaction between turbulence and combustion

The complexity of turbulence further increases when chemical reactions are also present. From the early studies in turbulent combustion, turbulence models have been transferred to combustion, leading to further complications. It is well known that combustion requires mixing between fuel and oxidizer at the molecular level and the way this occurs depends on the process of mixing. During the eddy break-up in turbulent combustion, also shear and strain rate play an important role: in fact, their presence increases the area of the interface between reactants, thus resulting in an enhancement of mixing. Molecular mixing of fuel and oxidizer takes place in regions of small eddies. The way combustion affects turbulent mixing is still not completely clear. Furthermore, interaction between turbulence and combustion seems to invalidate the classical scaling laws of turbulent flows [Peters,2000] [Bray-Swaminathan,2011] [Poinsot-Veynante,2005]. In fact, chemical reactions introduce additional time scales. From the above, we can conclude that classical approaches used for turbulent flows are not suitable when combustion and turbulence interact. Considering the Damköhler law already introduced in Chapter 1, in fast and slow chemistry processes, time and length scales of combustion are separated from those of turbulence in the inertial sub range.

One first aspect in combustion modeling is the comparison of length and time scales of the characteristic turbulent flows and those of chemical reaction and laminar flames. Furthermore, a second aspect concerns whether the laminar flame structure can exist in the turbulent flow. The Karlovitz number Ka, which was already introduced in Chapter 3, is one of the relevant parameters for this description. Since the smallest scale associated with turbulence is considered the Kolmogorov scale, it is conventional to introduce the Ka number to a Kolmogorov eddy [Law,2006]. A turbulent Ka number can be defined as :

$$Ka_L \approx \frac{\tau_L}{\tau_k}, \tag{5.1}$$

where τ_L is the laminar flame time scale and τ_k the Kolmogorov time scale. The dependence between the velocity ratio $\frac{u'_o}{s_L}$ and the turbulent Karlovitz number Ka_L reads:

$$\frac{u'_o}{s_L} = Ka_L^{2/3} \cdot \left(\frac{l_o}{l_L}\right)^{1/3}, \tag{5.2}$$

with l_o the integral length scale, l_L the flame length scale (which is equivalent to the flame thickness). In defining Ka_L, we have used the flame thickness as length scale. By using the reaction zone thickness l_R, with $l_R < l_L$, and the Kolmogorov length scale, a Ka number related to this new parameter is often used and reads:

$$Ka_R = \frac{\tau_R}{\tau_k}. \tag{5.3}$$

Finally, Reynolds number based on the integral scale Re_o reads:

$$Re_o = \frac{u'_o l_o}{\nu} = \frac{u'_o}{s_L}\frac{l_o}{l_L}. \tag{5.4}$$

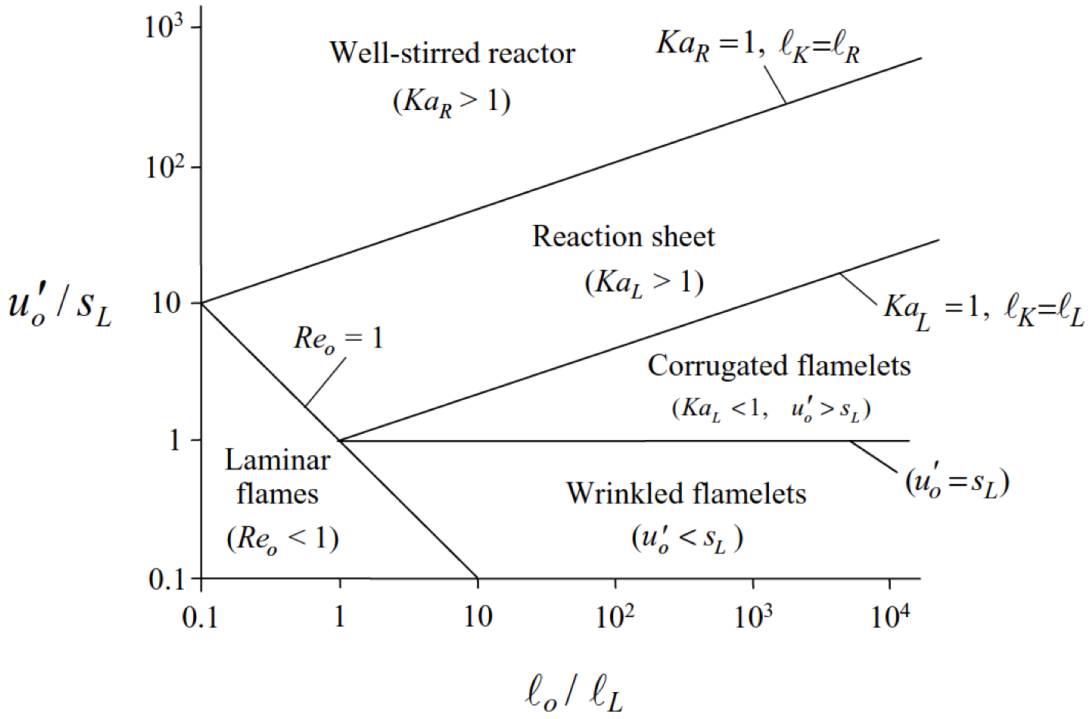

Figure 5.1: Borghi-Peters diagram for different turbulent combustion regimes (from [Law,2006]).

All these quantities presented above are used to describe different regimes of premixed turbulent combustion. A Borghi-Peters diagram [Peters,2000] is introduced in Figure 5.1 to show the different regimes in turbulent flows. The *laminar flame regime* is bounded in the triangle below $Re_o < 1$: here the turbulent intensity is weak and turbulence scales are small. The *wrinkled*

flamelet regime is characterized by $\frac{u'_o}{s_L} < 1$ and hence $Ka_L < 1$: in this regime u'_o can be interpreted as the turnover velocities of the large eddies. The flame surface here is weakly wrinkled. In the *corrugated flamelet regime*, the flame has the structure of a flamelet. Nevertheless, since the fluctuations are higher than s_L, there is a contortion of the flamelet upon crossing eddies, resulting in a distortion whose order is comparable with the size of the eddy. In the *reaction-sheet regime*, the flame behaves still like a flamelet, while the smaller turbulent scales can penetrate into the preheat zone, resulting in an enhancement of heat and mass transfer. Finally, in the *well-stirred reactor regime*, Kolmogorov eddies are smaller than the reaction zone thickness and thus they can penetrate in the reaction zone structure.

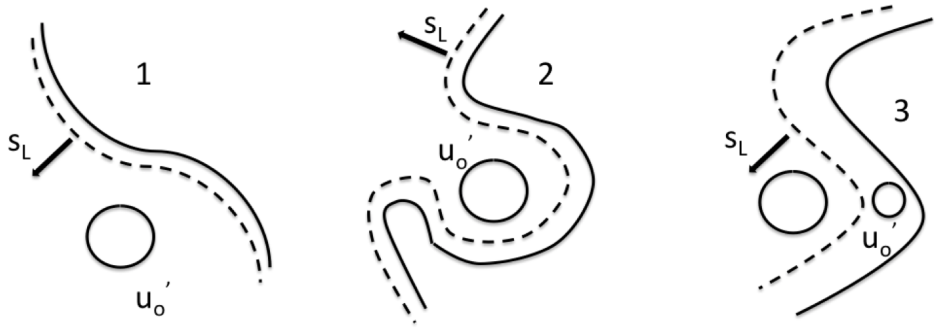

Figure 5.2: Schematic of different regimes case.

These 5 different regimes proposed in the Borghi-Peters diagram of Figure 5.1 can be summarized in 3 main categories of different flame-vortex interaction situations, presented in [Law,2006] [Peters,2000]: situation 1 shows the weak flame-vortex interaction since $u'_o < s_L$. In situation 2, $u'_o > s_L$ and thus a corrugated regime is present. In the end, the last situation, i.e. 3, shows a strong vortex-flame interaction, with smaller eddies penetrating and broadening inside the preheat zone of the flame, while the reaction layer is not perturbed.

5.3 Numerical approach for turbulence modeling

In the past, the primary approach to study turbulence was only experimental. However, detailed measurements are costly and time-consuming [Ferziger-Peric,2002]. As a result, numerical methods have an important role to play in studying turbulent flows. The major difficulty in solving turbulent flows numerically is that there is a much wider range of length and time scales, compared to the case of laminar flows. Therefore, turbulent flows are usually much more difficult and expensive to solve.

The most straightforward way to solve the governing system of equations of turbulent flows numerically is by fully resolving all spatial and temporal scales of the problem, i.e. through Direct

Numerical Simulation (DNS) [Germano,2000]. This approach requires a huge computational effort, and indeed it is not affordable for any practical calculations. The most common way of modeling turbulence is by means of averaging the Navier-Stokes equation in time, leading to Reynolds Averaged Navier Stokes (RANS) approach. Another approach is the filtering in space with Large Eddy Simulation (LES), [Pope,2000] where the unresolved contributions are modeled.

In DNS all the scales are solved. Therefore, the prohibitive costs related to the fine grid requirements, the precision of codes and, thus, the computational effort required, limits this approach to academic problems rather than industrial ones. The RANS model allows the use of coarse numerical grids and reduces numerical cost. On the other hand, since only mean flows are computed, models are required to represent the unclosed terms. The LES approach is an intermediate model between DNS and RANS. Variables are filtered either in spectral space, throughout the cut-off over a certain threshold wave number, or in physical space, with a weighted average over a given volume. The good aspect of LES is that most of the scales are resolved like in DNS and only the smallest ones have to be modeled.

In variable density flows, such as reacting flows [Poinsot-Veynante,2005], [Maas-Pope,1992], the well-known Reynolds averaging operation, which is generally applied to constant density flows, would lead to unclosed correlations between any averaged quantity and its density fluctuation [Poinsot-Veynante,2005]. In order to avoid this problem, a mass-weighted averaged is introduced, known as Favre averaging [Favre,1969], defined by:

$$\widetilde{\xi} = \frac{\overline{\rho\xi}}{\overline{\rho}}, \tag{5.5}$$

where $\overline{\xi}$ is the average of ξ.

Any quantity ξ can be split in a Favre mean and a fluctuating part $\xi = \widetilde{\xi} + \xi''$ (as with Reynolds averaging).

In cold flow turbulence [Pope,2000], by applying Favre averaging to the conservation equations, some quantities remain unclosed and need modeling. In the RANS approach, conservations equations are averaged in time. As a result of this averaging, the Reynolds stresses $-\overline{\rho}(\widetilde{u_i'' u_j''})$ need to be modeled since they are unclosed. This is generally performed by using an eddy viscosity model, as introduced by Boussinesq [Boussinesq,1877]. The eddy viscosity μ_t is not a fluid property, it depends on the state of turbulence and must be determined by the turbulence model. The simplest turbulence model is the one which considers a constant value for the eddy viscosity.

In the LES approach, the conservation equations are not averaged in time but filtered in space [Piomelli,1999] [Sagaut,2000]. The approach of spatially filtering the conservation Equations

[Poinsot-Veynante,2005] [Maas-Pope,1992] is performed by first introducing a basic filtered quantity $\overline{\xi}$, which reads:

$$\overline{\xi}(\mathbf{x}) = \int \xi(\mathbf{x}')G(\mathbf{x}-\mathbf{x}')d\mathbf{x}'. \tag{5.6}$$

where G is the filter convolution kernel, which uses a cut-off width Δ. The most used LES filters are the cut-off (spectral), the box and the Gaussian filters. All of them are normalized in order to have:

$$\int_{-\infty}^{+\infty}\int_{-\infty}^{+\infty}\int_{-\infty}^{+\infty} G(x_1,x_2,x_3)dx_1dx_2dx_3 = 1. \tag{5.7}$$

From the filtering operation, the scales which are smaller than the Δ are not resolved and have to be modeled, i.e. by using the so-called sub-grid modeling.

In cold flows, the sub-grid scale Reynolds stresses $\overline{\rho}(\widetilde{u_iu_j} - \widetilde{u}_i\widetilde{u}_j)$ have to be modeled by using the sub-grid eddy viscosity model. In literature, between the different models, the Smagorinsky [Smagorinsky,1963] and Germano [Germano-Piomelli,1991] models are among the most applied.

5.4 Turbulence modeling in reacting flows

Due to the interaction between turbulence and chemistry, extra terms in the conservation equations appear that need to be modeled. In order to explain the contribution of each term, the RANS and the LES approaches in the conservation equations for reacting flows are presented below. Filtering either in time or in space does not make the fluctuations disappear, thus the only advantage is that the fluctuation terms appear explicitly in the equations and they can be clearly modeled.

5.4.1 Reynolds Averaged Navier Stokes (RANS) approach

Conservation equations with Favre averaging for turbulent reacting flows by using a RANS approach read:

$$\frac{\partial\overline{\rho}}{\partial t} + \frac{\partial}{\partial x_i}(\overline{\rho}\widetilde{u}_i) = 0, \tag{5.8}$$

$$\frac{\partial\overline{\rho}\widetilde{u}_i}{\partial t} + \frac{\partial}{\partial x_i}\left(\overline{\rho}\widetilde{u}_i\widetilde{u}_j\right) = -\frac{\partial\overline{p}}{\partial x_j} + \frac{\partial}{\partial x_i}\left[\overline{\tau}_{ij} - \overline{\rho}(\widetilde{u_i''u_j''})\right], \tag{5.9}$$

$$\frac{\partial \overline{\rho}\widetilde{h}_s}{\partial t} + \frac{\partial}{\partial x_i}(\overline{\rho}\widetilde{u}_i\widetilde{h}_s) = \frac{\overline{Dp}}{Dt} + \frac{\partial}{\partial x_i}\left[\overline{\lambda\frac{\partial T}{\partial x_i}} - \overline{\rho}\left(\widetilde{u_i''h_s''}\right)\right] + \overline{\tau_{ij}\frac{\partial u_i}{\partial x_j}} - \frac{\partial}{\partial x_i}\overline{\left(\rho\sum_{k=1}^{N} U_{k,i}Y_k h_{s,k}\right)}, \tag{5.10}$$

$$\frac{\partial(\overline{\rho}\widetilde{Y}_k)}{\partial t} + \frac{\partial}{\partial x_i}(\overline{\rho}\widetilde{u}_i\widetilde{Y}_k) = \frac{\partial}{\partial x_i}\left[\overline{U_{k,i}Y_k} - \overline{\rho}\left(\widetilde{u_i''Y_k''}\right)\right] + \overline{\dot{\omega}}_k, \quad k = 1,\ldots,N_s. \tag{5.11}$$

From the previous equations, the following unclosed terms have to be modeled:

- The well-known *Reynolds stresses* $\widetilde{u_i''u_j''}$ as already mentioned for cold flows. Most combustion works [Poinsot-Veynante,2005] are based on the classical turbulence models developed for non-reacting flows, such as the $\kappa-\varepsilon$ model, rewritten in terms of Favre averaging.
- $\overline{\rho}\widetilde{u_i''Y_k''}$ can be modeled with a scalar assumption [Poinsot-Veynante,2005]:

$$\overline{\rho}\widetilde{u_i''Y_k''} = \frac{\mu_t}{Sc_t}\frac{\partial\widetilde{Y}_k}{\partial x_i}, \tag{5.12}$$

  where μ_t is the already introduced turbulent viscosity, Sc_t the turbulent Schmidt Number for the k species.
- $\overline{U_{k,i}Y_k} \approx -\overline{\rho}\overline{D_k}\frac{\partial\widetilde{Y}_k}{\partial x_i}$, where D_k is the mean species molecular diffusion coefficient [Poinsot-Veynante,2005].
- The chemical source term for the species $\overline{\dot{\omega}}_k$ which is an important parameter in the combustion modeling.

The conservation equations with the RANS approach can be extended to the transport equation for the scalar $\mathscr{Y}$, for the solution of the FGM problem. By replacing the equation of species Y_i with the scalar progress variable $\mathscr{Y}$, by keeping in mind that the scalar quantity is split in a mean component and a fluctuating one, the $\mathscr{Y}$ transport equation reads [Poinsot-Veynante,2005]:

$$\frac{\partial\overline{\rho}\widetilde{\mathscr{Y}}}{\partial t} + \frac{\partial\overline{\rho}\widetilde{u}_j\widetilde{\mathscr{Y}}}{\partial x_j} = \frac{\partial}{\partial x_j}\left(\widetilde{\rho D_{\mathscr{Y}}\frac{\partial\mathscr{Y}}{\partial x_j}} - \overline{\rho}\widetilde{u_j''\mathscr{Y}_j''}\right) + \overline{\dot{\omega}}_{\mathscr{Y}}. \tag{5.13}$$

On the left hand side of the equations, the terms are closed, while in the right hand side there are two terms, which have to be modeled, namely:

- $\widetilde{\overline{\rho} u_j'' \mathscr{Y}_j''} = -\frac{\mu_t}{Sc_t} \frac{\partial \widetilde{\mathscr{Y}}}{\partial x_i}$,

which has a similar form with respect to Equation 5.12. Finally, the source term is modeled with the so-called *closure model* which is proposed in Section 5.5.

By now we can re-write Equation 5.13 in a more complete form, which shows all the modeled quantities:

$$\frac{\partial \overline{\rho} \widetilde{\mathscr{Y}}}{\partial t} + \frac{\partial \overline{\rho} \widetilde{u}_j \widetilde{\mathscr{Y}}}{\partial x_j} = \frac{\partial}{\partial x_j} \left[\left(\overline{\rho D_{\mathscr{Y}}} + \frac{\mu_t}{Sc_t} \right) \frac{\partial \widetilde{\mathscr{Y}}}{\partial x_j} \right] + \overline{\dot{\omega}}_{\mathscr{Y}}. \tag{5.14}$$

The partial differential Equation 5.14, along with 5.8, 5.9, 5.10, compose the system of equations to solve in the CFD solver, by using the FGM approach and RANS modeling.

5.4.2 Large Eddy Simulation (LES)

In LES, the filtering approach is applied to the conservation equations for reacting flows yielding the following equations:

$$\frac{\partial \overline{\rho}}{\partial t} + \frac{\partial}{\partial x_i} (\overline{\rho} \widetilde{u}_i) = 0, \tag{5.15}$$

$$\frac{\partial \overline{\rho} \widetilde{u}_i}{\partial t} + \frac{\partial}{\partial x_i} \left(\overline{\rho} \widetilde{u}_i \widetilde{u}_j \right) + \frac{\partial \overline{p}}{\partial x_j} = \frac{\partial}{\partial x_i} \left[\overline{\tau}_{ij} - \overline{\rho} (\widetilde{u_i u_j} - \widetilde{u}_i \widetilde{u}_j) \right], \tag{5.16}$$

$$\begin{aligned} \frac{\partial \overline{\rho} \widetilde{h}_s}{\partial t} + \frac{\partial}{\partial x_i} (\overline{\rho} \widetilde{u}_i \widetilde{h}_s) = \frac{\overline{Dp}}{Dt} + \frac{\partial}{\partial x_i} \left[\overline{\lambda \frac{\partial T}{\partial x_i}} - \overline{\rho} \left(\widetilde{u_i h_s} - \widetilde{u}_i \widetilde{h}_s \right) \right] + \overline{\tau_{ij} \frac{\partial u_i}{\partial x_j}} \\ - \frac{\partial}{\partial x_i} \overline{\left(\rho \sum_{k=1}^{N} U_{k,i} Y_k h_{s,k} \right)}, \end{aligned} \tag{5.17}$$

$$\begin{aligned} \frac{\partial (\overline{\rho} \widetilde{Y}_k)}{\partial t} + \frac{\partial}{\partial x_i} (\overline{\rho} \widetilde{u}_i \widetilde{Y}_k) = \frac{\partial}{\partial x_i} \left[\overline{U_{k,i} Y_k} - \overline{\rho} \left(\widetilde{u_i Y_k} - \widetilde{u}_i \widetilde{Y}_k \right) \right] + \overline{\dot{\omega}}_k, \\ k = 1, \ldots, N_s, \end{aligned} \tag{5.18}$$

where $\overline{\frac{Dp}{Dt}}$ can be written as

$$\overline{\frac{Dp}{Dt}} = \frac{\partial \overline{p}}{\partial t} + \overline{u_i \frac{\partial p}{\partial x_i}}. \tag{5.19}$$

Considering the set of previous equations, a few unclosed quantities (a total of four) must be modeled:

- Sub-filter Reynolds stresses ($\widetilde{u_i u_j} - \widetilde{u}_i \widetilde{u}_j$). This term requires the so-called sub-grid scale turbulence model.
- Sub-filter Species fluxes ($\widetilde{u_i Y_k} - \widetilde{u}_i \widetilde{Y}_k$) and enthalpy fluxes ($\widetilde{u_i h_s} - \widetilde{u}_i \widetilde{h}_s$).
- Filtered laminar diffusion fluxes for species ($\overline{U_{k,i} Y_k}$) and enthalpy ($\overline{\lambda \frac{\partial T}{\partial x_i}}$). As in RANS approach, these molecular fluxes may be either neglected or modeled by using simple gradient models [Poinsot-Veynante,2005].
- Filtered chemical reaction rate $\overline{\dot{\omega}}_k$. As in the RANS, the modeling of this term is proposed in Section 5.5.

The first three unresolved terms above can be modeled by applying several approaches, which are available in literature. Since the description of these methods is out of the scope of this thesis, more details can be found in [Pope,2000], [Maas-Pope,1992] and [Germano-Piomelli,1991].

The set of conservation equations with LES modeling are 5.15, 5.16, 5.17. In order to apply the FGM approach, as presented for the RANS case, the equation for the scalar $\mathscr{Y}$ with LES modeling reads:

$$\frac{\partial \overline{\rho} \widetilde{\mathscr{Y}}}{\partial t} + \frac{\partial \overline{\rho} \widetilde{u}_j \widetilde{\mathscr{Y}}}{\partial x_j} = \frac{\partial}{\partial x_j} \left(\left(\frac{\lambda}{c_p} + \frac{\mu_t}{Sc_t} \right) \frac{\partial \widetilde{\mathscr{Y}}}{\partial x_j} \right) + \overline{\dot{\omega}}_\xi. \tag{5.20}$$

5.5 Presumed PDF modeling approaches

The modeling of the chemical source term is also known as *closure* of the combustion modeling. In the literature, a common approach which is used for chemistry modeling is the presumed Probability Density Function (PDF) approach [Williams,1958]. This statistical approach implies that, in order to model the source term, a presumed PDF shape is utilized. In general, a PDF function can take any shape and exhibit different extremes (see Figure 5.5). It contains information on the mean value of the variable, on its variance and on all higher moments. For many combustion applications, however, PDF functions often present common

features, suggesting that these functions can be described using a limited number of parameters [Poinsot-Veynante,2005]. Both in the RANS and LES case, a possible approach is then to assume that the PDF has a fixed shape, parameterized using, for example, only one or two parameters [Williams,1958].

A model based on a presumed form [Bray,Champion,2006] for the sub-grid scale probability density function of a scalar such as the progress variable $\mathscr{Y}$ is presented for the source term and reads:

$$\overline{\dot{\omega}}_{\mathscr{Y}} = \int_0^1 \overline{\dot{\omega}_{\mathscr{Y}}(\mathscr{Y})} P(\mathscr{Y}) d\mathscr{Y}. \tag{5.21}$$

β-PDF functions are generally employed to presume the PDF because they are able to cover shapes ranging from uni or bi-modal distributions to Gaussian shapes. The β-PDF is therefore considered a suitable probability distribution $P(\mathscr{Y})$ in modeling of the source term. The β distribution is presented as follows:

$$P(\mathscr{Y}) = \frac{\Gamma(\alpha+\beta)}{\Gamma(\alpha)\Gamma(\beta)} \mathscr{Y}^{\alpha-1}(1-\mathscr{Y})^{\beta-1}, \tag{5.22}$$

where Γ is the gamma function [Davis,1959] and the two parameters α and β are given by:

$$\alpha = \overline{\mathscr{Y}} \left(\frac{\overline{\mathscr{Y}}(1-\overline{\mathscr{Y}})}{\widetilde{\mathscr{Y}''^2}} - 1 \right), \; \beta = \left(\frac{\alpha}{\overline{\mathscr{Y}}} \right) - \alpha. \tag{5.23}$$

The β-PDF shape has the merit of including singularities near the end points, as shown in its behavior, and at the same time is simple to compute (see Figure 5.5).

In practice, the β-PDF approach is used to construct a table where the filtered chemical quantities depend on the filtered value $\overline{\mathscr{Y}}$ and its sub-grid variance $\widetilde{\mathscr{Y}''^2}$. While constructing the table, the β-PDF integrals have to be calculated carefully and need to be checked for their convergence. The integration of each flamelet through the β-PDF approach is called also convolution. This new database calculated with the convoluted quantities is called *Turbulent Manifold*.

There are several methods used in literature [Kaul,2011], [Knudsen,2012] to provide a suitable model for $\widetilde{\mathscr{Y}''^2}$. A transport equation for the variance can be used [Knudsen,2012], but also a simpler gradient model is often adopted in the LES case[Kaul,2009]:

$$\widetilde{\mathscr{Y}''^2} \approx \frac{a^2 \Delta_k^2}{12} \left(\frac{\partial \overline{\mathscr{Y}}}{\partial x_k} \right)^2, \tag{5.24}$$

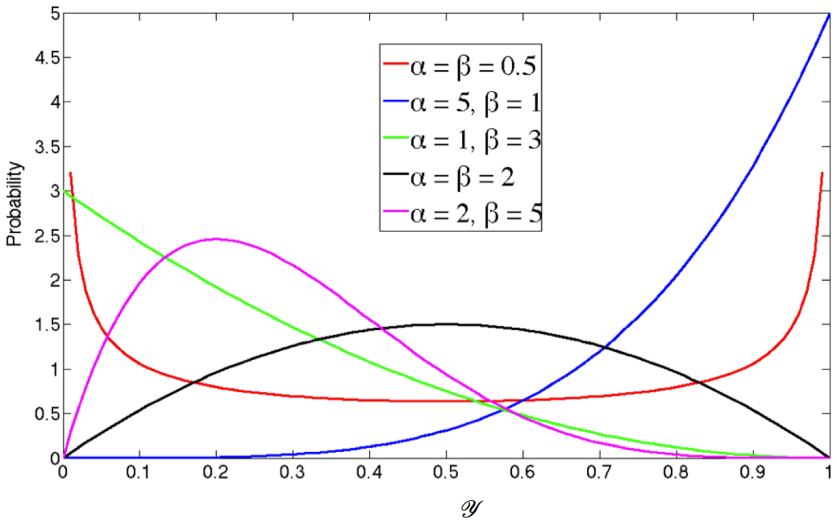

Figure 5.3: Different shapes of β-PDF distribution.

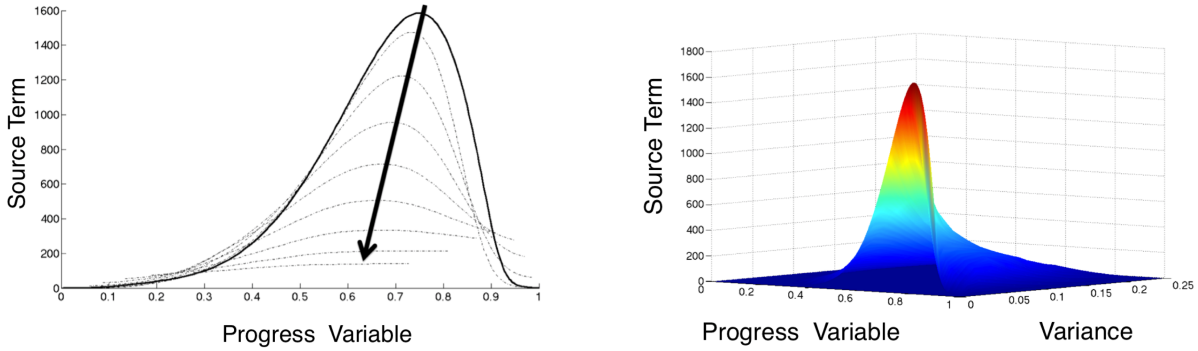

(a) 2D view

(b) 3D view

Figure 5.4: Filtered source term with β-PDF approach.

where Δ_k is related to the grid length, a can be assumed as constant. For smooth fields on the scale of Δ_k, we can deduce $a = 1$ from a simple Taylor expansion [Vreman,2009].

In Figure 5.4, an example of β-PDF convolution is shown: the chemical source term is illustrated for different values of variance. The arrows in Figure 5.4a indicates the increase of variance values. According to β-PDF approach, the variance levels are bounded between 0 and 0.25. Figure 5.4a shows the correspondent 3D version of the plot.

Chapter 6

2D FGM: progress variable and variance. Adiabatic DLR Jet Flame

" Ὅπερ ἔδει δεῖξαι"
"What was required to be proved"
Early validation statement in scientific problems - Euclid

The following work has been carried out in cooperation with Siemens AG. The geometry of the burner has been provided by Deutsches Zentrum für Luft-und Raumfahrt (German Aerospace Center) [DLR].

The contents of this Chapter has been published in the ASME Turbo Expo 2014 proceedings (Dusseldorf 2014) [Fancello,2014] with the title *Turbulent combustion Modeling using Flamelet-Generated Manifolds for Gas Turbine applications in OpenFOAM*.

6.1 Introduction

The recent developments in reducing pollutions and creating both an efficient and clean combustion system imply particular attention to the design requirements, especially related to industrial gas turbine applications. In recent years, although the progress in modeling has increased dramatically, combustion still needs a large computational effort. The Flamelet-Generated Manifolds (FGM) method is considered a good solution with an accuracy which can be comparable with detailed chemistry simulations results. The aim of this work is to figure out the

performance of FGM by using OpenFOAM ® as combustion solver. As a test case, a confined lean jet flame has been employed. For this configuration, an extensive experimental data set, including PIV and Raman data [DLR], is available.

6.2 Experimental setup - the DLR jet flame

The understanding of lean jet stabilized flames plays an important role in the design process of novel gas turbine combustors based on the flox ® concept [Lammel,2010], [Roediger,2012], [Lammel,2011]. In a preliminary experiment, a single burner nozzle was arranged in a rectangular confinement with optical access. Figure 6.1 shows a schematic drawing of the geometry configuration. The cylindrical single nozzle with an inner diameter d, where $d = 10\ mm$, was protruded $2\,d$ above the burner base plate. This tube was confined by a rectangular combustion chamber with edge lengths of $a \times b = 5\ d \times 4\ d$ and an overall height of $h = 60\ d$. The nozzle was positioned at 3.5 d distance from the combustion chamber wall referring to the longer side a, and centered at 2 d distance in perpendicular direction. The walls of the combustion chamber were made of quartz plates with reasonable thickness to minimize heat exchange with the surrounding. The experimental test rig is shown in Figure 6.3. The off-center positioning of the nozzle, between the surrounding quartz glass walls, allowed the formation of a distinct recirculation zone on one side, which drew a link between this configuration and the pronounced inner recirculation zone of an enhanced flox ® burner as presented in 6.2.

The straight tube before the nozzle exit had a length of $l_{\text{tube}} > 40\ d$. Dry air was fed into an electrical preheater consisting of a heating cartridge with a temperature stability of $\Delta T_{\text{ph}} < 2$ K. The fuel, such as methane or hydrogen, was added to the preheated air inside a static mixer through radial injection in the mass flow.

Confined jet methane-air flames were operated in a restricted stoichiometry region at atmospheric pressure. Different preheat temperatures of $T_{\text{ph}} = 473 - 673\ K$ and different jet velocities $U_{jet} = 90 - 150\ m/s$ have been applied in the experimental tests. Thermo-acoustic pulsations were not observed at any of the operating conditions studied.

Both burner and combustion chamber have been mounted on a base plate and have been shifted relatively to the stationary laser measurement setups. Laser Raman scattering has been applied to the flames and evaluated on a single shot basis, in order to simultaneously determine the major species concentrations and the temperature. Planar velocity fields have been measured by using the particle image velocimetry (PIV) technique.

Laser Raman scattering has been used for point wise measurements of the concentrations of oxygen, nitrogen, methane, hydrogen, carbon monoxide, carbon dioxide and water together with temperature. The beam of a flash lamp pumped a dye laser with high pulse energy that was focused in the combustion chamber. The Raman scattering has emitted from a volume of

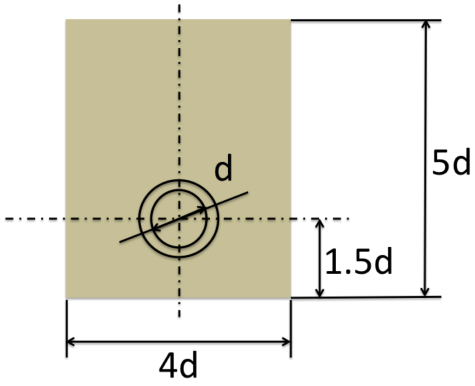

(a) side view

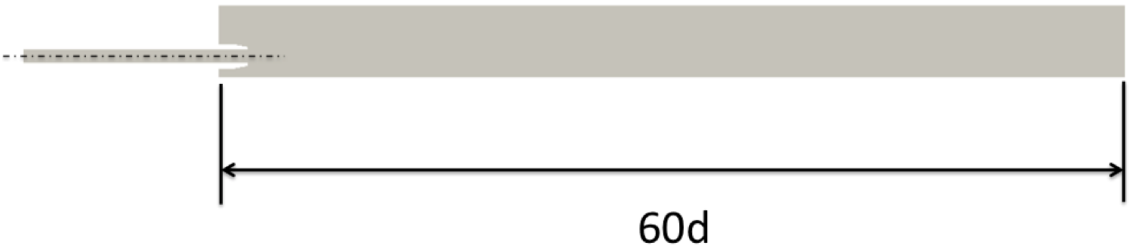

(b) longitudinal view

Figure 6.1: Schematic drawing of the DLR jet flame geometry.

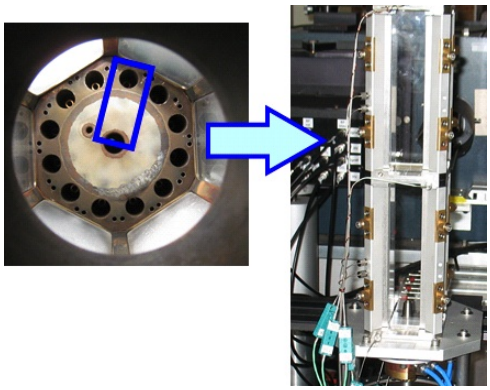

Figure 6.2: Configuration setup (Courtesy of DLR).

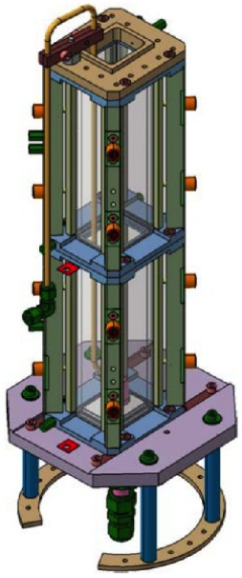

Figure 6.3: Confined single jet, experimental test rig (Courtesy of DLR).

0.17 mm^3 and has been collected by a lens and relayed to the entrance slit of a spectrograph. The dispersed and spatially separated signals from the different species have been detected by photomultipliers and have been sampled by boxcar integrators. The species number densities have been calculated from the signal intensities using calibration measurements. Finally, the temperature has been deduced from the total number density via the ideal gas law. At each measuring location, 200 single-pulse measurements have been performed within a scanning pattern of roughly 160 points.

The velocity field measurements have been performed by using a commercial PIV system provided by LaVision Flowmaster. Titanium dioxide particles have been added to the air flow upstream the combustor. A dual-pulse Nd:YAG laser has been used for illuminating the particles; the laser beam was formed into a light sheet and then crossed the combustion chamber. Thus, pairs of images of particle distributions with a short separation time of $\tau_{sep} < 11$ µs have been recorded with a CCD camera at a repetition rate of 5 Hz. From the image pairs, velocity fields have been calculated using a cross-correlation algorithm. The achieved spatial resolution was 2.2 $mm \times 2.2$ mm. The uncertainty of the velocity values is estimated to be 2.3 m/s. The recording time has been limited to ≈ 1000 image pairs due to contamination of windows with particles.

6.3 Numerical approach: adiabatic FGM-LES calculation

The modeling of turbulent chemistry is performed by using a Probability Density Function (PDF) approach, as described in Chapter 5. For relatively simple fuels such as methane, for which the *Le* number effects roughly cancel out, a β-PDF shape may be considered a reasonable

choice for the modeling of the sub-grid chemistry terms [Kaul,2011] [Poinsot-Veynante,2005] [Vreman,2009] [Donini,2013] [Fancello,2013] [CardosoDeSouza,2010]. The manifold is created in controlling variable space as already introduced for the laminar approach by using the following steps: (i) detailed chemistry simulations through the code CHEM1D [Somers,1994] (These calculations have been performed without considering heat loss effects); and (ii) convolution of the resulting manifold through a β-PDF approach (as explained in Chapter 5).

The adopted gas is a mixture of air-methane, with equivalence ratio $\phi = 0.7$, as described in the experimental data performed by DLR. GRI 3.0 mechanism [Smith,1999] and complex transport algorithm [Ern-Giovangigli,1994] have been considered for the detailed chemistry calculations.

Figure 6.4 illustrates the convoluted source term as function of progress variable and its variance through a β-PDF approach. The progress variable is limited between 0 and 1, while the variance ranges between 0 and 0.25.

The numerical tool OpenFOAM ® has different solvers for the solution of combustion problems [OpenFOAM-URL] [Wikki-URL]. Nevertheless, the compressible solver, *rhoPimpleFoam*, has been used for this purpose. In fact, this solver is usually considered for cold flow simulation. The choice of this solver has been done in order to consider compressibility effects, i.e. acoustics, in the future. In addition to the typical Navier-Stokes equations, extra equations for the controlling variable were added to the system. In this case, the solver is used with specific boundary conditions for pressure, known as non-reflecting boundary conditions [Alpert,2002], to avoid acoustic waves. This modified CFD solver uses both PISO [Issa,1986] and SIMPLE [Patankar,1972] [Kumar,2011] algorithms. An *ad hoc* library uploads and retrieves the manifold during the runtime. Thereby, an interpolation between the lookup values is applied. A *thermophysical* library [OpenFOAM-URL] calculates the density from the temperature, by applying the perfect laws gas. The equations to be solved are the continuity, momentum and energy equations. In addition to these ones, the progress variable equation is added to the system. This CFD solver is like the one presented in Chapter 4.

Some settings about the numerical discretization and schemes are presented as follows:

- the transient scheme is used, which has been discretized with an implicit Euler approach;
- the gradient and the divergence scheme, which are discretized with a linear Gauss method;
- the linear system solver, which is discretized with a pre-conditioned conjugate gradient solver for symmetric matrices (PCG) [Joubert,1994] with a diagonal incomplete-Cholesky (DIC) has been used for the solution of the density and pressure term; and
- the velocity and enthalpy terms, which are discretized with a pre-conditioned bi-conjugate gradient solver for asymmetric matrices (PBiCG) with a Diagonal Incomplete LU (DILU) pre-conditioner[Barrett,1994].

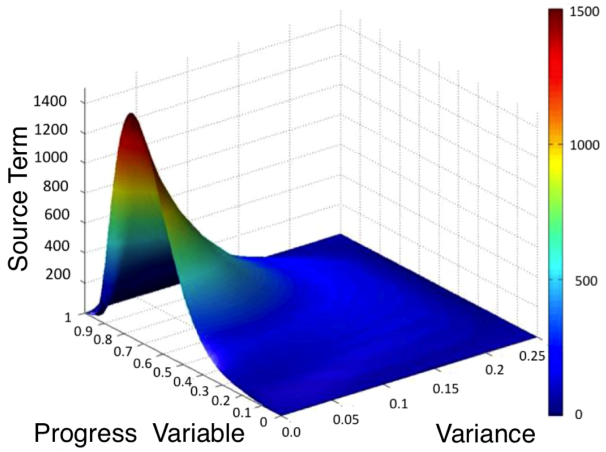

Figure 6.4: Source term as function of progress variable and variance, from turbulent manifold using β-PDF convolution. Pure Methane gas, $\phi = 0.7$.

The turbulence modeling has been performed throughout using the LES approach. The transport equation for the progress variable by using a LES approach was already presented in Equation 5.20. Following the Smagorinsky approach, the eddy viscosity is one component of the effective viscosity, μ_{eff}, which is defined as $\mu_{\text{eff}} = \mu + \mu_t$, where $\mu_t = C_s^2 \rho \Delta^2 |\bar{S}$, where C_s is a constant, Δ the characteristic length of the Smagorinsky eddies, and $\bar{S}$ the strain rate of the resolved field. In accordance with [Ferziger-Peric,2002], the eddy viscosity is usually damped near the wall with the van Driest damping model [vanDriest,1956]. A time step of $5 \cdot 10^{-7}$ s has been adopted resulting in a maximum Courant number of about 0.5 ensuring stable work of the PISO scheme.

Some details of the geometry mesh adopted for the simulation are shown in Figure 6.5. The mesh has been generated with ICEM-CFD [ICEM-CFD] as a structured multi-block mesh and converted into the OpenFOAM ® format. It consists of about 3.1 million hex cells. The mesh has been refined at the mixture inlet pipe walls, at the jet shear layers and at the combustion chamber walls. The average resolution in the jet lip area is about 40 cells across the jet diameter, as illustrated in Figure 6.5. The boundary condition specification was practically limited to the inlet conditions, by setting a uniform velocity of 150 m/s, in accordance to the experimental data.

The operating conditions are listed in Table 6.1.

6.4 Results and comments

The single jet flame has been chosen as a test case for the FGM method, since it contains the relevant combustion effects while having a relatively simple geometry and an extensive set of measurement data.

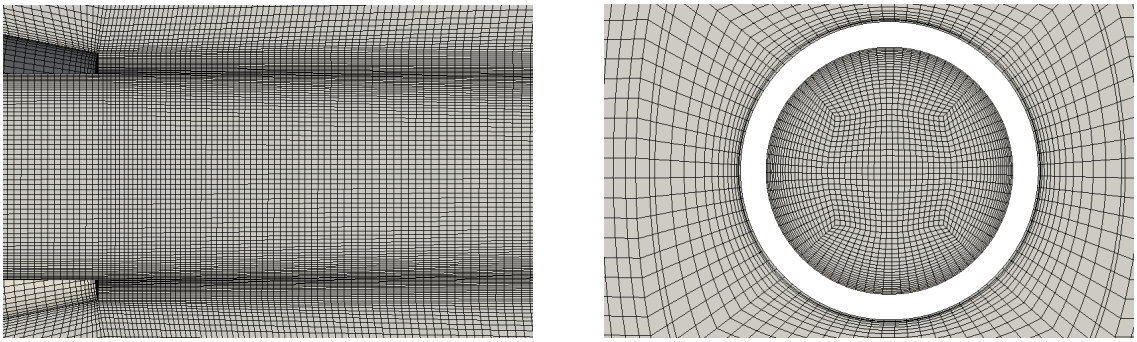

Figure 6.5: Computational mesh in the jet exit (left) and in the lip plane (right).

Table 6.1: Operating conditions in CFD calculations.

p	T_{ph}	U_{jet}	ϕ	Q_{air}	Q_{fuel}
$[bar]$	$[K]$	$[m/s]$		$[g/s]$	$[g/s]$
1	573	150	0.7	6.8	0.28

A total physical time of about 60 *ms* has been simulated. The time to achieve statistical convergence of the fields was relatively long due to the slow development of the recirculation system (resulting 30 *ms*). Figures 6.6 and 6.7 summarize these results with respect to velocity and temperature fields. Both averaged values and an instantaneous arbitrarily chosen snapshot are presented. In Figure 6.8 some corresponding experimental data are shown for comparison.

The velocity data clearly shows a pronounced recirculation zone above the jet. Its location is predicted quite correctly, but slightly shifted downstream. The wrinkled streamlines in Figure 6.6a indicate that the main recirculation vortex has not completely stabilized in the averaged time period. Several smaller vortices clearly emerge and might disappear after longer averaging. The velocity profiles at the jet axis and at the side axis, at location $x = 10D$, are shown in Figure 6.9 and Figure 6.10 respectively. Therefore we can assume the CFD results over-predict the potential core lengths noteworthy with respect to the PIV data. The off-axis values are in accordance to the PIV data.

The temperature distribution in the combustion chamber is shown in Figure 6.7. As expected,

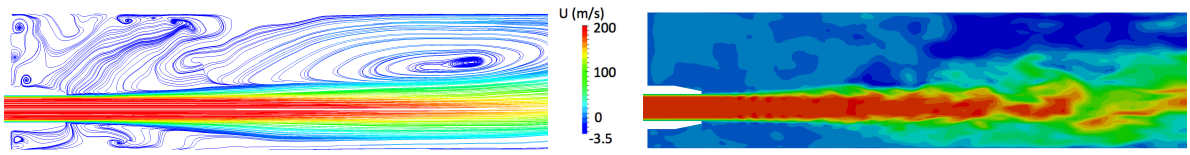

(a) mean U (b) instantaneous U

Figure 6.6: Simulation results - U field in a 2D plane considered in the streamwise direction.

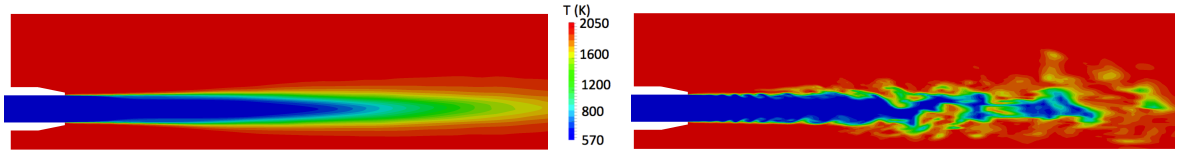

(a) mean T (b) instantaneous T

Figure 6.7: Simulation results - T field in a 2D plane considered in the streamwise direction.

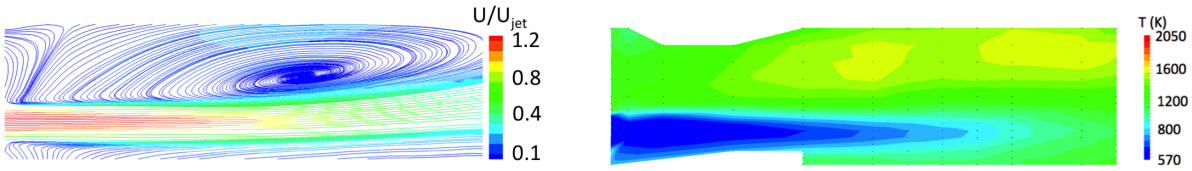

(a) PIV (b) Raman

Figure 6.8: PIV and Raman experimental data - Property of DLR.

since we are considering an adiabatic case, the results shows a clear over-prediction of the burnt gas temperature due to the lack of any heat loss effects included. In particular, the maximum reached temperature is about 2050 K.

The axial distribution of the temperature illustrated in Figure 6.9b reveals a much smoother growth of the axial temperature in the Raman data. As in the case for velocity, an over-prediction of the potential core length is also observed.

6.5 Conclusions

In this work, the FGM method applied to a turbulent test case has been presented. In general, the numerical setup described above was able to reproduce the physical behavior of the jet flame, but still cannot be considered of acceptable quality. The recirculation zone, which develops in the CFD solution, resembles the experimental results, despite the shifted location downstream. The most noticeable discrepancy between the numerical and experimental results lays in a too slow development of the jet shear layer, leading to a delayed mixing and an over-prediction of the potential core length. As a consequence, the CFD results show too steep gradients for both temperature and velocity in the profiles normal to the jet axis. A justification might lay in the employed adiabatic approach with respect to the heat loss effects, which are not considered. The average velocity fields are acceptable. Therefore, we may assume that the jet length over-prediction would be attributed to the turbulence modeling. A possible mitigation of these problems could be achieved by either a revision of the turbulence modeling approach or an extension of the domain upstream to the flame, in order to obtain an increased turbulence generation.

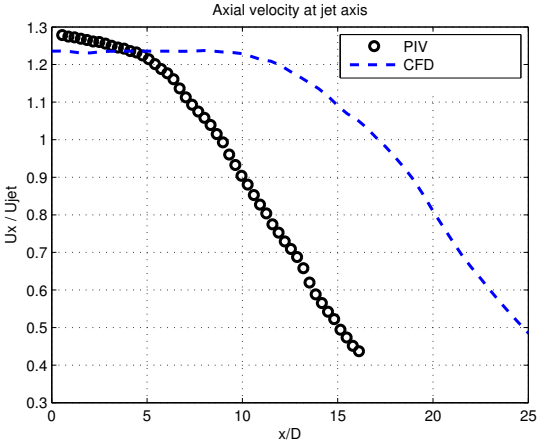

(a) axial U profile

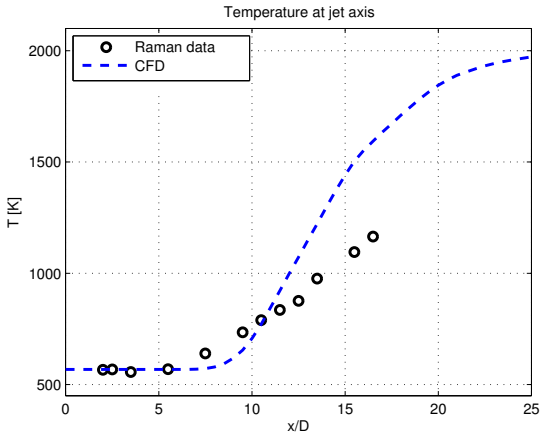

(b) axial T profile

Figure 6.9: Axial profiles.

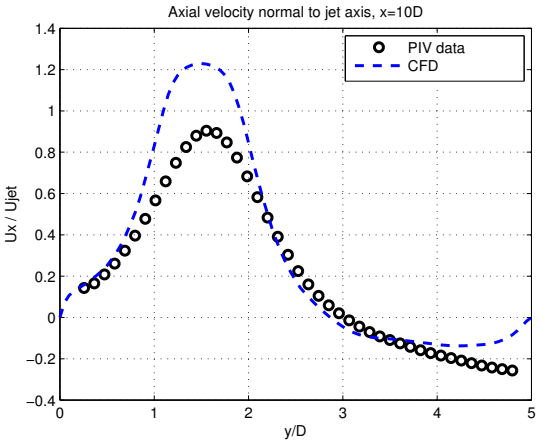

(a) cross U profile

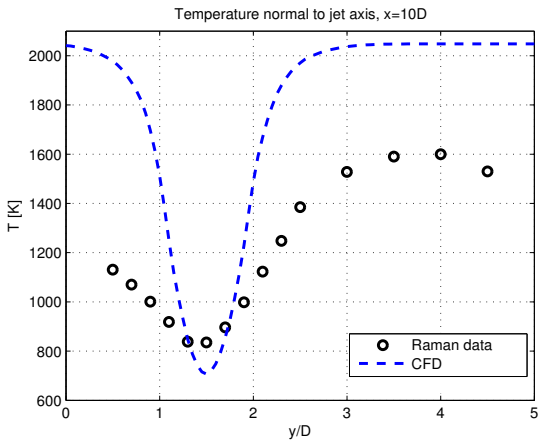

(b) cross T profile

Figure 6.10: Transversal profiles at $x = 10D$.

Finally, the next step will consist of an inclusion of heat loss effects in the turbulent manifold, which allows adding more peculiarities in the combustion modeling for industrial applications.

Chapter 7

3D FGM: inclusion of heat loss in turbulent combustion. Sudden-expansion flow

"Πάθει μάθος"
"Learning is suffering"

"Agamennon" - Aeschylus

The following work has been carried out together with the company CFD Engineering. A publication with title *Implementation of the Flamelet Generated Manifold technique in OpenFOAM for industrial burner combustion phenomena*, which describes the following part, is currently in preparation.

7.1 Motivation and outlook

The need of reducing fuel consumption and pollutant emissions in turbo-machinery applications is increasing quickly. As a consequence, new burner configurations and new working conditions are continuously developed and investigated. On the one hand, classical approaches are based on experimental activities, which are affected by high costs and by high demands related to the long times needed to do experiments. On the other hand, despite the application of numerical approaches to reactive simulations has increased significantly in the last decades, they are still time and resources demanding, especially when coupled with detailed chemistry modeling. Improvements have been achieved by formulating chemical reduction mechanisms, which are based on the simplification of the chemistry modeling, yielding a reduction in time

and resources. Among the most promising techniques, the Flamelet Generated Manifold (FGM) approach [vanOijen,2000] is receiving important attention due to the high accuracy and the lower computation effort, compared with detailed chemistry simulations. FGM found inspiration from the *flamelet* approach [Peters,2000], which treats a real multi-dimensional flame by considering it as a set of many 1D flames. Moreover, this method takes into account also convective and diffusive aspects, which is not the case for classical approaches techniques like ILDM [Maas-Pope,1992]. A manifold with reactive key properties is generated by solving detailed one-dimensional flames. In the CFD calculation, the manifold is read and the key properties are retrieved during the calculation runtime. In addition to the conservation equations for the flow, a limited amount of extra controlling variable equations for the chemistry is solved. In this work, the FGM technique is compared with respect to experimental and numerical results available in literature [Banhawy,1983] [Martin,2003], concerning a backward-facing step burner configuration in which a premixed methane-air configuration is used. This geometrical configuration has shown significant interest in the industrial field due to peculiarities of the resulting flow. In fact, real modern turbo-machinery burners rely on the stabilization effect induced by a recirculation region on the generated flame: the reactive field interacts with the turbulent flow in such a way that the flame speed equals the local flow velocity close to the recirculating bubble, where velocity values are typically low. A similar phenomenon is visible also in the backward-facing step configuration, where a recirculation region is generated after the inlet of the flow, inducing the anchoring of the flame structure. The available information on the local properties of the flow in such premixed turbulent flames is small. El Banhawy et al. [Banhawy,1983] have highlighted these problems through an experimental setup, including also the effects of heat loss, by cooling of the walls. In [Banhawy,1983], exhaustive data concerning both mean and variance fields of several quantities are provided. Thus this can be considered a significant benchmark for numerical reactive models. Prior work has already presented numerical comparisons with experimental data, for instance Guo et al. [Guo,2003] presented numerical results based on a EBU-Arrhenius model [Bray-Libby,1993] and a presumed joint PDF model, by providing a contours comparison in terms of mean temperature. Martin et al. [Martin,2003] proposed a numerical comparison using the CMC model, by showing mean and rms fields, and by providing iso-contours of different physical and reactive quantities. From the above mentioned works, it appears that heat loss effects are not taken into account in the modeling . Furthermore, only a 2D geometry has been used for these simulations. The present study proposes an application of the FGM technique, in order to validate the numerical modeling approach and, at the same time, to improve the numerical results currently available. The interaction of turbulence with reactive phenomena is investigated, providing both RANS and LES simulations. In particular, this work is the first case presenting LES regarding this configuration. In addition, heat loss effects are considered, resulting in significant improvements in the physical behavior. The results are compared with experimental and numerical data already available.

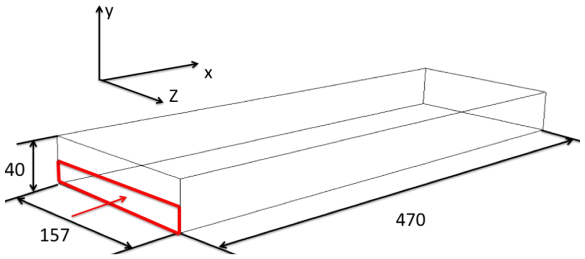

Figure 7.1: 3D Geometry of the test case, from [Banhawy,1983]. Dimensions are in *mm*.

7.2 Geometry configuration and experimental data

A sudden expansion flow geometry is presented here from the experimental work performed by El Banhawy et al. [Banhawy,1983]. The experimental data were measured in a combustion chamber. Before entering the chamber, the flow was forced to pass through different devices, resulting in a typical backward-facing step domain. This test case is taken into account since it has many peculiar characteristics typical of lean premixed gas turbine combustors, within an easy-to model geometry. Noteworthy aspect of this case is the presence of a recirculation region after the inlet. The inlet section is 20×157 *mm*, corresponding to the bottom half of the entire left boundary (see Figure 7.1); the outlet is placed on the right side and it includes the whole channel height. The chamber is 470 *mm* long in the streamwise direction. The entering flow is represented by a CH_4/air mixture with an equivalence ratio equal to 0.9 and a mass flow rate of 0.035 kg/s. The entering unburnt gas is considered to have a temperature equal to 300 K. The walls are cooled with a temperature of 360 K.

Experimental data of Banhawy et al. are presented in Figure 7.2 (reprinted under the permission of Elsevier). These data are presented by means of iso-countours in the cross section of the channel as shown in [Banhawy,1983]. Mean values of temperature, axial velocity and root mean square of velocity field are presented together with the mole fractions of O_2, CO and CO_2. One important aspect which can be observed regards mainly Figures 7.2c and 7.2d, where the variations of temperature and oxygen molar fractions, along the flame brush show quite a different behavior. From a flamelet point of view, a similar behavior was expected. From this first view, it has to be stated that the reproduction of these fields is probably not straightforward with the FGM method.

Since the experimental results show an almost 2D flow field, in accordance with [Martin,2003], a 2D computational domain is preliminarily studied. Afterwards, 3D simulations are performed as a second stage. The geometry configuration for the numerical modeling is shown in 3D and 2D configuration in Figures 7.1 and 7.3 respectively. In both figures, the red lines mark the inlet placed in the lower half height of the domain. Dimensions are given in *mm*. As a preliminary study for our numerical calculation, no channel inlet part before the combustion chamber has been modeled. Afterwards, this channel will be also included in order to model a more realistic flow condition. Figure 7.4 illustrates this geometry configuration adopted in the present work

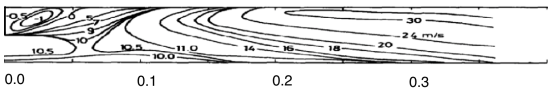

(a) Mean axial velocity

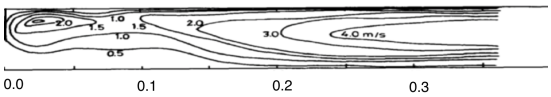

(b) RMS of velocity

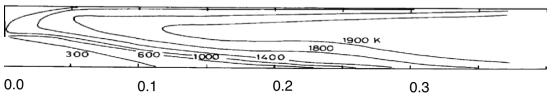

(c) Mean temperature

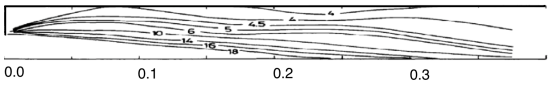

(d) O_2 molar fraction

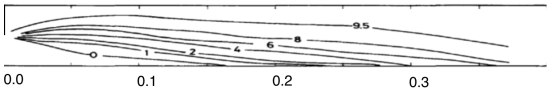

(e) CO_2 molar fraction

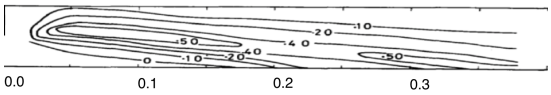

(f) CO molar fraction

Figure 7.2: Experimental data of Banhawy et al. [Banhawy,1983]. Numbers below indicate distance from inlet, dimensions are in *m*.

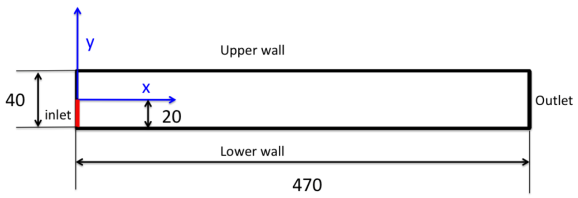

Figure 7.3: 2D Geometry of the test case, from [Banhawy,1983]. Dimensions are in *mm*.

with a channel length of 20 *mm*. Furthermore, a longer channel with respect to the one adopted in Figure 7.4 is also utilized, by considering a double channel length (40 *mm*).

7.3 Chemistry modeling and creation of turbulent manifold with heat loss

FGM is applied to this test case. In order to model the chemistry and create the turbulent manifold, a β-PDF approach is adopted, since it is considered a reasonable choice for the modeling of the sub-grid chemical terms [Vreman,2008] [Kaul,2011].

Before applying the β-PDF convolution to the manifold, a detailed chemistry calculation with heat loss is performed. A CH_4/air mixture with the equivalence ratio equal to 0.9 is computed by using CHEM1D [Somers,1994]. The transport model adopted is the complex EGlib [Ern-Giovangigli,1994], while the reaction mechanism is the GRI3.0 [Smith,1999]. As anticipated in Chapter 4, in order to consider heat loss effects, a series of flamelets is computed with varying enthalpy. The flamelets are converted in controlling variable space by using the progress variable $\mathscr{Y}$ and the enthalpy h as controlling variables. The progress variable $\mathscr{Y}$ is

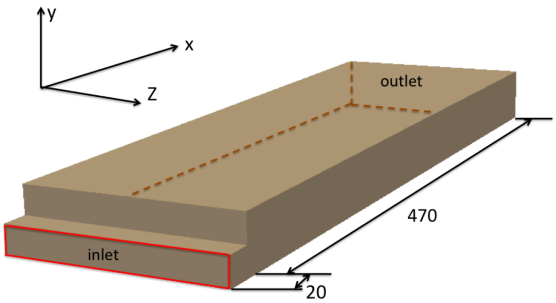

Figure 7.4: 3D Geometry of the test case, with addition of the inlet channel. Dimensions are in *mm*.

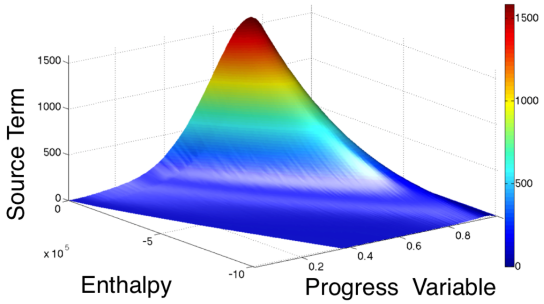

(a) Source term as function of progress variable $\mathscr{Y}$ and enthalpy h, from laminar manifold

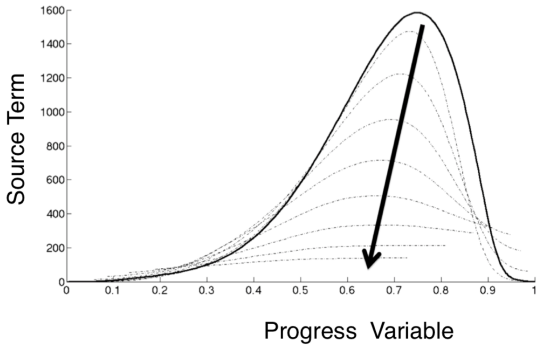

(b) Source term as function of progress variable $\widetilde{\mathscr{Y}}$ in turbulent manifold, with increasing variance $\widetilde{\mathscr{Y}''^2}$ levels, from 0 (bold curve) to 0.25 value, no heat loss

Figure 7.5: Laminar (a) and turbulent (b) manifold. CH_4-air mixture, $\phi = 0.9$, $\mathscr{Y} = O_2$, Complex EGlib transport, GRI 3.0 mechanism.

the mass fraction of O_2. In order to obtain the turbulent manifold, an integration is applied to the laminar manifold, using a β-PDF function in terms of $\mathscr{Y}$ as already described in chapter 5. Thereby, the relating field quantities are also function of the variance $\widetilde{\mathscr{Y}''^2}$. A δ function is used for h. Summarizing, this new 3D turbulent manifold is dependent on the mean progress variable $\widetilde{\mathscr{Y}}$, the enthalpy h and the progress variable variance $\widetilde{\mathscr{Y}''^2}$, resulting as the lookup values of the 3D manifold. In this turbulent manifold, as explained also in [Vreman,2008], the variables subjected to β-PDF integration are the progress variable source term, the species mass fractions, the density and the temperature, while values such as conductivity, specific heat, viscosity and thermal diffusivity are not convoluted. Figure 7.5 shows the laminar and turbulent manifolds: in Figure 7.5a, the source term as function of progress variable $\mathscr{Y}$ and enthalpy h is illustrated, while in Figure 7.5b, the convoluted source term, as function of progress variable $\mathscr{Y}$, for different variance $\widetilde{\mathscr{Y}''^2}$ levels, is shown. Regarding the variance levels considered within the β-PDF integration, as presented in Figure 7.5b, the levels are bounded between 0 (no turbulence) and 0.25.

7.4 CFD tool for turbulent FGM calculation

This work uses a new reactive pressure-based CFD solver, which includes the FGM modeling approach in the OpenFOAM ® environment. This solver is based on PISO [Issa,1986] (Pressure Implicit Split Operator) algorithm. In pressure-based algorithms, the momentum equation is solved directly. Moreover, a pressure-correction equation is obtained by joining continuity and momentum equations.

In addition to the Navier-Stokes equations, the transport equations for controlling variables are included. At each time step, the variables which are not solved in the equations are retrieved from the FGM manifold. For the 3D manifold, a *3-linear* interpolation among the lookup variables is performed.

While extra transport equations for progress variable $\widetilde{\mathscr{Y}}$ and the enthalpy h are solved during the calculation, regarding the progress variable variance $\widetilde{\mathscr{Y}''^2}$, an algebraic model [Kaul,2011] is considered, as already introduced in Chapter 5 (Equation 5.5).

To date, the RANS approach is considered the most feasible in an industrial environment. This enables the use of a two-dimensional mesh configuration, thus an important reduction in computational costs. In the RANS calculations, concerning momentum and enthalpy equations, a second-order centered scheme is utilized for both convective and diffusive terms. Regarding the progress variable transport equation, a bound blended scheme between the first and second order for the convective term is adopted, while the diffusive term is discretized by using the same scheme considered for the other equations.

LES provides a transient approach and is a compromise between the detailed turbulent flow approach by means of Direct Numerical Simulations (DNS) and the RANS approach. The sub-grid modeling and the grid resolution are important aspects of this approach, as already anticipated in Chapter 5. A three-dimensional configuration is required for LES, in order to capture the three-dimensional behavior of the flow.

Furthermore, the transient behavior of the flow is important for the correct development of the flow, especially for a configuration such as the sudden-expansion flow, where the recirculation zone and the stabilization of the flame play an important role.

In this work, different calculations have been performed for the sudden expansion flow configuration by using different turbulence modeling approaches. A series of unsteady RANS calculations is carried out by using both a parabolic inlet velocity profile and a constant velocity profile. The 2D configuration for RANS approach is the one illustrated in Figure 7.3. Afterwards, a LES approach has been also adopted by using four different inlet configurations. For some of the simulations, also an additional adiabatic computation is utilized to show the differences. A detailed list of the simulations is presented in Table 7.1 together with the corresponding inlet velocity profile adopted.

Table 7.1: List of different simulations performed.

Calculations	**Velocity profile**	Heat loss	Adiabatic
RANS-1	Parabolic profile	X	X
RANS-2	Constant profile	X	X
LES-1	Parabolic profile	X	
LES-2	Constant profile	X	X
LES-3	Mapped velocity profile and inlet channel (20 *mm*)	X	
LES-4	Mapped velocity profile and inlet channel (40 *mm*)	X	

7.5 RANS and LES boundary conditions

Regarding the turbulence modeling with RANS, a standard $k-\varepsilon$ approach is adopted in this work. In the LES simulations, a Smagorinsky approach for the modeling of the sub-grid eddy viscosity is employed.

Boundary conditions for progress variable are listed as follows: a fixed value representing the unburnt condition ($\mathscr{Y} = 0$) is imposed in the inlet, while in the outlet and in the walls a zero gradient condition is imposed.

Different velocity boundary conditions have been adopted for the different cases, as already anticipated in Table 7.1. In case RANS-1, a parabolic inlet profile with a maximum value of 13.5 m/s is set, resulting in an average value equal to 9.0 m/s. In RANS-2, a constant velocity profile has been adopted, with a value of 10.5 m/s. At the walls, a no-slip condition is imposed, while at the outlet a zero gradient behavior is assumed. The turbulence intensity is set equal to 3%. With regards to LES calculations, three different velocity profile approaches are considered here. In LES-1, a parabolic profile with an average value of 10.5 m/s is utilized. In LES-2, a constant velocity profile as presented in RANS-2 is adopted, in accordance with what was presented in [Martin,2003]. In LES-3 and LES-4 simulations, a small inlet channel has been included as well, with different length. The length of this channel has been imposed for LES-3 and LES-4 equal to 2 *cm* and 4 *cm* respectively. The velocity boundary conditions have been set in the following way: in order to have a fully developed flow, the inlet value for velocity is set by imposing the value of the velocity mapped at the distance of 1.5 *cm* downstream the inlet, before the expansion area. This method ensures that the inlet values of velocity are continuously updated and, after a transient, converge to the fully developed flow. This mapping technique is often used in LES and it is equivalent to having an infinitely long channel before the expansion area. This allows the flow to develop and there is no forced turbulence imposed. A constant mass flow rate equal to 0.035 kg/s is imposed in accordance with [Banhawy,1983]. The mapping procedure transfers the velocity profile from the reference interior plane to the inlet section, in such a way that a constant average value for velocity equal to 10.5 m/s is

imposed.

Pressure boundary conditions are set by imposing a fixed value equal to the atmospheric one at the outlet. Zero gradient conditions on both inlet and walls are imposed.

Regarding the enthalpy boundary conditions, a fixed value is imposed at inlet, corresponding to the adiabatic value. A zero gradient is imposed at the outlet. Usually, heat loss effects on walls are imposed by applying a fixed temperature value. In the present work enthalpy boundary conditions are imposed. In order to obtain the wall values for enthalpy, a table of these values as function of progress variable is retrieved by the manifold: these values of enthalpy are the corresponding ones with respect to a fixed temperature, which is exactly the temperature value imposed on the walls.

A Cartesian structured 2D mesh is used for the RANS calculation, made of 40000 elements: 500 elements in streamwise direction, with a Δx of $1 \cdot 10^{-3}$ m and 80 elements in spanwise direction, with a Δy of $0.5 \cdot 10^{-3}$ m. In the LES approach, a uniform three-dimensional mesh with a Δx of $1 \cdot 10^{-3}$ m is adopted. Regarding LES1-2-3 simulations, the averaged quantities have been obtained in the following way: a transient simulation has been performed up to 0.5 seconds, in order to reach a fully developed flow. In this simulation, a Δt increase from $1 \cdot 10^{-6}$ to $1 \cdot 10^{-5}$ s has been considered. Afterwards, another simulation with an extra interval of 0.2 seconds with a time step of $1 \cdot 10^{-5}$ s is performed and averaged values have been calculated during this last period. Figure 7.6 shows a qualitative propagation of the flame structure by means of some transient snapshots of the LES-3 case: iso-contours for $\mathscr{Y} = 0.5$, colored by the velocity magnitude, are shown for three different times (0.01, 0.02 and 0.5 s): in the first two time snapshots the flow is still developing (Figures 7.6a, 7.6b), while in Figure (7.6c) the flow can be considered sufficiently developed. For LES-4 simulation, a longer calculation time has been considered to reach a proper convergence. Further informations about the statistical convergence of LES-4 simulation are presented in Appendix B.3. Before presenting the results of the simulations, few informations regarding the grid adopted for LES calculations are given here. By considering a $Re = 8500$ for the present case, a correspondent Kolmogorov length scale η can be estimated by using the $Re^{3/4}$ law. Thus, $\eta \sim Re^{-3/4} \cdot \frac{D}{2} \sim 0.0113$ mm, with D the inlet channel height (20 mm). Considering $D/2$ as the correspondent integral length scale l_o, a *cut-off* length $l_{\mathrm{c/o}}$ [Poinsot-Veynante,2005] is defined as the length correspondent to the grid size (in this case 1 mm). All scales smaller than $l_{\mathrm{c/o}}$ are modeled while the larger ones are resolved. Considering that $\eta < l_{\mathrm{c/o}} < l_o$, then $l_{\mathrm{c/o}} = \eta \cdot \mathscr{Q}$ where $\mathscr{Q}$ is a coefficient whose value is $\mathscr{Q} = l_{\mathrm{c/o}}/\eta \sim 88$.

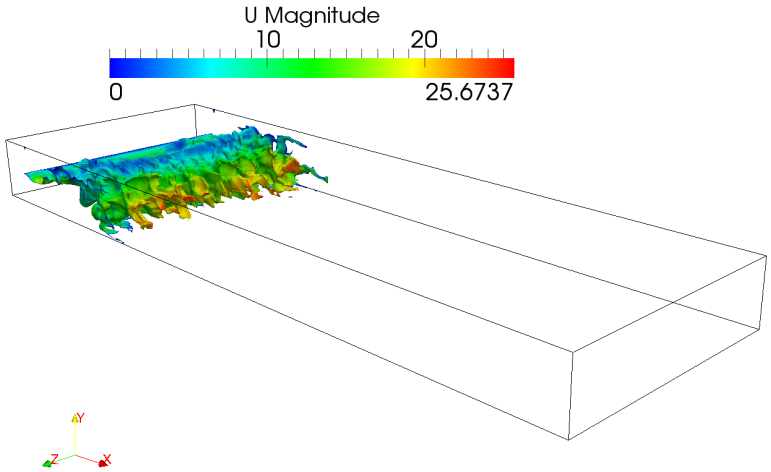

(a) 10 *ms*

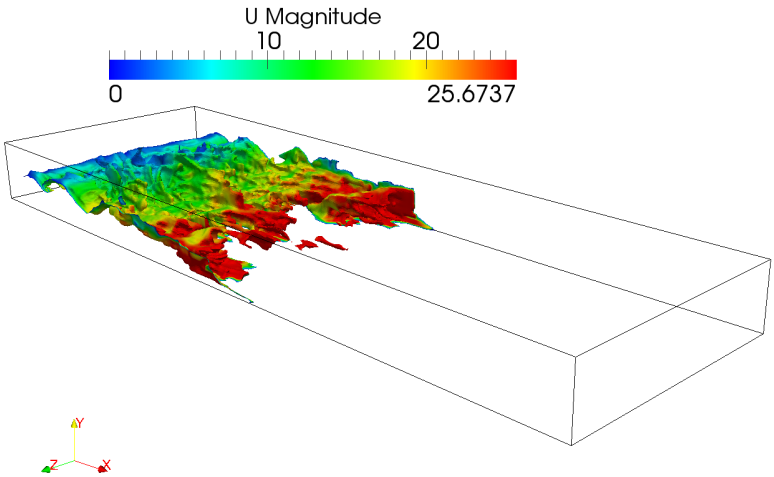

(b) 20 *ms*

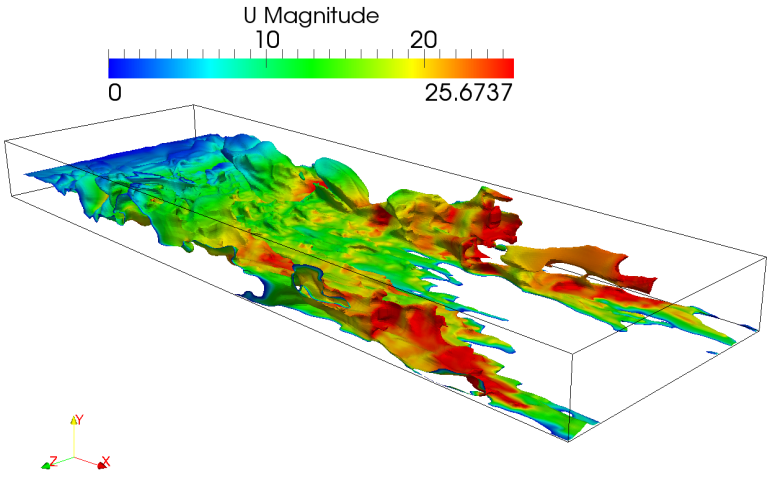

(c) 0.5 *s*

Figure 7.6: Transient simulation of LES-3 case. Isocontours of $\mathscr{Y} = 0.5$ colored by the velocity magnitude.

7.6 Results and discussion

7.6.1 Iso-contours and comparison with previous work

A comparison between the experimental results and those obtained from the FGM technique is performed in the present part by means of iso-contours. This comparison includes also the numerical results of [Martin,2003] (reprinted under permission of ASME). With respect to [Martin,2003], this work also considers heat loss, by including the dependency on the enthalpy. Thus this approach should be more realistic and consistent with the experimental data. In this Chapter, axial velocity and temperature iso-contours are presented. Regarding the other quantities, a comparison is presented in Appendix B.1 .

Figures 7.7 and 7.8 illustrate a comparison of the mean axial velocity with heat loss (7.7) and adiabatic (7.8) approaches respectively. The domain can be subdivided into three main interesting regions: (i) recirculation bubble in the upper left corner, (ii) the area downstream the inlet, and (iii) the acceleration zone downstream the flame front. The adiabatic condition shows shorter recirculation and acceleration regions compared to the heat loss results. By focusing on heat loss results, the recirculation zone is predicted satisfactorily in the RANS results, with a bubble size about 10% longer. In LES1-2-3 results, the recirculation bubble is approximately 20% longer, while in LES-4 this length is below 10%. In the area downstream the inlet, all iso-contours have values similar to the experimental case, but the LES-3 and LES-4 show values which are roughly 1 m/s lower. Nevertheless, LES-3 and LES-4 calculation show contour shapes which reproduce the experimental data more accurately with respect to the other simulations. This should be related to a more realistic boundary condition at the inlet: in the LES-3 and LES-4, a freely developing flow with the mapping velocity approach is assumed. It should be however noted that in LES-3 the velocity is mapped at a distance of 0.5 *cm* from the expansion area, while in LES-4 it is mapped at a distance of 2.5 *cm*. This difference can affect the correspondent flow field: in LES-3 the mapping location might be too close to the expansion area and might be affected by the expansion flow, while in LES-4 the mapping distance coordinate might be considered sufficiently far from the expansion area. In all other simulations, fixed values for velocity and turbulence are imposed in an approximated way, since no exact information was available for the inlet profile. The acceleration region best result between RANS results is obtained by the RANS-2, where the highest velocity region iso-contour is located in between 2 and 3 *cm* in the streamwise direction. Concerning the LES simulations, the best result is obtained by LES-4, where the highest velocity region begins at about 3 *cm* in streamwise direction.

Figures 7.9 and 7.10 illustrate the temperature iso-contours. Regarding temperature field, a distinction has to be made between the heat loss and adiabatic results. In results with heat loss, the cooling of the wall changes completely the iso-contour distribution with respect to the adiabatic approach. Due to these differences, the two approaches need to be evaluated separately. Concerning the adiabatic case in Figure 7.10, RANS results show a thinner flame front

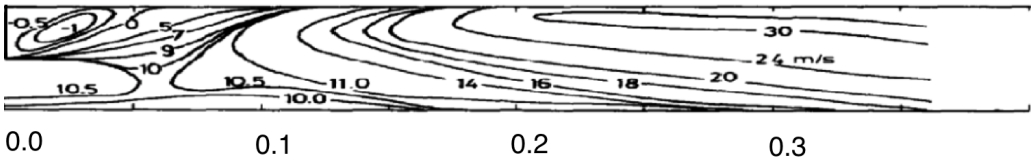

(a) El Banhawy et al. experimental results

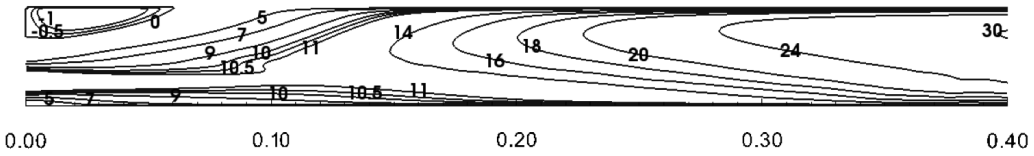

(b) RANS-1 simulation - Parabolic velocity profile

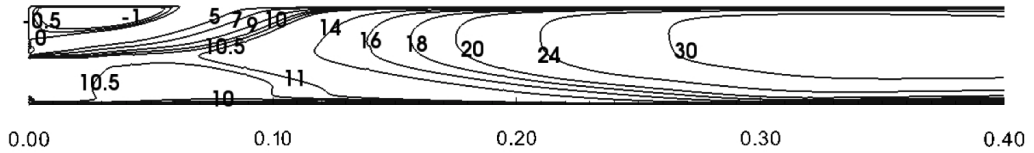

(c) RANS-2 simulation - Constant velocity profile

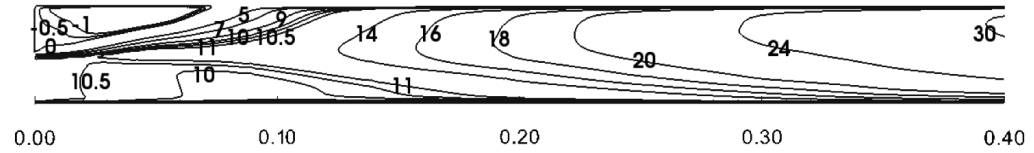

(d) LES-1 simulation - Parabolic velocity profile

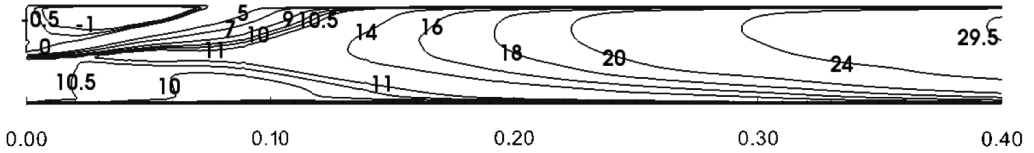

(e) LES-2 simulation - Constant velocity profile

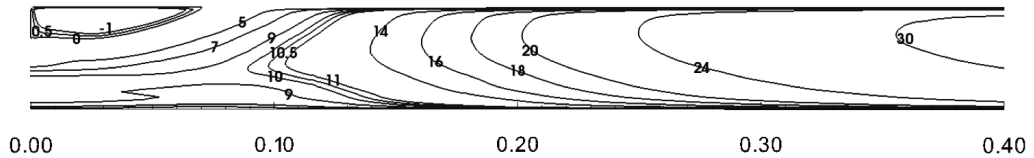

(f) LES-3 simulation - mapped profile

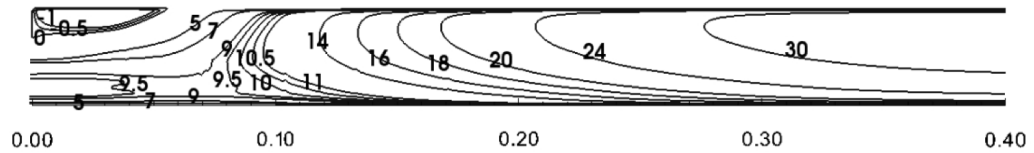

(g) LES-4 simulation - mapped profile

Figure 7.7: Isocontours of mean axial U. Comparisons of different simulations using the heat loss approach with [Banhawy,1983].

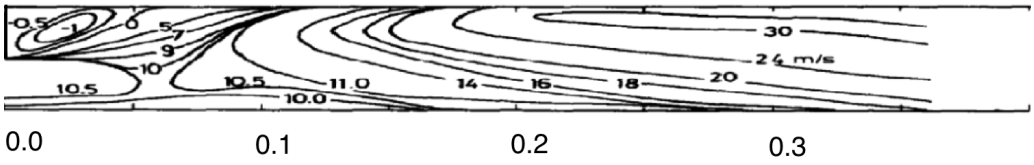

(a) El Banhawy et al. experimental results

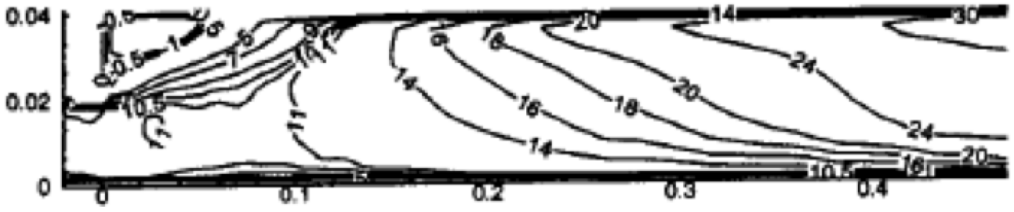

(b) Martin et al. numerical results

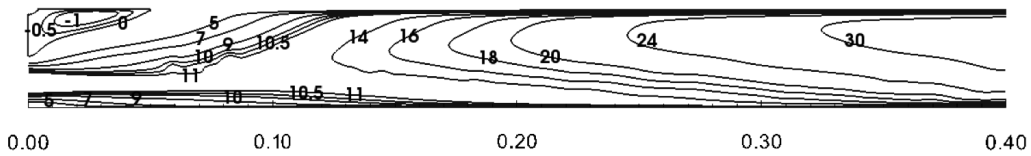

(c) RANS-1 simulation - Parabolic velocity profile

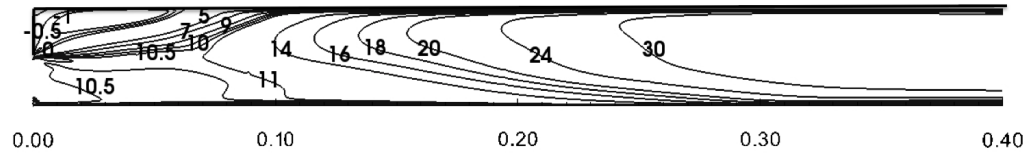

(d) RANS-2 simulation - Constant velocity profile

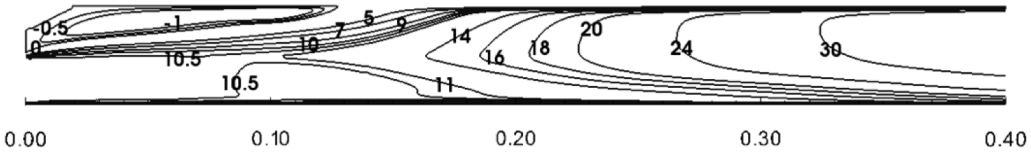

(e) LES-2 simulation - Constant velocity profile

Figure 7.8: Isocontours of mean axial U. Comparisons of different simulations using an adiabatic approach with [Banhawy,1983] and [Martin,2003].

and the iso-contour gradients are steeper, with respect to [Martin,2003]. The same behavior seen in RANS results is also visible In LES-2 adiabatic results. Moreover, in the same case (7.10e) the flame front is smeared along a greater region, resulting in lower gradient with a flame length which is extremely long; the anchoring zone of the flame between the inlet and the recirculation region is extremely long and flat. This can be due to the constant profile which is imposed in the inlet, without any turbulence perturbation. In this case, the turbulence develops further downstream.

Regarding the heat loss results, in RANS-1, RANS-2, LES-1 and LES-2 flame front iso-contours reach the bottom wall at a position which is further downstream with respect to the experimental data, resulting in a longer flame. On the other hand, in LES-3 and LES-4 the flame front iso-contours reach the bottom wall at a position which is more similar with respect to the experimental data, resulting in a shorter flame. This can be related to the more realistic condition imposed to the turbulence at the inlet section. However, between LES-3 and LES-4 small differences appear, due to the different flow regime related to the different mapping region, as already explained for the velocity field. Another aspect which should be noted in Figure 7.9 concerns how the iso-contours of the highest temperature values go back to the low streamwise coordinate: the best results are obtained by LES-2, while in all the other cases the highest temperature values go deep in the recirculation zone: the flame front equals the flow velocity upstream with respect to LES-2 and experimental results, due to the different approaches adopted in modeling the inlet profile.

7.6.2 Recirculation bubble

An important characteristic in this sudden expansion flow configuration is the presence of the recirculation bubble. In order to give an estimation of the bubble size with respect to the different simulations performed, an illustration of the recirculation zone is presented in Figures 7.11, 7.12 and 7.13. As evident in Figure 7.13, for a few cases also the corresponding cold case is presented, to show the differences in bubble recirculation. A resume of the corresponding lengths is provided in Table 7.2. In order to show these bubbles, the following procedures have been adopted: in RANS cases, streamlines are computed and visualized in the 2D plane. Since in LES the domain is three-dimensional, an appropriate quantity has been computed: the velocity vector is considered by neglecting the z component and the related streamlines are evaluated in the middle plane of the combustion chamber.

As expected, in cold flow cases, the recirculation bubbles are much longer with respect to the reactive cases. This is due to the different thermal field which is present in the cold flow condition, where there are no density changes and temperature gradients. On the other hand, in the reactive cases, the temperature increases and the density drops correspondingly, and therefore the main flow can expand quickly, reducing the bubble dimension. Same considerations could be made by comparing the adiabatic and heat loss results (in the adiabatic cases temperatures

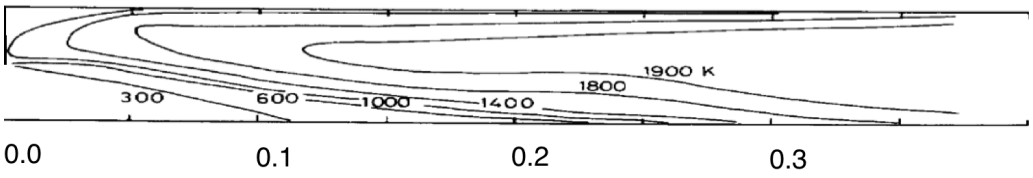

(a) El Banhawy et al. experimental results

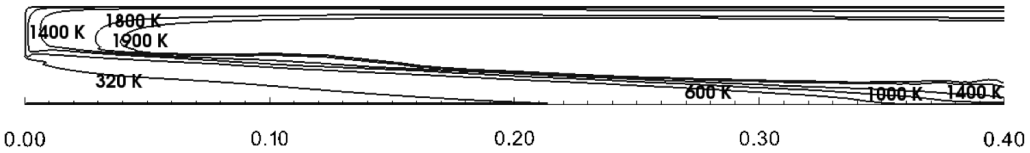

(b) RANS-1 simulation - Parabolic velocity profile

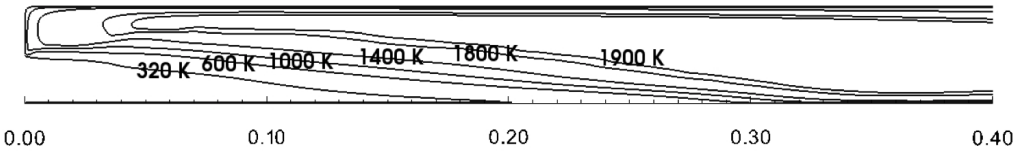

(c) RANS-2 simulation - Constant velocity profile

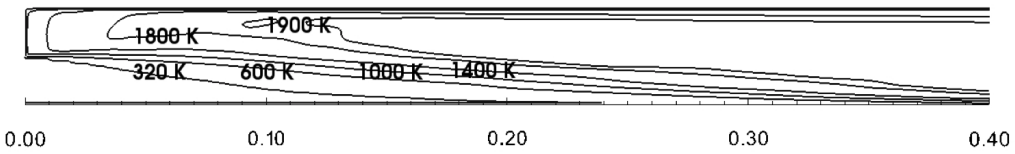

(d) LES-1 simulation - Parabolic velocity profile

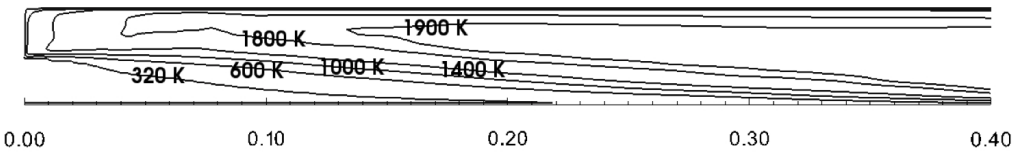

(e) LES-2 simulation - Constant velocity profile

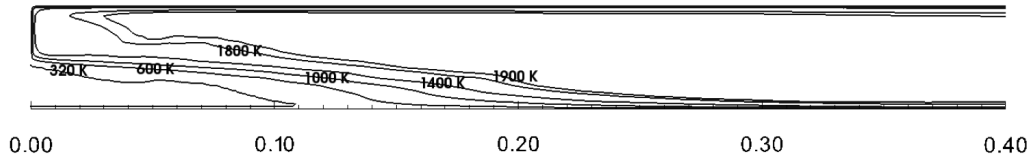

(f) LES-3 simulation - mapped profile

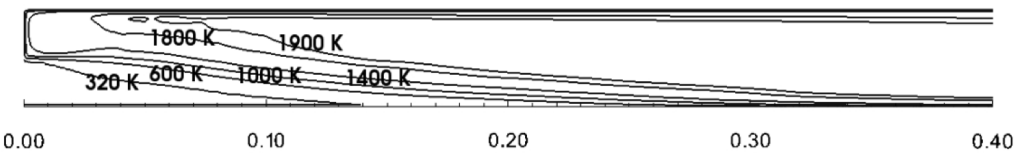

(g) LES-4 simulation - mapped profile

Figure 7.9: Isocontours of mean T. Comparisons of different simulations using the heat loss approach with [Banhawy,1983].

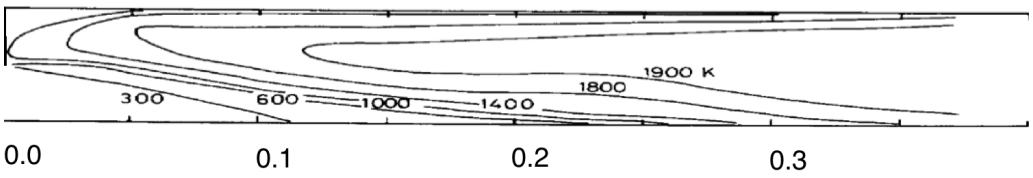

(a) El Banhawy et al. experimental results

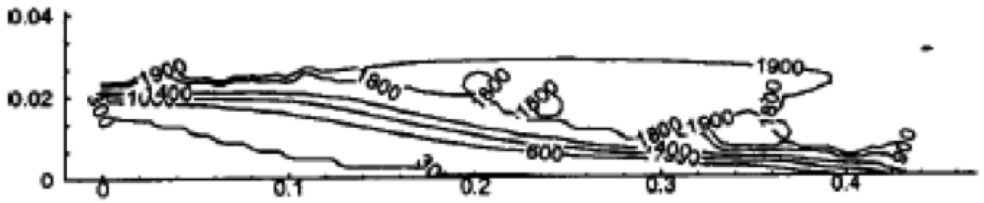

(b) Martin et al. numerical results

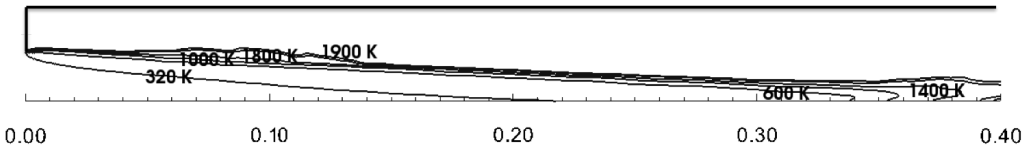

(c) RANS-1 simulation - Parabolic velocity profile

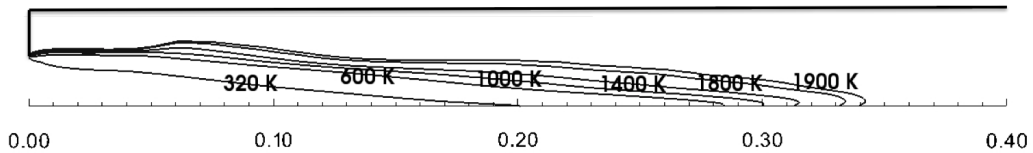

(d) RANS-2 simulation - Constant velocity profile

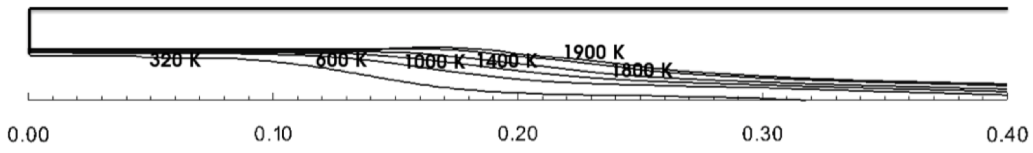

(e) LES-2 simulation - Constant velocity profile

Figure 7.10: Isocontours of mean T. Comparisons of different simulations using an adiabatic approach with [Banhawy,1983] and [Martin,2003].

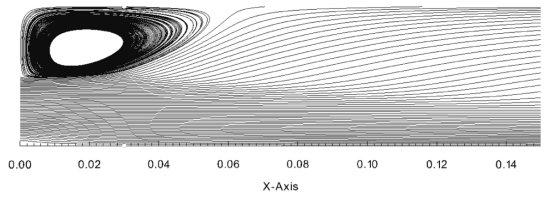

(a) RANS-1 with heat loss

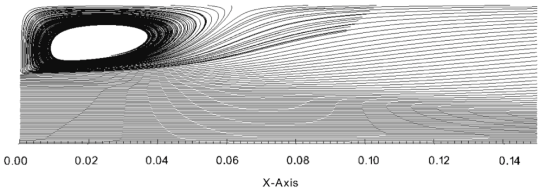

(b) RANS-2 with heat loss

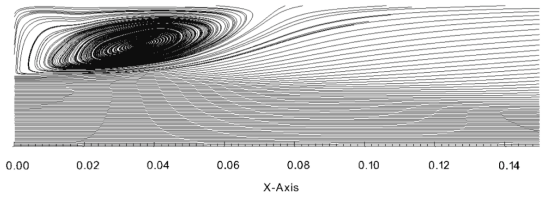

(c) LES-1 with heat loss

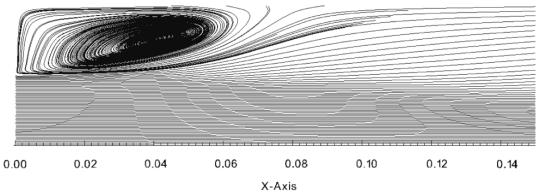

(d) LES-2 with heat loss

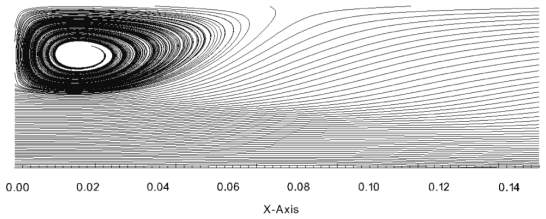

(e) LES-3 with heat loss

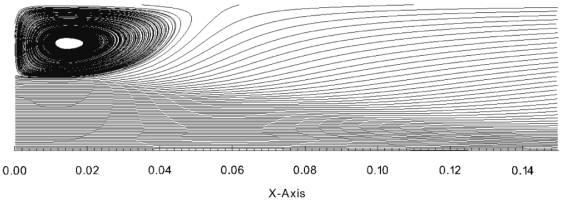

(f) LES-4 with heat loss

Figure 7.11: Recirculation bubble iso-lines for heat loss cases.

reach the maximum values). However, only in RANS simulations the recirculation bubble in the heat loss approach are longer with respect to the corresponding adiabatic cases. Opposite to RANS, in LES this behavior is not observed. Last consideration concerns the heat loss results: the RANS solutions have a shorter bubble dimension with respect to the LES ones. Moreover, among the LES simulations, the LES-3 has the longest bubble size, approximately 20% more with respect to the bubble size measured in [Banhawy,1983]. The only exception in LES results regards the LES-4 results, which are the most similar to the experimental data ones: in this configuration, the recirculation bubble length is about 0.5 *cm*. To conclude, LES-4 configuration results to have the best prediction in the recirculation length among the various simulations.

7.6.3 Cross profiles

A cross profile analysis has been carried out in order to compare the different simulation approaches. Figures from 7.14 and 7.15 show the cross profiles of temperature, O_2 and CO_2 molar fractions for different distances from the inlet. A series of cross profiles are presented for different distances in the streamwise direction (0.04 - 0.28 *m*). In this work, only profiles for $x = 0.04$ *m* and $x = 0.28$ *m* are presented. On the left column of each picture, heat loss results are presented while adiabatic results are presented on the right column. The cross profiles express the

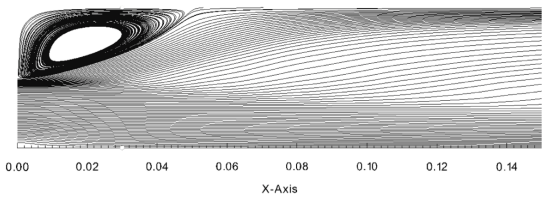

(a) RANS-1 with adiabatic approach

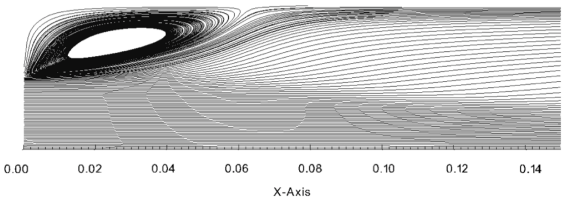

(b) RANS-2 with adiabatic approach

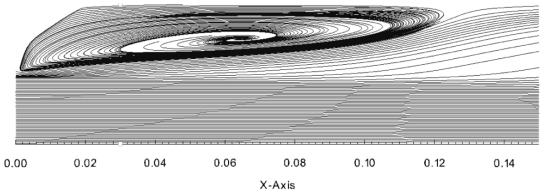

(c) LES-2 with adiabatic approach

Figure 7.12: Recirculation bubble iso-lines for adiabatic cases.

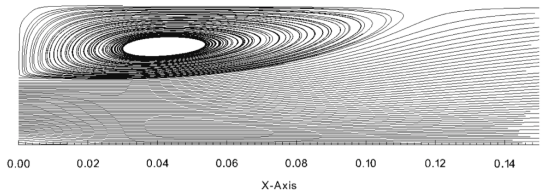

(a) RANS-1 - cold case

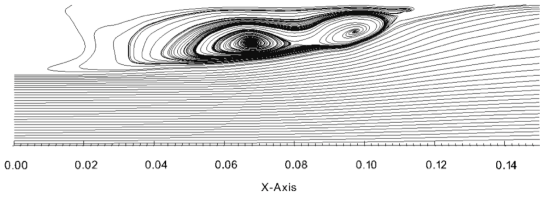

(b) LES-2 - cold case

Figure 7.13: Recirculation bubble iso-lines for cold cases.

Table 7.2: Estimation of recirculation bubble lengths.

CASE	Heat loss	Adiabatic	Cold
RANS-1	0.054	0.048	0.112
RANS-2	0.062	0.062	n.a.
LES-1	0.07	n.a.	n.a.
LES-2	0.074	0.12	0.12
LES-3	0.088	n.a.	n.a.
LES-4	0.05	n.a.	n.a.

evolution of the three mentioned quantities. The interpretation can be done as follows: LES-1 and LES-2 profiles are shifted downstream with respect to the other profiles while LES-3 is showing an early evolution of the quantities. This can be explained with the fact that the LES-1 and LES-2 simulations have different inlet conditions with respect to the LES-3. In LES-3, the inlet condition allows the flow to enlarge faster inside the combustion chamber, reducing the flame length. In LES-3, profiles are similar with respect to the other LES ones, but they are all shifted upstream. In LES-4, profiles are located between the LES-3 and RANS-2. Concerning RANS simulations, RANS-1 results show steeper gradients with respect to RANS-2.

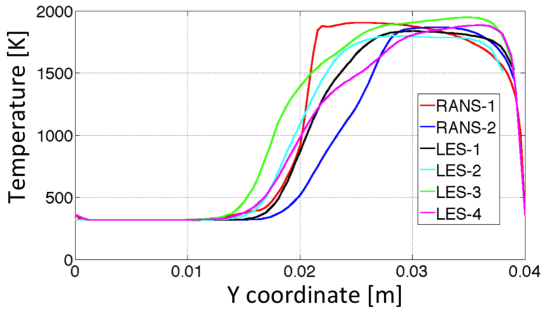

(a) Temperature - heat loss case

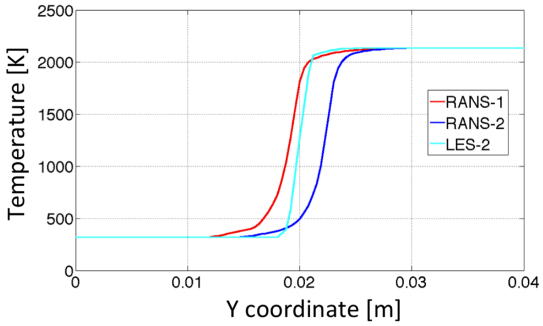

(b) Temperature - adiabatic case

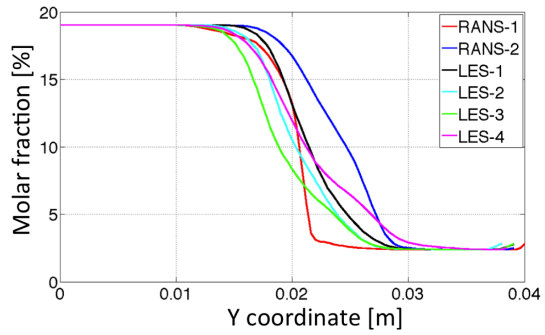

(c) O_2 molar fraction - heat loss case

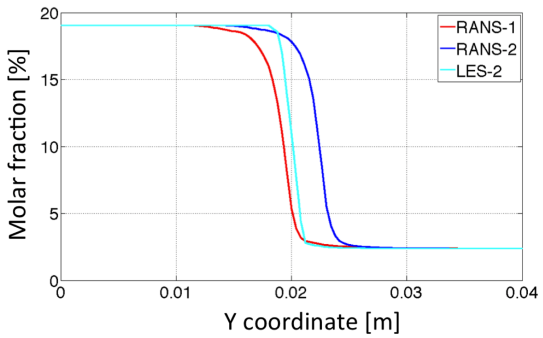

(d) O_2 molar fraction - adiabatic case

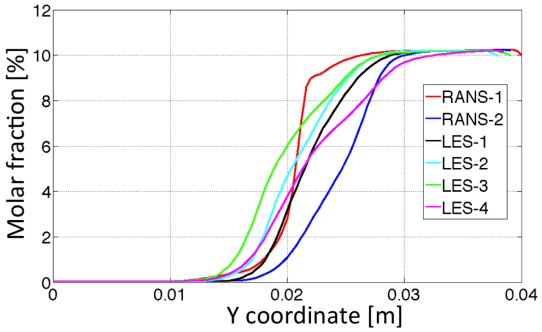

(e) CO_2 molar fraction - heat loss case

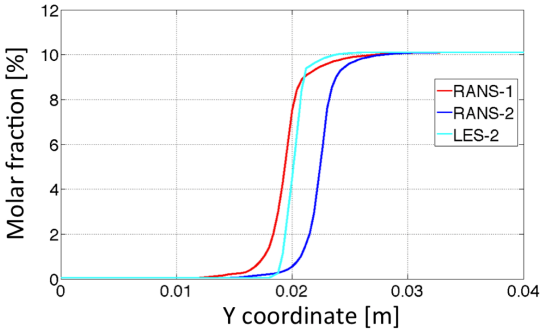

(f) CO_2 molar fraction - adiabatic case

Figure 7.14: Cross behavior along y coordinate of temperature, O_2 and CO_2 molar fractions for $x = 2D = 0.04\ m$ for both heat loss and adiabatic cases.

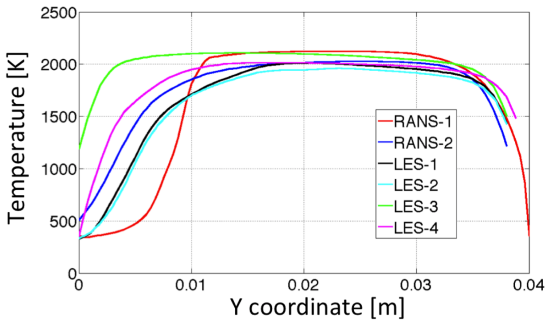

(a) Temperature - heat loss case

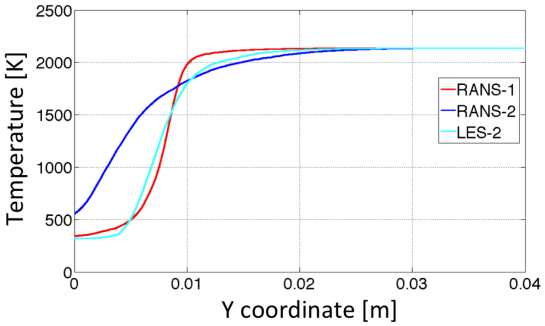

(b) Temperature - adiabatic case

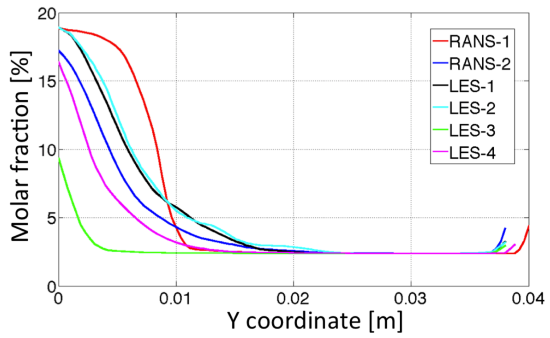

(c) O_2 molar fraction - heat loss case

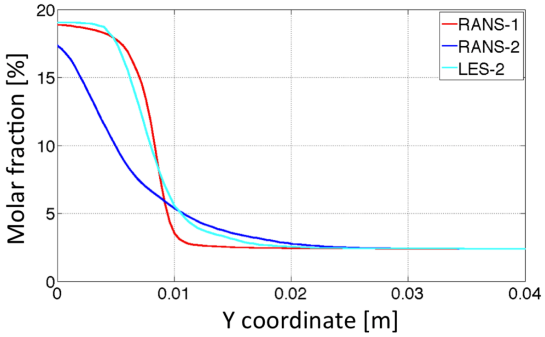

(d) O_2 molar fraction - adiabatic case

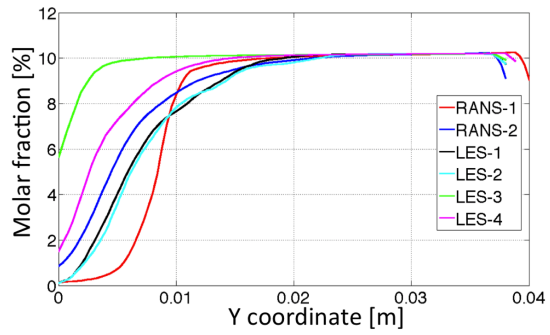

(e) CO_2 molar fraction - heat loss case

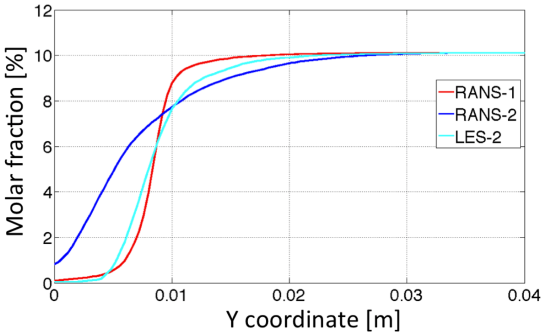

(f) CO_2 molar fraction - adiabatic case

Figure 7.15: Cross behavior along y coordinate of temperature, O_2 and CO_2 molar fractions for $x = 14D = 0.28\ m$ for both heat loss and adiabatic cases.

7.6.4 Flame length estimation

A flame length study is performed as well. The results obtained with the different simulations are presented and compared with estimations of the flame length regarding the experimental results in [Banhawy,1983] and the numerical results in [Martin,2003].

The flame length is defined as the axial distance from the inlet where the average temperature is reached at the bottom wall. The value of the average temperature T_{av} is calculated by using Equation 7.1:

$$T_{av} = T_{min} + \frac{T_{max} - T_{min}}{2}, \tag{7.1}$$

where T_{max} and T_{min} are the maximum and minimum values respectively in the middle plane of the combustion chamber. $T_{av} = 1200K$ for the adiabatic case.

This evaluation of the flame length can also be proposed for the X_{O_2} and X_{CO_2} molar fraction percentages by using the same assumption, as indicated in Equations 7.2 and 7.3:

$$X_{O_2} = X_{O_2-min} + \frac{X_{O_2-max} - X_{O_2-min}}{2}, \tag{7.2}$$

$$X_{CO_2} = X_{CO_2-min} + \frac{X_{CO_2-max} - X_{CO_2-min}}{2}. \tag{7.3}$$

A comparison is presented for the different simulations, both with heat loss and adiabatic approaches. The flame length estimated from [Banhawy,1983] and [Martin,2003] is presented by showing two vertical lines, both of them estimated by taking into account the iso-contours values previously shown.

In each plot, the evolution of each quantity (T, X_{O_2} and X_{CO_2}) is also superposed as function of the streamwise coordinate x along the bottom wall. For each curve, the corresponding flame length for the current results is indicated.

In this Section, only RANS-2 (Figure 7.16), LES-3 (Figure 7.17) and LES-4 (Figure 7.18) results are illustrated. The other cases are presented in Appendix B.2.

RANS-1 results in Figure 15 show that the flame length is longer with respect to the experimental data of roughly 0.3 m, but closer to [Martin,2003]. RANS-2 results show a closer correspondence to the experimental data, although the flame length is little bit longer. The same considerations can be made concerning the corresponding adiabatic cases.

LES-1 and LES-2 results in Figures 14 16 show a clear over-prediction of the flame length with respect to both experimental data and numerical results from [Martin,2003]. This is probably

Table 7.3: Estimation of flame lengths in terms of temperature for different calculations and comparison with experimental data and numerical previous work - Dimensions are in m.

Experimental data from [Banhawy,1983]	0.28	
Numerical results from [Martin,2003]	0.4	
Simulations with OpenFOAM ®	Heat loss	Adiabatic
RANS-1	0.42	0.375
RANS-2	0.33	0.31
LES-1	0.45	n.a.
LES-2	0.46	> 0.5
LES-3	0.28	n.a.
LES-4	0.37	n.a.

due to an erroneous level of turbulence generated at the flame front by shearing flows: the absence of such velocity fluctuations affects the flame shape which results to be longer in the streamwise direction and thinner in the spanwise direction, in comparison with [Banhawy,1983] and [Martin,2003] .

On the other side, for the LES-3 results, the flame lengths appear to be closer to the ones of [Banhawy,1983]. In particular, considering the T field, the flame is about 5% longer, while considering X_{O_2} and X_{CO_2} the flame is $5-10\%$ shorter with respect to the reference data. Flow shearing is probably better reproduced leading to a larger fluctuating flow near the flame front and a shorter flame. LES-4 results show a longer flame length with respect to the LES-3 simulation, resulting more similar to RANS-2 results.

Table 7.3 summarizes the different flame lengths in terms of temperature for the different calculations.

A statistical analysis related to the latest configuration LES-4 is presented in 8. This analysis describes few quantities which have been recorded during the transient simulations, by using few probes in the middle plane of the geometry.

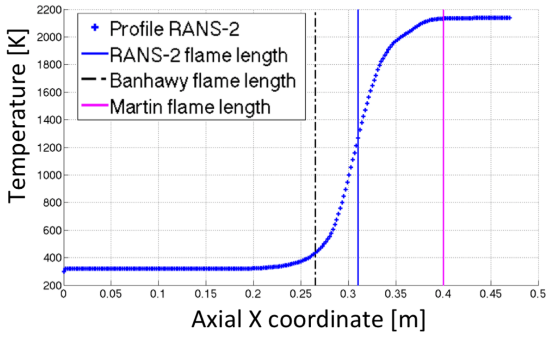

(a) RANS-2 case with heat loss - Temperature profiles

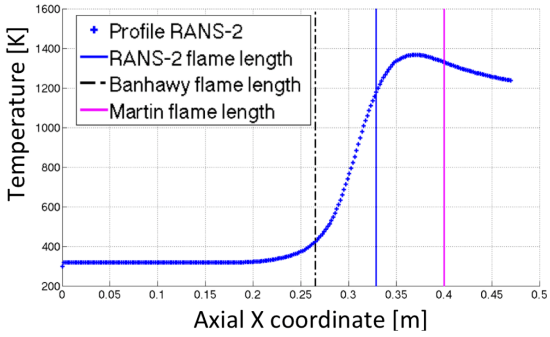

(b) RANS-2 adiabatic case - Temperature profiles

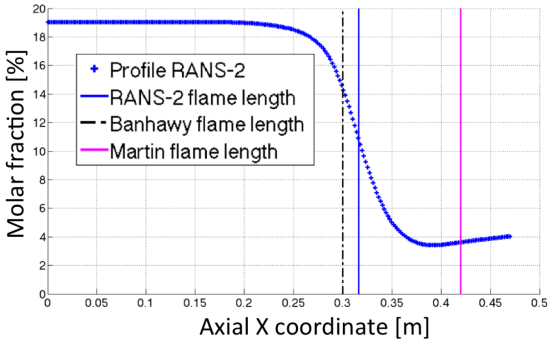

(c) RANS-2 case with heat loss - X_{O_2} profiles

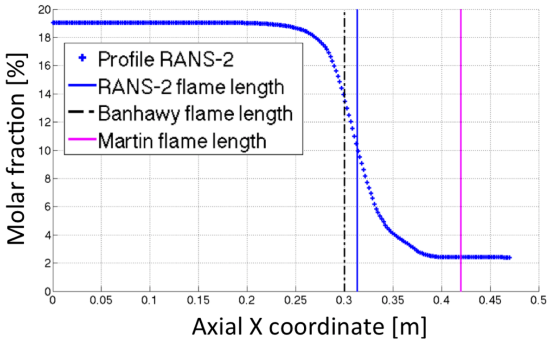

(d) RANS-2 adiabatic case - X_{O_2} profiles

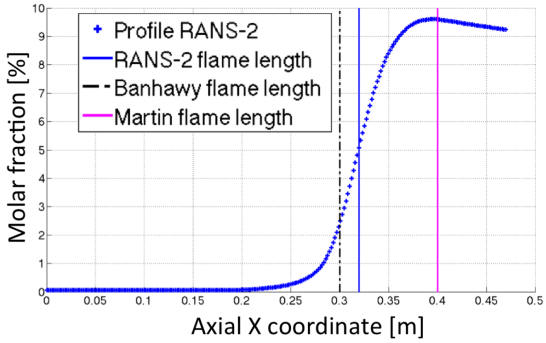

(e) RANS-2 case with heat loss - X_{CO_2} profiles

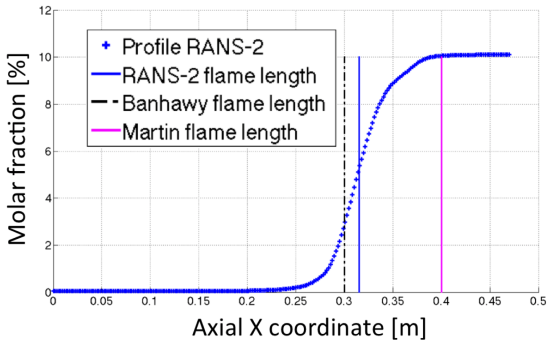

(f) RANS-2 adiabatic case - X_{CO_2} profiles

Figure 7.16: RANS-2 case. Estimation of flame length using T, X_{O_2} and X_{CO_2}. Comparison of different simulations with [Banhawy,1983] and [Martin,2003] flame lengths.

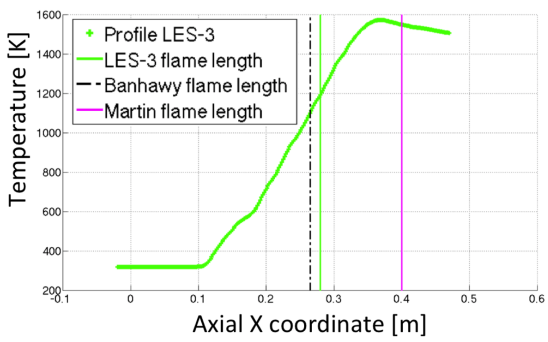

(a) LES-3 case with heat loss - Temperature profiles

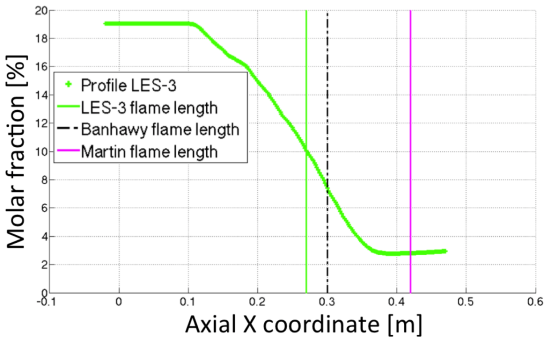

(b) LES-3 case with heat loss - X_{O_2} profiles

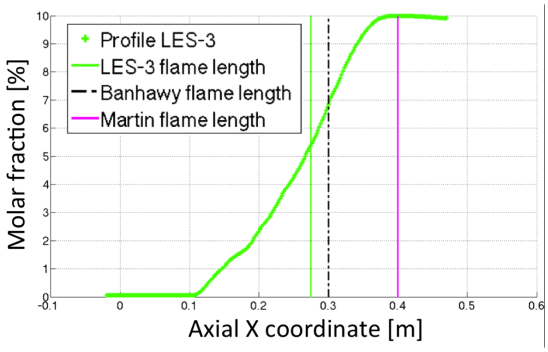

(c) LES-3 case with heat loss - X_{CO_2} profiles

Figure 7.17: LES-3 case. Estimation of flame length using T, X_{O_2} and X_{CO_2}. Comparison of different simulations with [Banhawy,1983] and [Martin,2003] flame lengths.

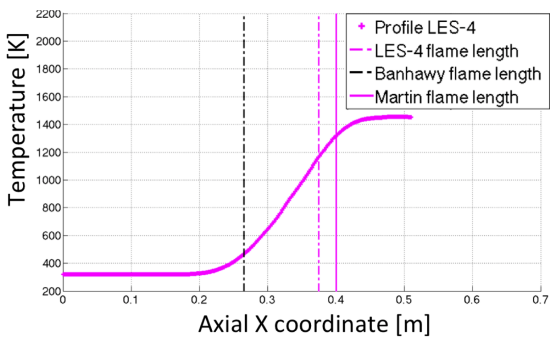

(a) LES-4 case with heat loss - Temperature profiles

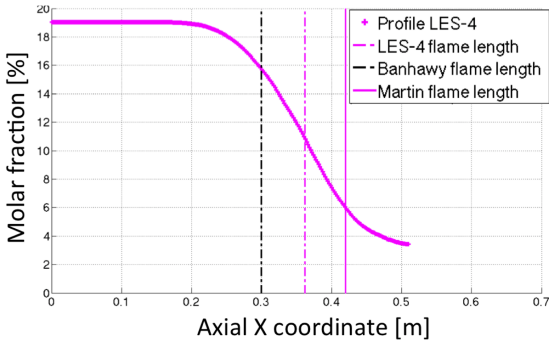

(b) LES-4 case with heat loss - X_{O_2} profiles

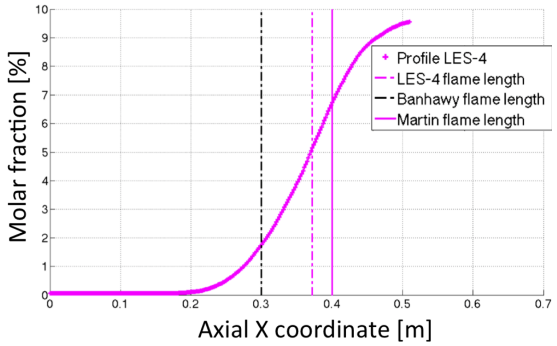

(c) LES-4 case with heat loss - X_{CO_2} profiles

Figure 7.18: LES-4 case. Estimation of flame length using T, X_{O_2} and X_{CO_2}. Comparison of different simulations with [Banhawy,1983] and [Martin,2003] flame lengths.

7.7 Conclusions

In the present Chapter, a pressure-based reactive solver has been developed connecting the CFD standard approach to the FGM reduction method technique.

The resulting code has been satisfactorily applied to a sudden expansion flow configuration. This geometry is considered of great importance for the flow phenomena which are observed. In particular, the flow recirculation and the flame stabilization play an important role. This configuration has been used to perform reactive-CFD simulations with FGM approach by using both RANS and LES modeling with different velocity inlet conditions. Results have been compared with experimental data. Important effects such as heat loss phenomena have been included in this combustion configuration, providing better results with respect to previous numerical works. Furthermore, a saving in calculation time is achieved considerably with respect to detailed chemistry calculations, considering that detailed chemistry still results not significantly feasible in practical combustion configurations. An exhaustive description of the different simulations has been presented and few important quantities, such as recirculation bubbles and flame length, have been estimated and compared with reference data. Among the different simulation approaches, the latest one with a LES approach has shown the best correspondence with respect to the experimental data. In this configuration, the inclusion of the inlet channel,

which provides a fully developed flow in the inlet section, has become of great importance in reaching a more realistic flow condition. In conclusion, FGM has been employed with standard turbulence approaches resulting in a valid solution for the combustion modeling, while giving a reasonable accuracy in terms of temperature and species predictions, which is comparable to detailed chemistry results.

Chapter 8

Conclusions and Recommendations

"Ο μῦθος δηλοῖ ὅτι..."
Lit. "The meaning of the story is ... (used as a conclusive statement in a story)"

Aesop

Gas turbine combustion has reached an increasing attention in the last decades. Thereby, fuel flexibility, combustion efficiency and environmental issues such as pollution emissions in turbomachinery configurations are considered of primary importance. The reaching of these standards and the development of efficient combustion systems have become a great challenge, since new configurations for burners have been required. Classical research approaches on the basis of experimental techniques have been always very expensive and time consuming. Similarly, numerical design of detailed combustion systems have been also very demanding considering the problem of the huge computational effort required for the solution of the whole reactive system. Reduction chemistry methods have improved the efficiency in numerical studies and the computational time, since they have considered the combustion process by solving a small amount of the partial differential transport equations. By adopting this inspiration, the Flamelet Generated Manifold (FGM) technique has become an affirmed reduction method and, therefore, can be applied to real burner configurations by reaching a high standard efficiency in numerical computation and, at the same time, having an accuracy comparable to the detailed chemistry approaches. By using a manifold built from the detailed chemistry calculation, a multidimensional combustion calculations solves the transport equation for few controlling variables. During these calculations, key variables such as chemical source term, temperature,

and diffusivity are retrieved from the manifold. To summarize, the multidimensional flame is calculated by tabulating the chemistry of a series of one-dimensional flames.

In this work, the FGM technique is exploited and applied to an open source code known as OpenFOAM ®İn chapter 4, laminar combustion is studied and the FGM performances are shown on a simple two-dimensional geometry called *flame in a box*. However, prior studies focused on stationary solutions of this geometry. Thus no prior work has shown transient effects and dynamic aspects to date. Thereby, a *dynamic flame in a box* has been investigated. This has been performed by using both an adiabatic and a non adiabatic approach in the study of the flame. Moreover, a compressible code is adopted for which particular care in pressure boundary conditions has to be given. Heat loss is considered by including progress variable and enthalpy as controlling variables. By considering heat loss effects in this configuration, we have shown that, under certain conditions, a stationary solution cannot be reached and, therefore, transient approaches are of great importance in combustion analysis. Proper non-reflecting boundary conditions are needed to circumvent flame oscillations due to the pressure waves in the domain. To conclude, the obtained results show that the implementation in the code has been successful.

In chapter 5, the interaction between turbulence and combustion is discussed. In order to model the sub-grid aspects of the chemistry terms, a β-PDF approach has been considered a proper choice and an algebraic model for the variance of the progress variable is used. Thereby, the variance becomes a new controlling variable of the so-called turbulent manifold. The approach described above is suitable for relatively simple gases such as methane, for which there is a balance between molecular and thermal diffusion. In chapter 6, a joint work with Siemens AG on a single jet analysis has been performed by means of FGM applied to LES turbulent modeling. Results have been validated with experimental data by using an adiabatic approach: results have shown reasonable prediction of the flow field, beside some differences which have been related to limitations of the manifold; in fact, in this approach no heat loss has been taken into account while this aspect should be included in the analysis. Chapter 7 presented another burner configuration and FGM is applied to turbulent flows with heat loss inclusions, in collaboration with CFD Engineering. A sudden expansion flow has been employed and both RANS and LES approaches have been utilized. Results have demonstrated a good reproduction of experimental data available. Recirculation bubbles, cross profiles and flame estimations have been illustrated for different calculations and they have been compared with experimental data and prior numerical work. Moreover, significant improvements of previous numerical results available in literature have been achieved.

To conclude, presumed β-PDF approach have shown satisfactory results for relatively simple fuels such as methane. Future works should be focused on adding hydrogen in the fuel. With the future aim of doing a proper RANS and LES simulation in turbulent hydrogen combustion configurations, the modeling part requires some statistical approaches. An analysis of DNS results can be the starting point of such work. The analysis of these turbulent data can become the instrument to find suitable sub-grid modeling for the chemistry of hydrogen-based fuels.

Bibliography

[Aguerrea,2013] Aguerrea, H.J., Damiana, S.M., Gimeneza, J.M. and Nigroa, N.M., Modeling of compressible fluid problems with openfoam using dynamic mesh technology, Mecanica Computacional Vol XXXII, 995-1011, Mendoza, Argentina, 2013.

[Alpert,2002] Alpert, B., Greengard, L. and Hagstrom, T., Non reflecting boundary conditions for the time dependent wave equation, Journal of Computational Physics, 180, 270-296, 2002.

[Anderson,1984] Anderson, D.A., Tannehill, J.C., and Pletcher, R.H., Computational Fluid Mechanics and Heat Transfer, McGraw-Hill Book Company, New York, 1984.

[Banhawy,1983] El Banhawy, Y., Sivasegaram, S. and Whitelaw, J., Premixed, turbulent combustion of a sudden-expansion flow, Combustion and Flame, 50, 153-165, 1983.

[Barrett,1994] Barrett, R., Berry, M., Chan, T.F., Demmel, J., Donato, J.M., Dongarra, J., Eijkhout, V., Pozo, R., Romine, C. and Vorst, H.V.D., Templates for the Solution of Linear Systems: Building Blocks for Iterative Methods, SIAM, Philadelphia, 1994.

[Bird,1960] Bird, R.B., Stewart, W.E. and Lightfoot, E.N., Transport Phenomena, John Wiley and Sons, 1960.

[Boussinesq,1877] Boussinesq, J., Essai sur la theorie des eaux courantes, Memoires presentes par divers savants a l'Academie des Sciences, 23 (1), 1-680, 1877.

[Bray-Swaminathan,2011] Swaminathan, N. and Bray K. N. C., Turbulent Premixed Flames, Cambridge University Press, 2011.

[Bray,Champion,2006] Bray, K.N.C., Champion, M., Libby, P.A. and Swaminathan, N., Finite rate chemistry and presumed PDF models for premixed turbulent combustion, Combustion and Flame, 146, 665-673, 2006.

[Bray-Libby,1993] Bray, K.N.C., Libby, P.A., Recent developments in the BML model of premixed turbulent combustion, Turbulent reacting flows, Academic Press, New York 1993.

[CardosoDeSouza,2010] Cardoso de Souza, T., Bastiaans, R.J.M., Geurts, B.J. and Goey, L.P.H. de, Numerical Analysis of a Swirl Stabilized Premixed Combustor with the Flamelet Generated Manifold approach, Proceedings of the Direct and Large - Eddy Simulation 8, Eindhoven, The Netherlands, 2010.

[CardosoDeSouza,2011] Cardoso de Souza, T., Bastiaans, R.J.M., Geurts, B.J. and Goey, L.P.H. de, Les and Rans of premixed combustion in a gas-turbine like combustor using the flamelet generated manifold approach, Proceedings of ASME Turbo Expo 2011 GT2011, Vancouver, Canada, 2011.

[CHEM1D-URL] http://www.combustion.tue.nl/flamecodes/chem1d/

[Chen,2014] Chen, G., Xiong, Q., Morris, P.J., Paterson, E.G., Sergeev, A. and Wang, Y., OpenFOAM for Computational Fluid Dynamics, Notices of the AMS, 61(4), 2014.

[Comsol-URL] http://www.comsol.com

[Davis,1959] Davis, P., Leonhard Euler's Integral: A Historical Profile of the Gamma Function, The American Mathematical Monthly, 66(10), 1959.

[DLR] COORETEC-turbo 2.1.4, Hochtemperaturverbrennung, Messkampagne Eigengeschlossene Jetflamme, Deutsches Zentrum für Luft und Raumfahrt.

[Donini,2013] Donini, A., Martin, S.M., Bastiaans, R.J.M., Oijen, J.A. van and Goey, L.P.H. de, High pressure jet flame numerical analysis of CO emissions by means of the flamelet generated manifolds technique, Proceedings of the 11th International Conference of Numerical Analysis and Applied Mathematics, Rhodos, Greece, 2013.

[Donini,2014] Donini, A., Advanced turbulent combustion modeling for gas turbine application, PhD thesis, 2014.

[Drake,1988] Drake, M.C. and Blint, R.J., Structure of Laminar opposed-flow diffusion flames with CO/H2/N2 fuel., Combustion Science Technoogy, 61, 187-224, 1988.

[vanDriest,1956] Driest, E.R. van, On turbulent flow near a wall, Journal of the Aeronautical Sciences, 23, 1007-1011, 1956.

[Ern-Giovangigli,1994] Ern, A. and Giovangigli, V., Multicomponent Transport Algortihms Lectures Notes in Physics, Series Monographs, Springer Verlag, Berlin, 1994.

[Fancello,2013] Fancello, A., Bastiaans, R.J.M. and Goey, L.P.H. de, Towards numerical simulation of turbulent hydrogen combustion in OpenFOAM, Proceedings of the American Institute of Physics, 1558, 168-171, 2013.

[Fancello,2014] Fancello, A., Panek, L., Lammel, O., Krebs, W., Bastiaans, R.J.M. and Goey, L.P.H. de, Turbulent combustion modeling using Flamelet Generated Manifolds for gas turbine applications in OpenFOAM, Proceedings of TurboExpo 2014, Dusseldorf, Germany, 2014.

[Favre,1969] Favre, A., Statistical equations of turbulent gases, Problems of hydrodynamics and continuum mechanics, 231-266, SIAM, Philadelphia, 1969.

[Ferziger-Peric,2002] Ferziger, J. H. and Peric, M., Computational Methods for Fluid Dynamics, Third Edition, Springer Verlag, Berlin, 2002.

[Germano-Piomelli,1991] Germano, M., Piomelli, U., Moin, P. and Cabot, W. H., A dynamic subgrid-scale eddy viscosity model, Physics of Fluids, A 3, 1760-1765, 1991.

[Germano,2000] Germano, M., Fundamentals of Large Eddy Simulation in Advanced Turbulent Flows Computations, edited by R. Peyret and E. Krause, pp. 81-130, Springer, 2000.

[deGoey-TenThijeBoonkkamp,1997] Goey, L.P.H. de and Thije Boonkkamp, J.H.M. ten, A mass based definition of flame stretch for flames with finite thickness, Combustion Science and Technology, 122, 399, 1997.

[deGoey-TenThijeBoonkkamp,1999] Goey, L.P.H. de and Thije Boonkkamp, J.H.M. ten, A Flamelet description of premixed laminar flames and the relation with flame stretch, Combustion and Flame, 119, 253-271, 1999.

[deGoey,2007] Goey, L.P.H. de, Hermanns, R.T.E. and Bastiaans, R.J.M., Analysis of the asymptotic structure of stoichiometric premixed CH4-H2-air flames, Proceedings of Combustion Institute, 31(1), 1031-1038, 2007.

[Goswami,2014] Goswami, M., Bastiaans, R.J.M., Konnov, A.A. and Goey, L.P.H. de, Laminar burning velocity of lean H2-CO mixtures at elevated pressure using the heat flux method, International Journal of Hydrogen Energy, 39, 1485-1498, 2014.

[Guo,2003] Guo, Z. M., Zhang, H. Q., Chan, C. K. and Lin W. Y., Presumed joint probability density function model for turbulent combustion, Fuel, 82, 1091-1101, 2003.

[Felippa,2001] Felippa, C. A., A Historical Outline of Matrix Structural Analysis: A Play in Three Acts, Computers and Structures, 79(14), 1313-1324, 2001.

[Hawken,1990] Hawken, D. M., Tamaddon-Jahromi, H. R., Townsend, P. and Webster, M. F., A Taylor-Galerkin based algorithm for viscous incompressible flow, International Journal for Numerical Methods in Fluids, 10, 327-351, 1990.

[Hirschfelder,1964] Hirschfelder, J.O., Curtis, C.F. and Bird, R.B., Molecular theory of gases and liquids, Wiley, New York, 1964.

[ICEM-CFD] http://www.ansys.com/

[ICON-URL] http://www.iconcfd.com/

[IGCC-project] http://www.h2-igcc.eu/

[Issa,1986] Issa, R. I., Solution of the Implicitly Discretized Fluid Flow Equation by Operator Splitting, Journal of Computational Physics, 62, 40-65, 1986.

[Joubert,1994] Joubert, W., PCG: a software package for the iterative solution of linear systems on scalar, vector and parallel computers, Proceedings of Scalable High-Performance Computing Conference, Knoxville, USA, 1994.

[Kaul,2009] Kaul, C. M., Raman, V.,Balarac, G. and Pitsch H., Numerical errors in the computation of subfilter scalar variance in large eddy simulations, Physics of Fluids, 21, 055102, 2009.

[Kaul,2011] Kaul, C.M. and Raman V., A posteriori analysis of numerical errors in subfilter scalar variance modeling for large eddy simulation, Physics of Fluids, 23, 2011.

[Kee,1986] Kee, R.J. and Miller, J.A., A structured approach to the computational modeling of chemical kinetics and molecular transport in flowing systems, Springer Series in Chemical Physics, 47, 1986.

[Kee,2003] Kee, R. J., Coltrin, M E. and Glarborg, P., Chemically Reacting Flow: Theory and Practice, John Wiley and Sons, 2003.

[Knudsen,2012] Knudsen, E., Richardson, E. S., Doran, E.M., Pitsch, H. and Chen J. H., Modeling scalar dissipation and scalar variance in large eddy simulation: Algebraic and transport equation closures, Physics of Fluids, 24, 055103, 2012.

[Kroger,2010] Kröger, H., Hassel, E., Nikolai, K. and Wendig D., LES of Premixed Flame Propagation in a Free Straight Vortex, Flow Turbulence and Combustion, 84, 513-541, 2010.

[Kumar,2011] Sashi Kumar, G.N., Mahendra, A.K. and Gouthaman, G., Understanding the Compatibility of Thermal Mass Flow Meter with Various Process Gases, Journal Chemical Engineering Process Technology, doi:10.4172/2157-7048.S1-002, 2011.

[Lam-Goussis,1991] Lam, S. H. and Goussis, D. A., Conventional asymptotics and computational singular perturbation for simplified kinetics modelling, in Reduced Kinetic Mechanisms and Asymptotic Approximations for Methane-Air Flames, Chapter 10: Conventional asymptotics and computational singular perturbation for simplified kinetics modeling, 227-242, ed. by Smooke, Springer Verlag, Berlin, 1991.

[Lammel,2010] Lammel, O., Schutz, H., Schmitz, G., Luckerath, R., Stohr, M., Noll, B., Aigner, M., Hase, M. and Krebs, W., Flox(r) combustion at high power densitiy and high flame temperatures, Journal of Engineering for Gas Turbines and Power, 132, 2010.

[Lammel,2011] Lammel, O., Stohr, M., Kutne, P., Dem, C., Meier, W. and Aigner, M., Experimental analysis of confined jet flames by laser measurement techniques, Journal of Engineering for Gas Turbines and Power, 134, 2011.

[Law,1988] Law, C. K., Cho, P., Mizomoto, M. and Yoshida, Flame curvature and preferential diffusion in the burning intensity of Bunsen flames, Proceedings of Combustion Institute, 21, 1803-1809, 1988.

[Law,1994] Law, C.K. and Faeth, G.M., Progress in energy combustion science, 20, 65-113, 1994.

[Law,2006] Law, C.K., Combustion Physics, Cambridge University Press, 2006.

[vanLeer,1991] Leer, B. van, Lee, W. T. and Roe, L., Characteristic time-stepping or local preconditioning of the Euler equations, American Institute of Aeronautics and Astronautics Journal, 91, 1991.

[LeVeque,2002] LeVeque, R., Finite Volume Methods for Hyperbolic Problems, Cambridge University Press, 2002.

[Nilsson,2008] Nilsson, H., Page, M., Beaudoin, M., Gschaider, B. and Jasak, H., The openfoam turbomachinery working group, and conclusions from the turbomachinery session of the third openfoam workshop, Proceeding of the 24th Symposium on Hydraulic Machinery and Systems October 27-31, Foz do Iguassu, Brazil, 2008.

[vanOijen,2000] Oijen, J.A. van and Goey, L.P.H. de, Modelling of premixed laminar flames using flamelet-generated manifolds, Combustion Science and Technology, 161, 113-137, 2000.

[VanOijen,2002-thesis] Oijen, J.A. van, Flamelet-generated manifolds: development and application to premixed laminar flames, PhD thesis, 2002.

[vanOijen,2002] Oijen, J.A. van and Goey, L.P.H. de, Modelling of premixed counterflow flames using the flamelet-generated manifold method, Combustion Theory Modelling, 6, 463-478, 2002.

[Ong,2012] Ong, R. H., King, A. J. C., Mullins, B. J., Cooper, T. F. and Caley M. J., Development and Validation of Computational Fluid Dynamics Models for Prediction of Heat Transfer and Thermal Microenvironments of Corals, PLoS One, 7(6), 2012.

[OpenFOAM-URL] http://www.openfoam.org

[Maas-Pope,1992] Maas, U. and Pope, S.B., Simplifying Chemical Kinetics: Intrinsic Low-Dimensional Manifolds in Composition Space, Combustion and Flame, 88, 239 - 264, 1992.

[Martin,2003] Martin, S.M., Kramlich, J.C., Kosaly, G. and Riley, J.J., The Premixed Conditional Moment Closure Method Applied to Idealized Lean Premixed Gas Turbine Combustors, Journal of Engineering for Gas Turbines and Power, 125(4), 895-900, 2003.

[Park,2013] Park, S., Park, S.W., Rhee, S.H., Lee, S.B., Choi, J-E and Kang, S.H., Investigation on the wall function implementation for the prediction of ship resistance, International journal naval architecture ocean engineering, 5, 33-46, 2013.

[Pashami,2010] Pashami, S., Asadi, S. and Lilienthal, A.J., Integration of openfoam flow simulation and filament-based gas propagation models for gas dispersion simulation, Proceedings of the Open Source CFD International Conference, 2010.

[Patankar,1972] Patankar, S.V. and Spalding, D.B., A calculation procedure for heat, mass and momentum transfer in three-dimensional parabolic flows,International journal of Heat and Mass Transfer, 15(10), 1787-1806, 1972.

[Peters,1991] Peters, N., Reducing Mechanisms, in Reduced kinetic mechanisms and asymptotic approximations for methane-air flames: a topical volume, edited by M. D. Smooke, Lecture Notes in Physics, 384, Springer-Verlag, Berlin, 1991.

[Peters,2000] Peters, N., Turbulent Combustion, Cambridge University Press, 2000.

[Piomelli,1999] Piomelli, U., Large-eddy simulation achievements and challenges, Progress in Aerospace Sciences, 35, 335-362, 1999.

[Poinsot-Veynante,2005] Poinsot, T. and Veynante D., Theoretical and Numerical Combustion, Second Edition, R.T. Edwards Inc., 2005.

[Pope,2000] Pope, S.B., Turbulent Flows, Cambridge University Press, 2000.

[Reynolds,1895] Reynolds, O., On the dynamical theory of incompressible viscous fluids and the determination of the criterion, Philosophical Transactions of the Royal Society of London, 186, 123-164, 1895.

[Rezaei,2013] Rezaei, F., Roohi Goolkhatmi, E. and Pasandideh Fard, M., Large Eddy Simulation of compressibile flow around naca 0012 airfoil at stall condition, Proceedings of Ankara International Aerospace Conference, 2013.

[Richardson,1922] Richardson, L. F., Weather Prediction by Numerical Process, Cambridge University Press, 1922.

[Roediger,2012] Roediger, T., Lammel, O., Aigner, M., Beck, C., W. and Krebs, W., Part load operation of a piloted flox(r) combustion system, Journal of Engineering for Gas Turbines and Power, 135, 2012.

[Ronney,1998] Ronney, P. D., Understanding Combustion Processes Through Microgravity Research, Proceedings of 27th International Symposium on Combustion, Boulder, USA, 1998.

[Sagaut,2000] Sagaut, P., Large Eddy Simulation for incompressible flows, Springer Verlag, Berlin, 2000.

[Smagorinsky,1963] Smagorinsky, J., General circulation experiments with the primitive equations, Monthly Weather Review, 91, 99-164, 1963.

[Smith,1999] Smith, G. P., Golden, D. M., Frenklach, M., Moriarty, N. W., Eiteneer, B., Goldenberg, M., Bowman, C. T., Hanson, R. K., Song, S., Gardiner Jr and W.C., Grimech 3.0, URL: http://www.me.berkeley.edu/gri mech, 1999.

[Smooke-Giovangigli,1991] Smooke, M.D. and Giovangigli, V., Formulation of the premixed and nonpremixed test problems, in Reduced kinetic mechanisms and asymptotic approximations for methane-air flames, edited by M.D. Smooke, pp. 128, Springer Verlag, Berlin, 1991.

[Somers,1994] Somers, L.M.T., The Simulation of Flat Flames with Detailed and Reduced Chemical Models PhD Thesis, 1994.

[Spalding,1961] Spalding, D.B., Mixing and chemical reaction in steady confined turbulent flames, Thirteenth symposium (international) on combustion, The Combustion Institute, 649-657, 1971.

[Towsend,1987] Townsend, P. and Webster, M. F., In Transient/Dynamic Analysis and constitutive Laws for Engineering Materials, Proceedings of the International Conference of Numerical Methods in Engineering: Theory and Applications-Numeta, 87(2), T12/1-11, 1987.

[Turkel,1987] Turkel, E., Preconditioned methods for solving the incompressible and low speed compressible equations, Journal of Computational Physics, 72, 277-298, 1987.

[Turkel,1997] Turkel, E., Radespiel, R. and Kroll, N., Assessment of preconditioning methods for multidimensional aerodynamics, Computers and Fluids, 26(6), 613-634, 1997.

[Versteeg,1995] Versteeg, H. and Malalasekera W., An introduction to computational fluid dynamics: the finite volume method, Longman Scientific and Technical, 1995.

[Vreman,2008] Vreman, A.W., Albrecht, B.A., Oijen, J.A. van, Goey, L.P.H. de and Bastiaans, R.J.M., Premixed and non-premixed generated manifolds in large-eddy simulation of Sandia flame D and F, Combustion and Flame, 153(3), 394-416, 2008.

[Vreman,2009] Vreman, A. W. , Oijen, J.A. van, Goey, L.P.H. de and Bastiaans, R.J.M., Subgrid Scale Modeling in Large-Eddy Simulation of Turbulent Combustion Using Premixed Flamelet Chemistry, Flow Turbulence Combustion, 82, 511-535, 2009.

[Warnatz,1996] Warnatz, J., Maas, U. and Dibble, R.W., Combustion, Springer Verlag, Berlin, 1996.

[Weller,1997] Fureby, C., Tabor, G., Weller, H. and Gosman, A.D., A Comparative Study of Sub Grid Scale Models in Homogeneous Isotropic Turbulence, Physics of Fluids, 9(5), 1416-1429, 1997.

[Whittaker,1967] Whittaker, E. T. and Robinson, G., The Error Function, The Calculus of Observations: A Treatise on Numerical Mathematics, 179-182, Ed. New York Dover, 1967.

[Wikki-URL] http://www.wikki.co.uk/

[Wilke,1950] Wilke, C. R., A viscosity equation for gas mixture, Journal of Chemical Physics, 18, 1950.

[Williams,1958] Williams, F. A. The conservation equations for multicomponent gas mixtures in arbitrary coordinate systems, Journal of the Aeronautical Sciences, 25(5), 343, 1958.

[Williams,1985] Williams, F. A., Combustion Theory 2nd edition, Addison-Wesley, 1985.

[Xisto,2010] Xisto, C.M., Pascoa, J.C., Oliveira, P.J. and Nicolini, D.A., Implementation of A 3D Compressible Mhd Solver able to model transonic flows, Proceedings of 5th European Conference on Computational Fluid Dynamics, Eccomas CFD, 2010.

Nomenclature

Latin Symbols

$\mathbf{g}$	gravitational acceleration field $[m \cdot s^{-2}]$
$\mathbf{q}$	heat flux $[J \cdot m^{-2} s^{-1}]$
$\mathbf{u}, \mathbf{U}$	velocity of the flow field $[m \cdot s^{-1}]$
$\mathbf{u}_f$	velocity of flame surface $[m \cdot s^{-1}]$
a	applied strain rate $[s^{-1}]$
A_c	pre-exponential constant $[-]$
c_p	heat capacity at constant pressure $[J \cdot kg^{-1} \cdot K^{-1}]$
c_v	heat capacity at constant volume $[J \cdot kg^{-1} \cdot K^{-1}]$
D	diffusion coefficient $[m^2 \cdot s^{-1}]$
D_{im}	mixture-averaged diffusion coefficient $[m^2 \cdot s^{-1}]$
e	specific energy $[J \cdot kg^{-1}]$
E_a	activation energy $[J \cdot mol^{-1}]$
erf	error function $[-]$
h	enthalpy $[m^2 \cdot s^{-2}]$
K	mass-based stretch rate $[s^{-1}]$

k reaction rate coefficient $[-]$

K_A area stretch rate $[s^{-1}]$

Ka Karlovitz number $[-]$

Ka_t turbulent Karlovitz number $[-]$

$l_{\mathrm{c/o}}$ cut-off length scale $[m]$

l_o integral length scale $[m]$

Le Lewis number $[-]$

M molar mass $[kg \cdot mol^{-1}]$

m mass burning rate $[kg \cdot m^{-2} \cdot s^{-1}]$

Ma Mach number $[-]$

n molar concentration $[mol \cdot m^{-3}]$

N_s number of species $[-]$

p pressure $[Pa]$

p_i partial pressure $[Pa]$

PV progress variable $[-]$

R curvature radius $[m]$

R^0 gas universal constant $J \cdot mol^{-1}K^{-1}]$

Re Reynolds number $[-]$

s coordinate perpendicular to flame surface $[m]$

s_A, s_L laminar burning velocity $[m \cdot s^{-1}]$

Sc Schmidt number $[-]$

Sc_t turbulent Schmidt number $[-]$

t time $[s]$

T temperature $[K]$

X_i species mole fraction $[-]$

x_i spatial coordinate in the i direction $[m]$

x_k grid coordinate in the k direction $[m]$

Y_i species mass fraction $[-]$

Z_i mixture fraction $[K]$

$\mathscr{A}_i$ chemical symbol for species i [-]

$\mathscr{H}$ enthalpy flux $[J \cdot m^{-2} \cdot s^{-1}]$

$\mathscr{M}$ Markstein number $[-]$

$\mathscr{Y}$ general scalar variable $[-]$

Greek Symbols

β temperature exponent $[-]$

Δ filter width $[m]$

δ_f flame thickness $[m]$

δ_r reaction layer $[m]$

$\dot{\omega}_i$ chemical source term $[kg \cdot m^{-3} \cdot s^{-1}]$

$\dot{\omega}_{\mathscr{Y}}$ scalar source term $[s^{-1}]$

η Kolmogorov length scale $[m]$

Γ Gamma function $[-]$

κ curvature of the flame surface $[m^{-1}]$

λ thermal conductivity $[W \cdot K^{-1} \cdot m^{-1}]$

μ dynamic viscosity $[kg \cdot m^{-1} \cdot s^{-1}]$

μ_t turbulent eddy viscosity $[kg \cdot m^{-1} \cdot s^{-1}]$

ν kinematic viscosity $[m^2 \cdot s^{-1}]$

ν'_{li}, ν''_{li} molar stoichiometric coefficient [-]

$\overline{\xi}$ Averaged quantity

ϕ equivalence ratio $[-]$

ρ density $[kg \cdot m^{-3}]$

σ area field $[m^2]$

τ_k Kolmogorov time scale $[-]$

$\widetilde{\xi}$ Favre filtering quantity

ξ'' Fluctuating quantity

$\boldsymbol{\tau}$ viscous stress tensor $[kg \cdot m^{-1} \cdot s^{-2}]$

Miscellaneous

Δt time step $[s]$

Δx grid spacing $[m]$

Subscript

ad adiabatic condition

b burnt region

i species index

il inner layer

l reaction layer

M mass based

u unburnt region

Superscript

0 no stretched condition

Appendix A - Laminar flow calculations

Comparison between OpenFOAM ® and Comsol Multiphysics with $\rho = const$

The purpose of this part is to show a comparison of results between OpenFOAM ® and Comsol Multyphysics [Comsol-URL]. These calculations are done with incompressible flow. The purpose of this comparison is to show the differences in results between an open source and a commercial software. These solvers differ for the discretization method: OpenFOAM ® uses the Finite Volume Method (FVM) approach [LeVeque,2002] while Comsol uses the Finite Element Method (FEM) [Felippa,2001] one. The manifold data which are taken into account in this calculations are only the progress variable and the source term. This is performed in order to be consistent with the results available from Comsol Multiphysics. The diffusion coefficient for the progress variable is considered as a constant value in the simulation and its value is set to $1.8 \cdot 10^{-5}\ m^2/s$.

As a temporary assumption, the real density change in the flame front is not taken into account, resulting in considering the density of the flow constant along the flame structure. This is not correct from the physical point of view. This assumption is used for a comparison purpose. Of course, Comsol Multiphysics simulations have been performed with the same approximation. By imposing a constant density results in a mere simplification. In fact, as evident in combustion, a fresh mixture, i.e. the unburnt zone of the flame, is affected by a higher density respect to the burnt gas zone. As a result, the flow should be affected by this density variation which occurs along the flame front and, therefore, the transport of the quantities should be also affected by this density change. Evidently, this aspect should be included in the features of the solver. By keeping this temporary assumption in mind, as a preliminary work, the density is temporarily considered constant.

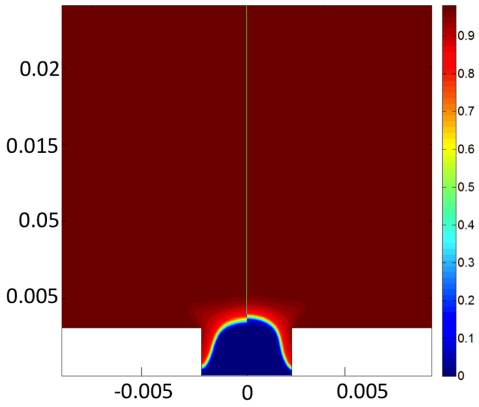

(a) Open FOAM (left) and Comsol (right) after a time of $t = 0.015\ s$

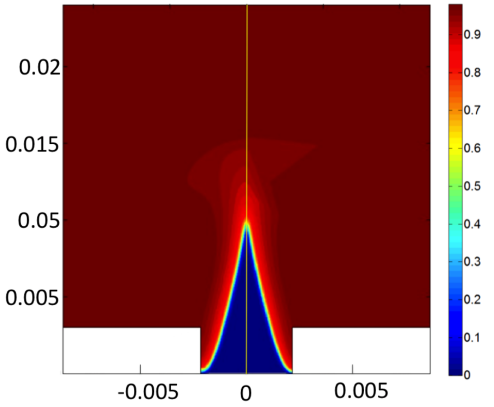

(b) Open FOAM (left) and Comsol (right) with stabilized flame

Figure 1: Comparison between Open FOAM (left) and Comsol (right) with the transient and stabilized flame.

Table 1: Grid size of different calculations. Dimensions are in m.

Name of the grid	Grid size Δx
a	$8 \cdot 10^{-4}$
b	$4 \cdot 10^{-4}$
c	$2 \cdot 10^{-4}$
d	$1 \cdot 10^{-4}$
e	$2.5 \cdot 10^{-5}$
f	$1.87 \cdot 10^{-5}$

Figure 1a shows a comparison between the results obtained with OpenFOAM ® on the left side, and Comsol, on the right side. This result is captured during the transient of the flame, before its stabilization. Beside a small difference from the result in the left side, it is evident that the two outputs are not so different.

As represented in Figure 1b, a comparison of the stationary solution is provided. It can be observed that the flame height, given by OpenFOAM ® and Comsol, are essentially the same and, therefore, it is evident that both results are alike.

In addition to this comparison, a grid refinement is proposed here. A series of different grids have been applied in the OpenFOAM ® and Comsol calculations as listed in Table 1:

The examination of the spatial convergence of a simulation is a straightforward method for determining the order of discretization error in the CFD simulation [Ferziger-Peric,2002] [Anderson,1984].

The height error is here defined as the root square of the difference between the finest grid result flame height with respect to the height obtained with the other grids:

$$\mathrm{Err} = \sqrt{y_{\mathrm{ref}} - y_i}. \tag{1}$$

The reference height is $y_{\mathrm{ref}} = 0.99001\ cm$, by using the grid size f (from Table 1)

The error is normalized, by dividing its value to a reference length l_{ref}, defined as the half width of the inlet, which is 3 mm:

$$\mathrm{Err}_{\mathrm{normalized}} = \frac{\mathrm{Err}}{l_{\mathrm{ref}}}. \tag{2}$$

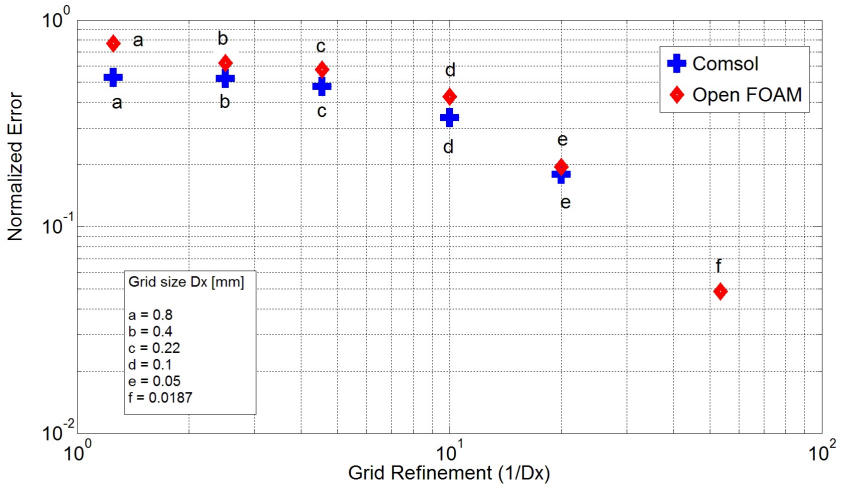

Figure 2: Discretization error plot of the Y coordinate respect to the finest mesh.

From the grid resolution study, an impression of the discretization error, respect to the finest grid result ($\Delta x = 0.0187\ mm$), is given in Figure 2.

Compressible solver

As explained in Chapter 4, an implementation of this PIMPLE algorithm for a compressible application is explained in [Xisto,2010] [Ong,2012] [Aguerrea,2013]. As already known, the SIMPLE algorithm is used to solve steady-state problems where the treatment of the non-linear effects of the velocity during the resolution is more important than the precise determination of the pressure field. As each iteration is equivalent to a pseudo time step, the properties are under relaxed in order to stabilize the method and improve convergence. On the other hand, the PISO algorithm is suitable for transient simulations where it is necessary to fully solve the velocity-pressure coupling for each time step. The non-linear effects of the velocity are reduced

setting small time steps characterized by Courant numbers below one. In transient compressible cases, the error due to the non-linear effects of the velocity are more important because of the compressibility. Therefore, the momentum equation is located in an outer loop named PIMPLE and the momentum balance can be recalculated many times as number of PIMPLE iterations [Aguerrea,2013]. The energy equation can be located in the PIMPLE loop or either in the PISO loop. When a thermodynamic property (temperature, density or pressure) vary rapidly in time, the energy equation should be located inside the PISO loop in order to improve the pressure-temperature coupling [Aguerrea,2013].

A scheme of the PIMPLE algorithm, as proposed by [Aguerrea,2013], is shown in Figure 3.

The coupling of the solver with the FGM implementation is performed in the following steps:

- A *look-up* system reads the variables of the manifold and interpolates them.
- A *thermophysical library*, based on compressibility, calculates the temperature T based on the energy equation and it updates the value with the manifold values. Thermophysical models are concerned with the energy, heat and physical properties.

  The *thermophysicalProperties* dictionary is read by any solver that uses the thermophysical model library. The thermophysical modelling starts with a layer that defines the basic equation of state and then adds more layers of modelling that derive properties from the previous layer(s).[OpenFOAM-URL].
- Density ρ cannot be imposed in the calculation, but it is obtained by using the T value and retrieving ρ from the gas law.

Chem1D - Lewis constant

As presented in Chapter 4 for $Le = 1$, a Lewis constant transport approach is proposed here, in order to show the differences with $Le = 1$ case. In Figure 4, a few variables from this 2D manifold calculations, are proposed. As shown in Figure 4a, each enthalpy level is not straight, as for the $Le = 1$ case, but locally changes due to preferential diffusion effects.

Grid convergence

From the 2D-FGM stationary solution proposed in Chapter 4, a grid convergence study is here proposed. A grid convergence graph is shown in Figure 5. The standard grid is composed by 17400 element. The two refinements are performed respectively with 69600 elements and 278400 elements. The convergence is studied along the symmetry line, between $y = 0$ and $y = 11$ mm. A good convergence is already achieved with the middle size grid.

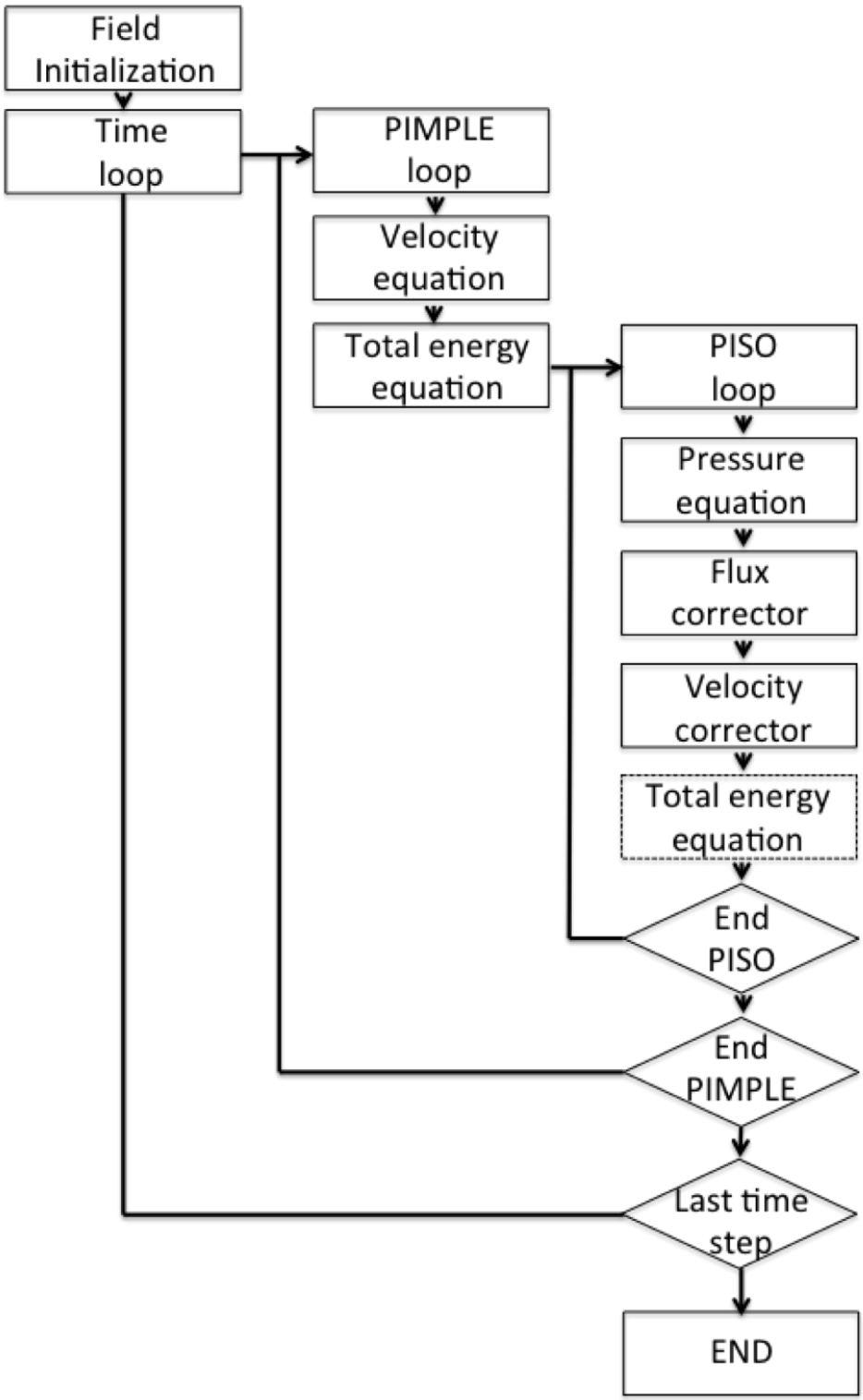

Figure 3: Scheme of PIMPLE algorithm as proposed by [Aguerrea,2013].

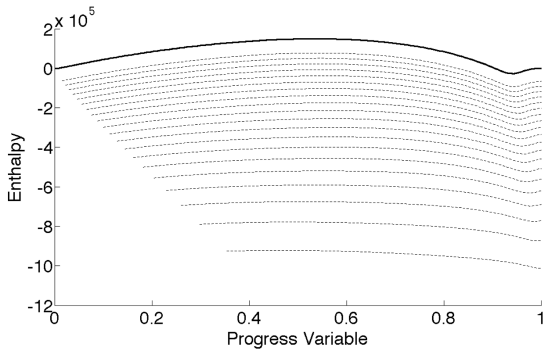

(a) Enthalpies level

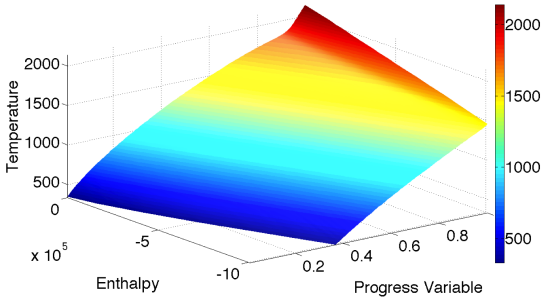

(b) Temperature

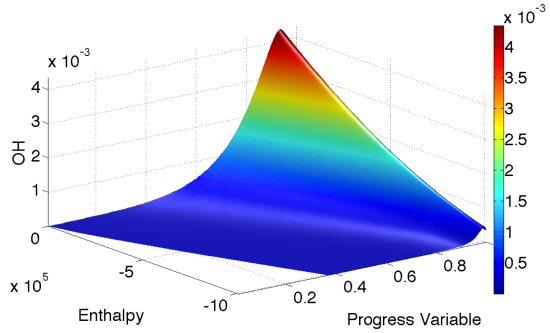

(c) *OH*

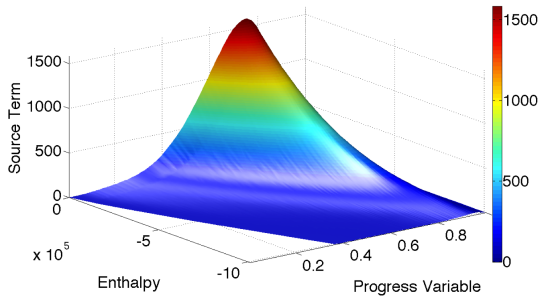

(d) Source term

Figure 4: Overview of different variables calculated from a 2D manifold. Fuel: pure methane with $\phi = 0.9$. Controlling variables: $\mathscr{Y}_{O_2}$ and h. Transport approach: $Le = 1$ constant.

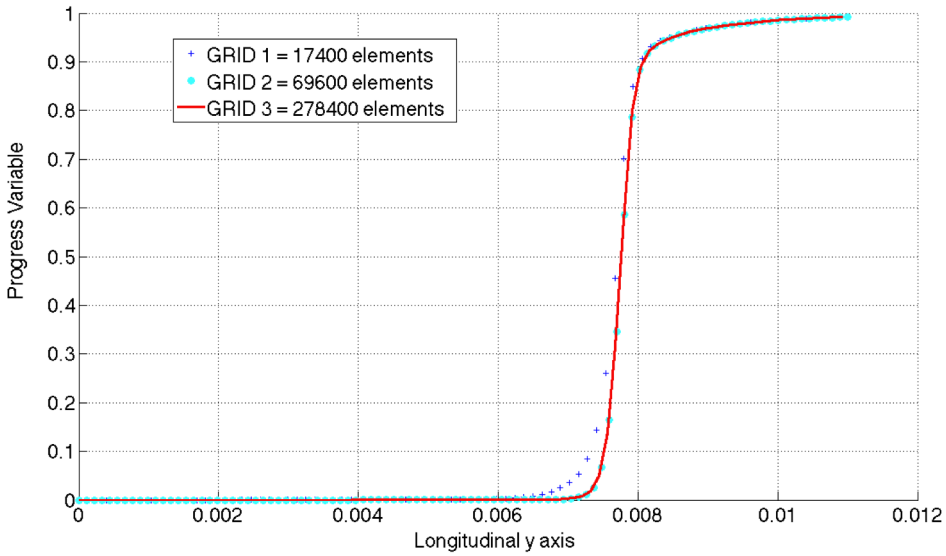

Figure 5: Grid convergence of progress variable $\mathscr{Y}_{O_2}$ along a line placed in the y axis, between 0 and 11 *mm*.

Appendix B - Sudden expansion flow calculations

The following part provides an exhaustive illustration of the results described in Chapter 7, which have not been completely illustrated.

Iso-contours

Figures 6 and 7 show the root mean square of velocity field. Field values are satisfactorily predicted. However, the iso-contour distributions do not match the experimental results correctly in any case.

Figures 8 - 13 illustrate the iso-contours for O_2, CO_2 and CO molar fraction. The main differences which appear in these results are between heat loss and adiabatic approaches, due to the different distribution of the species in the domain. The species distribution is similar to the temperature distribution, since the values of the species are retrieved from the manifold and they are therefore consistent with the temperature iso-contours. In particular, in RANS-1 results for O_2 and CO_2, a steep gradient is present as was shown for the temperature iso-contours. The same considerations made about the flame length based on temperature iso-contours can be extended to the analysis of O_2 and CO_2 molar fractions iso-contours, as will be discussed further on. Regarding O_2 and CO_2 values, they are consistent with the experimental data in terms of minimum and maximum value, while CO molar fraction shows an over-prediction of the values with respect to the experimental data: highest CO molar fraction values are located across the flame front as expected, but their values are almost twice.

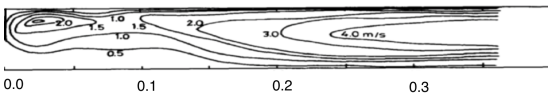

(a) El Banhawy et al. experimental results

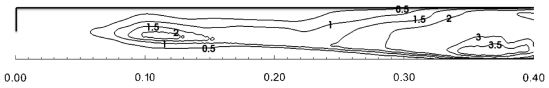

(b) RANS-1 simulation - Parabolic velocity profile

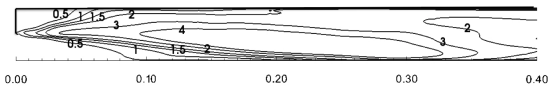

(c) RANS-2 simulation - Constant velocity profile

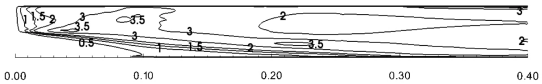

(d) LES-1 simulation - Parabolic velocity profile

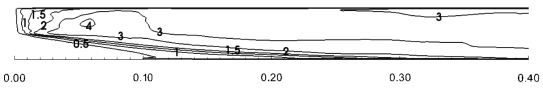

(e) LES-2 simulation - Constant velocity profile

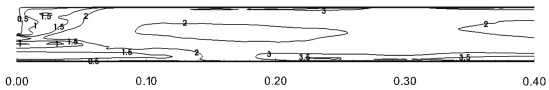

(f) LES-3 simulation - mapped profile

Figure 6: Isocontours of root mean square of U. Comparisons of different simulations using the heat loss approach with [Banhawy,1983].

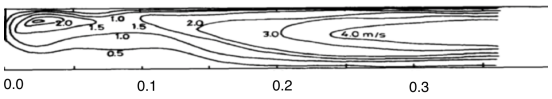

(a) El Banhawy et al. experimental results

(b) Martin et al. numerical results

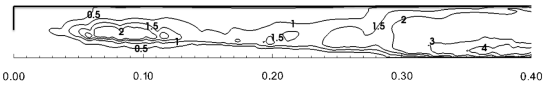

(c) RANS-1 simulation - Parabolic velocity profile

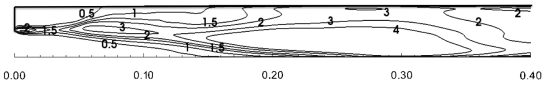

(d) RANS-2 simulation - Constant velocity profile

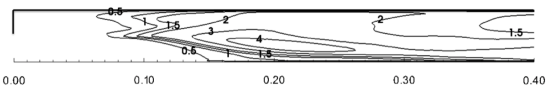

(e) LES-2 simulation - Constant velocity profile

Figure 7: Isocontours of root mean square of U. Comparisons of different simulations using an adiabatic approach with [Banhawy,1983] and [Martin,2003].

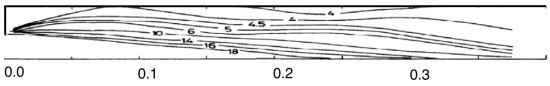

(a) El Banhawy et al. experimental results

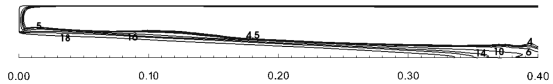

(b) RANS-1 simulation - Parabolic velocity profile

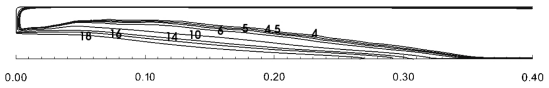

(c) RANS-2 simulation - Constant velocity profile

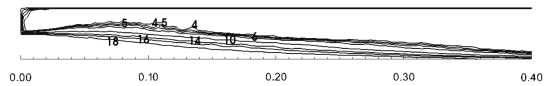

(d) LES-1 simulation - Parabolic velocity profile

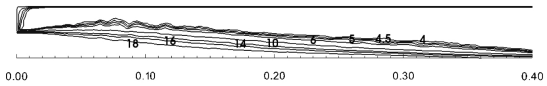

(e) LES-2 simulation - Constant velocity profile

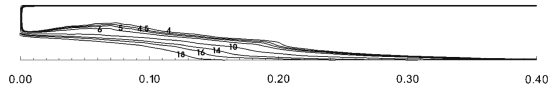

(f) LES-3 simulation - mapped profile

Figure 8: Isocontours of mean O_2 molar fraction. Comparisons of different simulations using the heat loss approach with [Banhawy,1983].

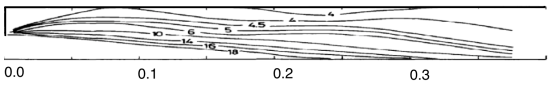

(a) El Banhawy et al. experimental results

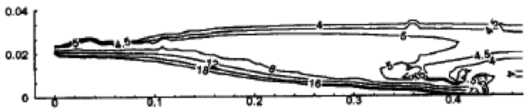

(b) Martin et al. numerical results

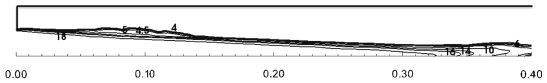

(c) RANS-1 simulation - Parabolic velocity profile

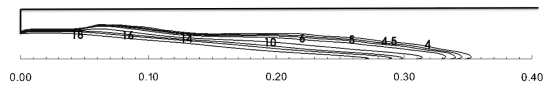

(d) RANS-2 simulation - Constant velocity profile

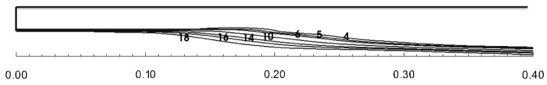

(e) LES-2 simulation - Constant velocity profile

Figure 9: Isocontours of O_2 molar fraction. Comparisons of different simulations using an adiabatic approach with [Banhawy,1983] and [Martin,2003].

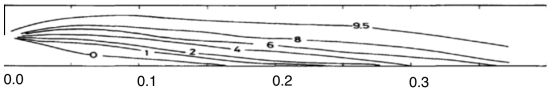

(a) El Banhawy et al. experimental results

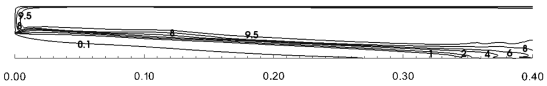

(b) RANS-1 simulation - Parabolic velocity profile

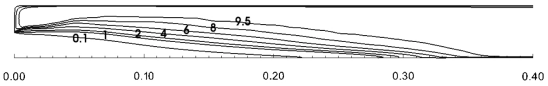

(c) RANS-2 simulation - Constant velocity profile

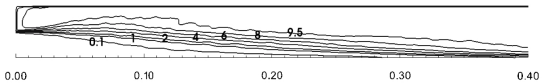

(d) LES-1 simulation - Parabolic velocity profile

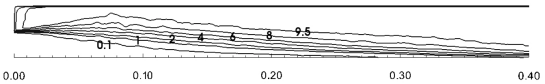

(e) LES-2 simulation - Constant velocity profile

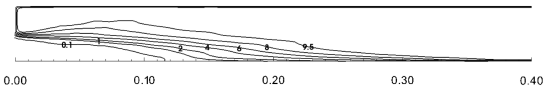

(f) LES-3 simulation - mapped profile

Figure 10: Isocontours of mean CO_2 molar fraction. Comparisons of different simulations using the heat loss approach with [Banhawy,1983].

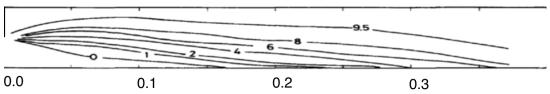

(a) El Banhawy et al. experimental results

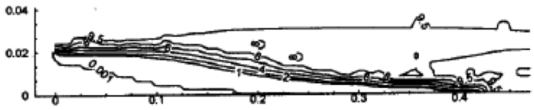

(b) Martin et al. numerical results

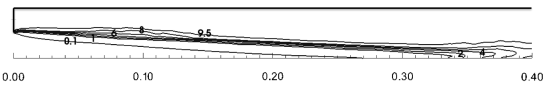

(c) RANS-1 simulation - Parabolic velocity profile

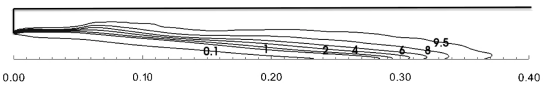

(d) RANS-2 simulation - Constant velocity profile

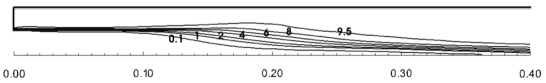

(e) LES-2 simulation - Constant velocity profile

Figure 11: Isocontours of CO_2 molar fraction. Comparisons of different simulations using an adiabatic approach with [Banhawy,1983] and [Martin,2003].

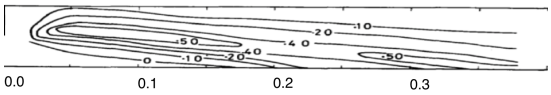

(a) El Banhawy et al. experimental results

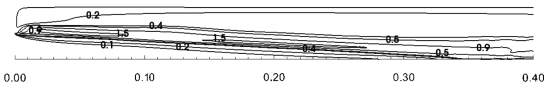

(b) RANS-1 simulation - Parabolic velocity profile

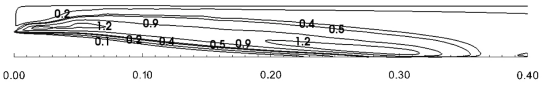

(c) RANS-2 simulation - Constant velocity profile

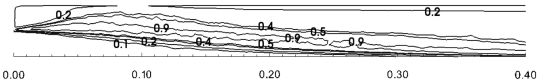

(d) LES-1 simulation - Parabolic velocity profile

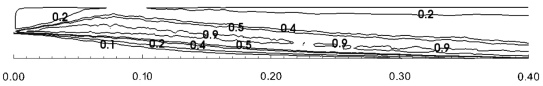

(e) LES-2 simulation - Constant velocity profile

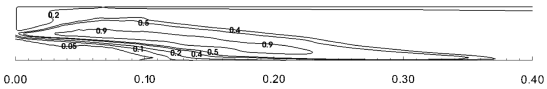

(f) LES-3 simulation - mapped profile

Figure 12: Isocontours of mean *CO* molar fraction. Comparisons of different simulations using the heat loss approach with [Banhawy,1983].

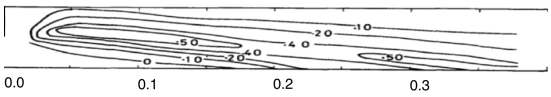

(a) El Banhawy et al. experimental results

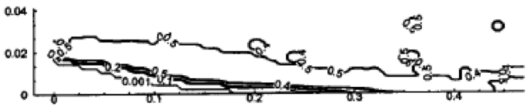

(b) Martin et al. numerical results

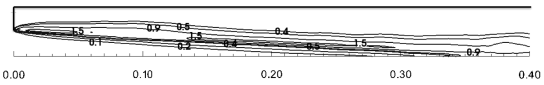

(c) RANS-1 simulation - Parabolic velocity profile

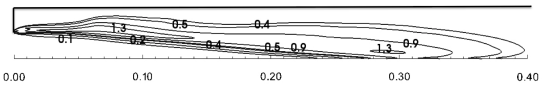

(d) RANS-2 simulation - Constant velocity profile

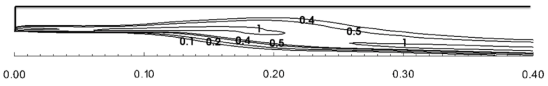

(e) LES-2 simulation - Constant velocity profile

Figure 13: Isocontours of *CO* molar fraction. Comparisons of different simulations using an adiabatic approach with [Banhawy,1983] and [Martin,2003].

Flame length estimation

In this Section, the results of RANS-1, LES-1 and LES-2 regarding the flame length estimations are illustrated (see Figures 14-16), as already introduced in Chapter 7, Section 7.6.4.

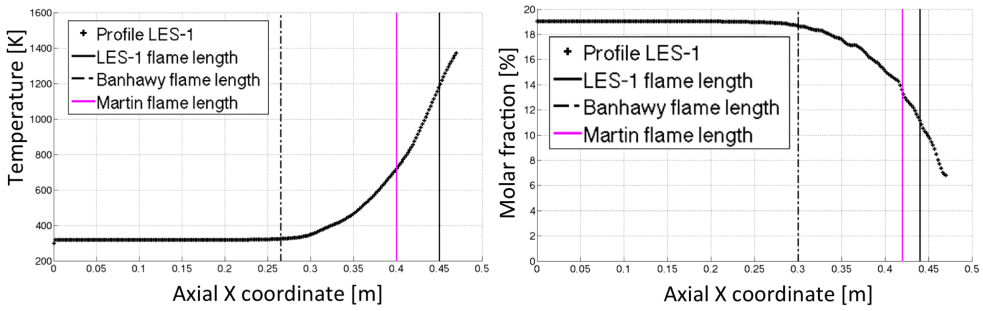

(a) LES-1 case with heat loss - Temperature profiles

(b) LES-1 case with heat loss - X_{O_2} profiles

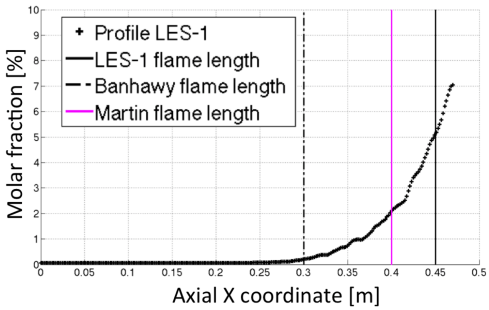

(c) LES-1 case with heat loss - X_{CO_2} profiles

Figure 14: LES-1 case. Estimation of flame length using T, X_{O_2} and X_{CO_2}. Comparison of different simulations with [Banhawy,1983] and [Martin,2003] flame lengths.

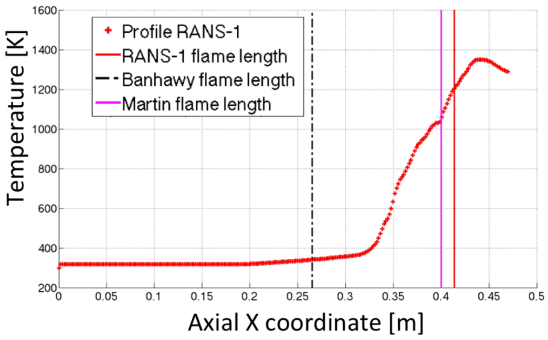

(a) RANS-1 case with heat loss - Temperature profiles

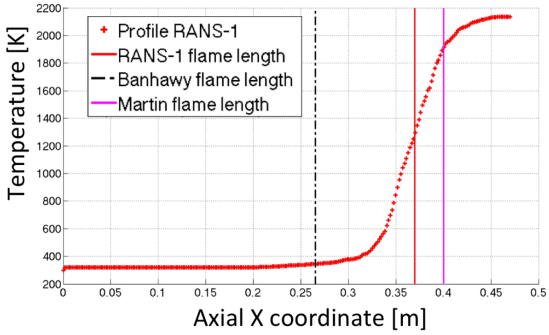

(b) RANS-1 adiabatic case - Temperature profiles

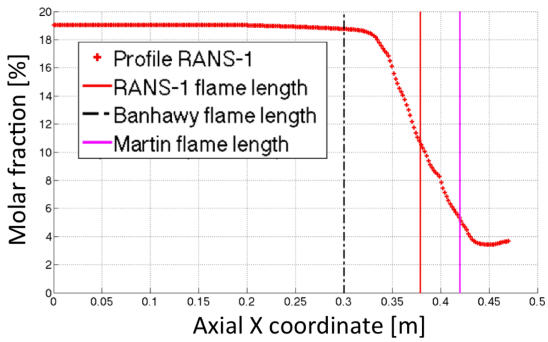

(c) RANS-1 case with heat loss - X_{O_2} profiles

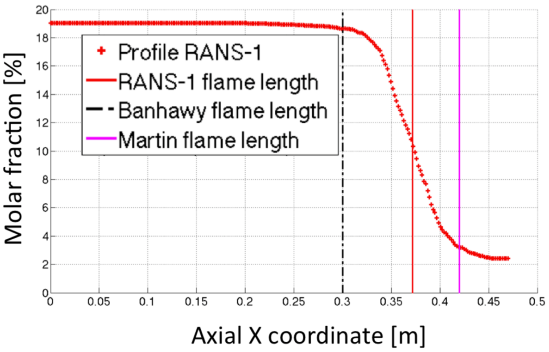

(d) RANS-1 adiabatic case - X_{O_2} profiles

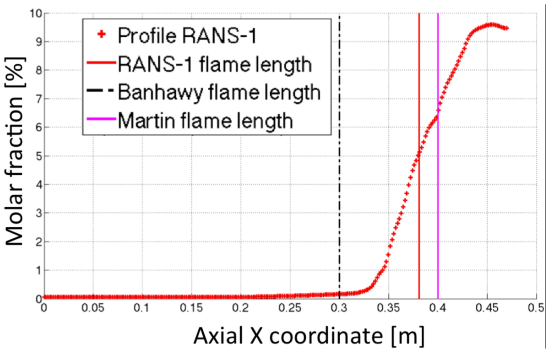

(e) RANS-1 case with heat loss - X_{CO_2} profiles

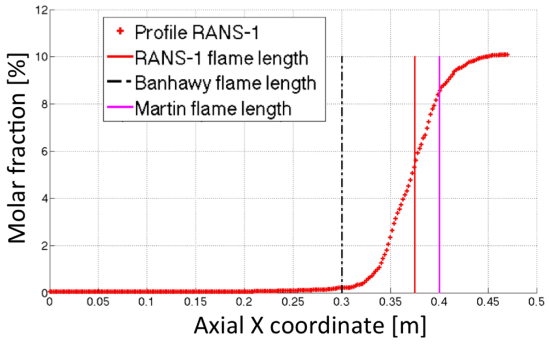

(f) RANS-1 adiabatic case - X_{CO_2} profiles

Figure 15: RANS-1 case. Estimation of flame length using T, X_{O_2} and X_{CO_2}. Comparison of different simulations with [Banhawy,1983] and [Martin,2003] flame lengths.

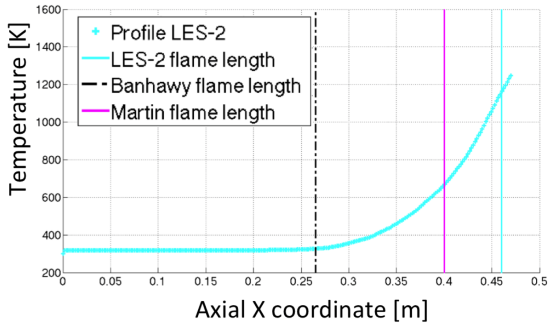

(a) LES-2 case with heat loss - Temperature profiles

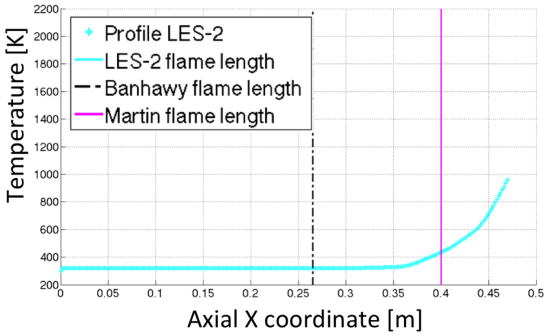

(b) LES-2 adiabatic case - Temperature profiles

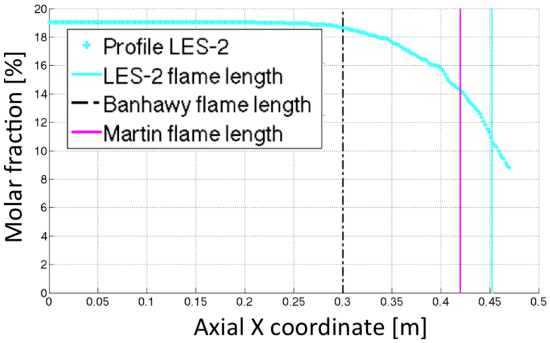

(c) LES-2 case with heat loss - X_{O_2} profiles

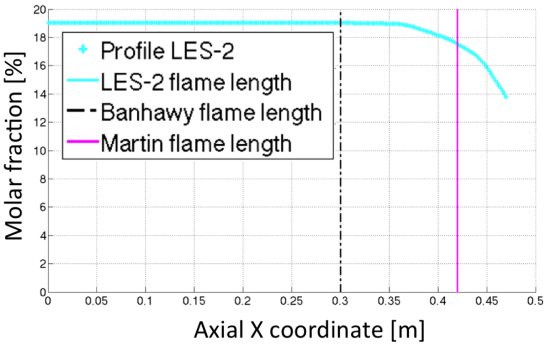

(d) LES-2 adiabatic case - X_{O_2} profiles

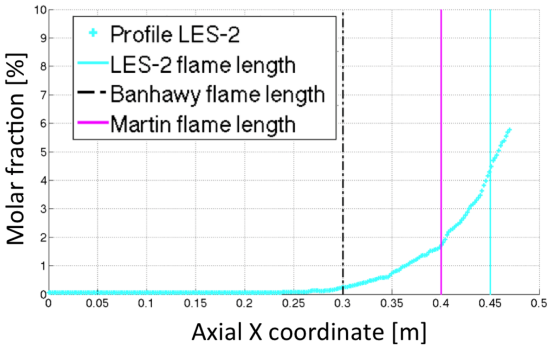

(e) LES-2 case with heat loss - X_{CO_2} profiles

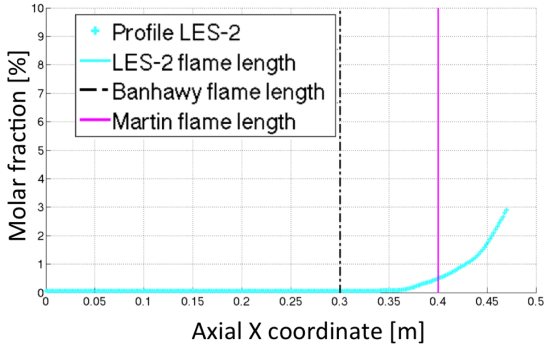

(f) LES-2 adiabatic case - X_{CO_2} profiles

Figure 16: LES-2 case. Estimation of flame length using T, X_{O_2} and X_{CO_2}. Comparison of different simulations with [Banhawy,1983] and [Martin,2003] flame lengths.

Statistical analysis of LES-4 results

A statistical analysis of the transient simulation LES-4 is presented here, as introduced in Chapter 7. This analysis is developed to show the time signals of the velocity field and the statistical convergence. 12 points placed in the middle plane perpendicular to the z direction are used as probes for the signal sampling. Figure 17 shows the points distribution while Figure 18 gives the exact coordinates of these points in the expansion area (no points are considered in the inlet channel).

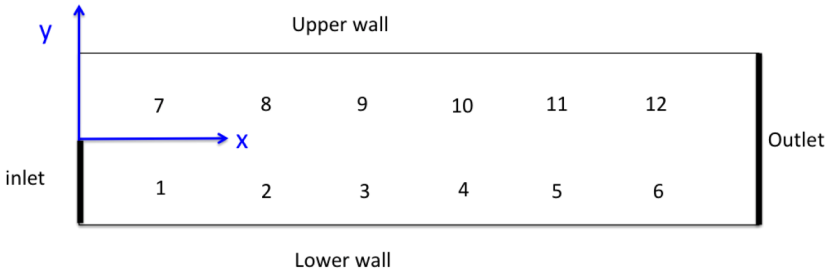

Figure 17: Scheme of different points used for the statistical analysis.

Point	Coordinate (x,y)
1	(0.0392,-0.01)
2	(0.1176,-0.01)
3	(0.196,-0.01)
4	(0.2744,-0.01)
5	(0.3528,-0.01)
6	(0.4312,-0.01)
7	(0.0392,0.01)
8	(0.1176,0.01)
9	(0.196,0.01)
10	(0.2744,0.01)
11	(0.3528,0.01)
12	(0.4312,0.01)

Figure 18: Points Locations coordinates.

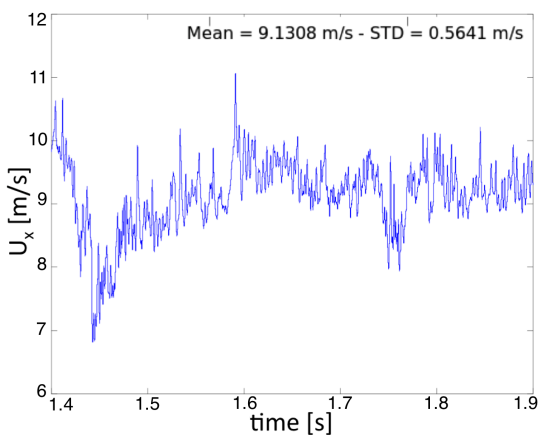

(a) Point 1

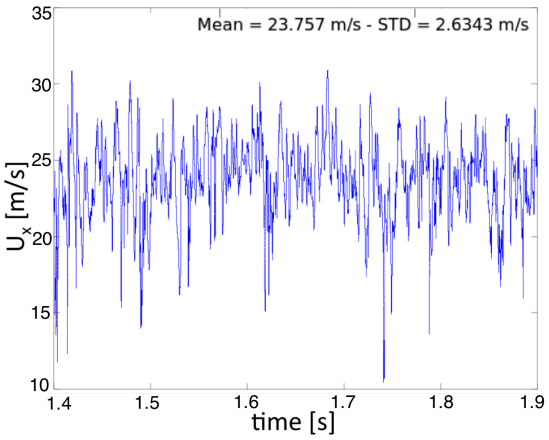

(b) Point 4

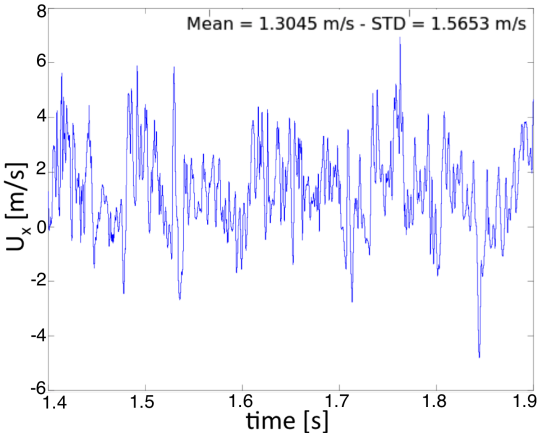

(c) Point 7

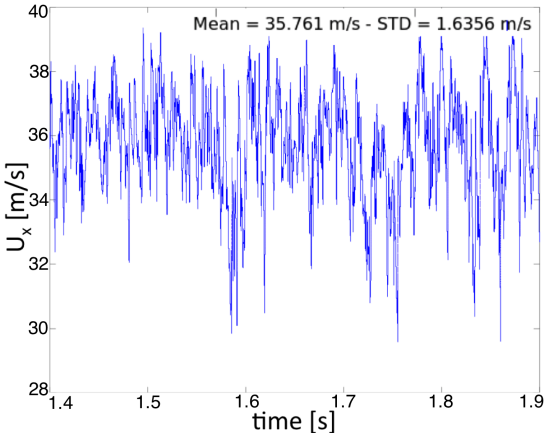

(d) Point 12

Figure 19: U_x time signals for 4 different points (see figure 18) - LES-4 case.

Time signals

For the sake of simplicity, only 4 points are going to be presented in the analysis: point 1, 4, 7 and 12. Point 1 is placed after the inlet, point 4 in a region very close to the flame front, point 7 in the recirculation region and, finally, point 12 is placed very close to the upper outlet region. Time signals are presented for the three velocity components in Figures 19-21 for the interval time 1.4 - 1.9 seconds. The signals in these points show a fully developed and converged flow.

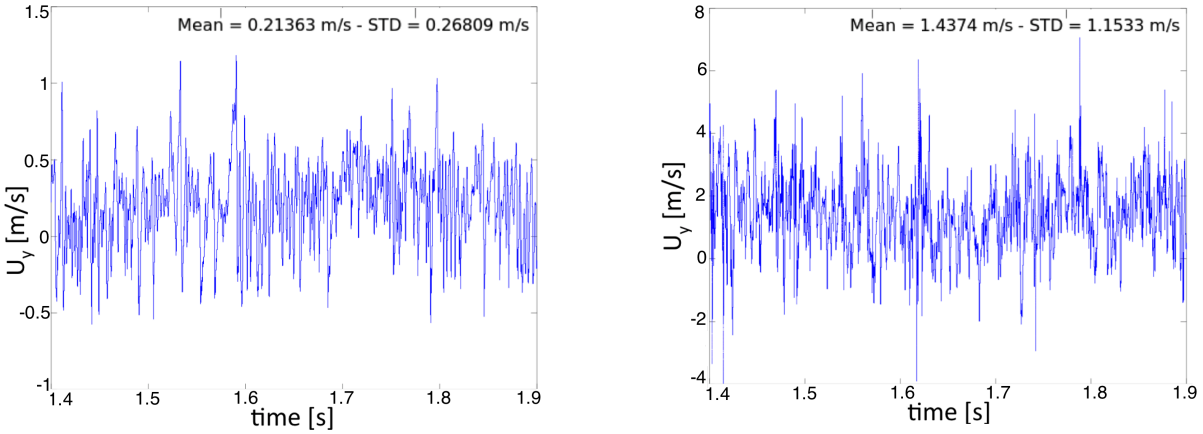

(a) Point 1

(b) Point 4

(c) Point 7

(d) Point 12

Figure 20: U_y time signals for 4 different points (see figure 18) - LES-4 case.

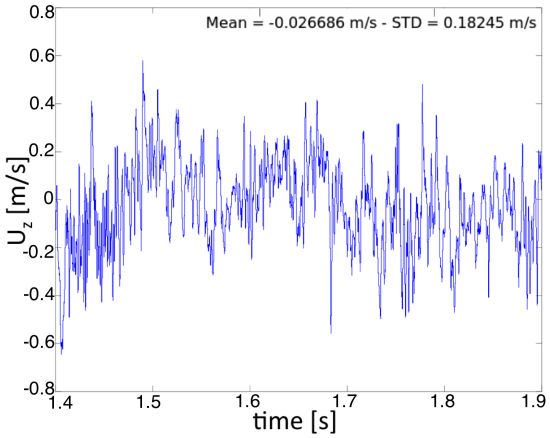

(a) Point 1

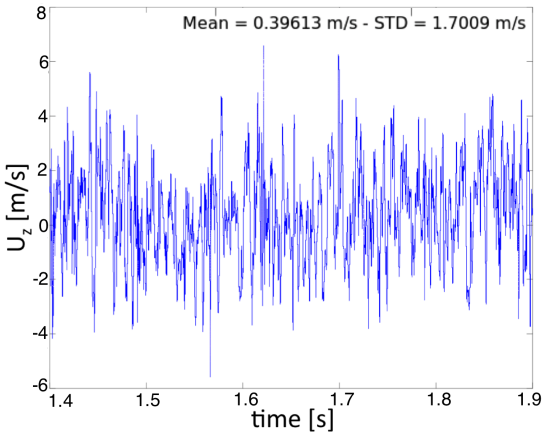

(b) Point 4

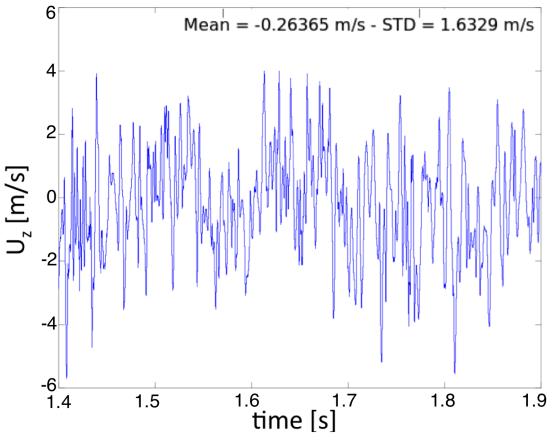

(c) Point 7

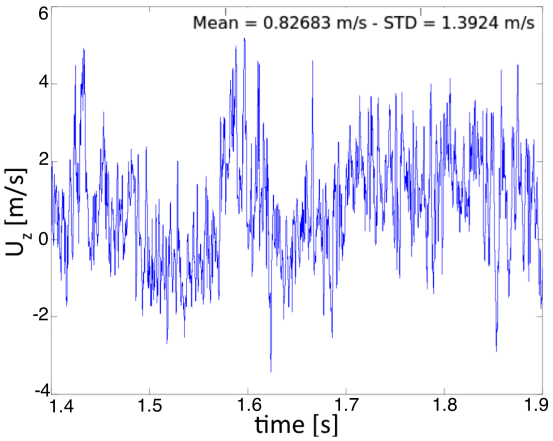

(d) Point 12

Figure 21: U_z time signals for 4 different points (see figure 18) - LES-4 case.

Statistical convergence

Statistical convergence of a certain quantity is achieved once its time averaged signal stabilizes to a certain value, with increasing the averaging time. In order to apply this concept, three different time intervals have been considered for which the time averages have been calculated over increasing sub-periods: 0.7-1.2 s, 1.2-1.7 s and 1.4-1.9 s. All the intervals are 0.5 s long; the first 0.7 s (about 14 flow times) of the simulations have been neglected since signals pass through transient behavior. Each interval has been subdivided into 1000 uniform smaller periods $\mathscr{T}$.

For each of these smaller periods, the time averaged quantity $\overline{f}$ has been calculated by adopting the following formula:

$$\overline{f} = \frac{1}{\mathscr{T}} \int_{t_0}^{t_0+\mathscr{T}} f(t)dt \approx \frac{\Delta t}{\mathscr{T}} \sum_{k=1}^{\mathscr{T}/\Delta t} f_k, \tag{3}$$

where Δt is the integration time step (5×10^{-7} s) and t_0 the initial time of averaging (0.7, 1.2, 1.4 s).

The statistical convergence of U_x is illustrated for the three different time intervals in Figure 22 for the points 1, 4, 7 and 12. For all points, it is evident that the convergence is reached after a time of 0.4 seconds for each considered interval.

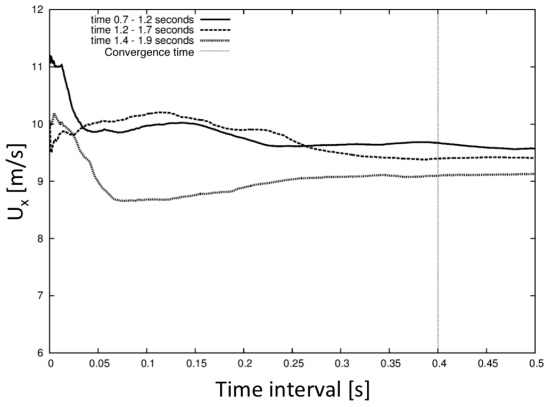

(a) Point 1

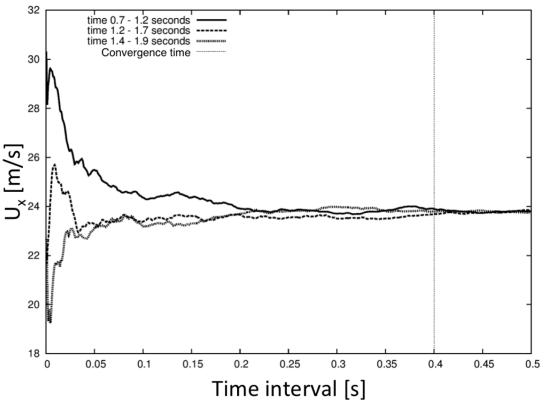

(b) Point 4

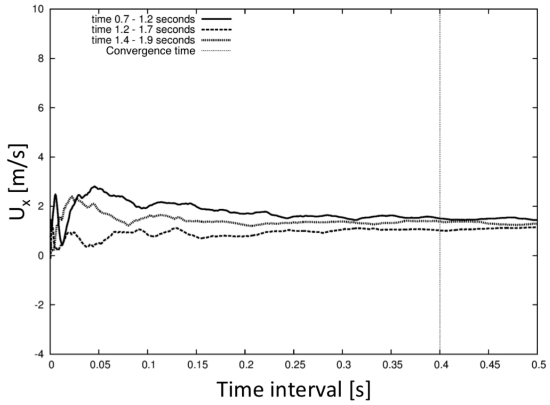

(c) Point 7

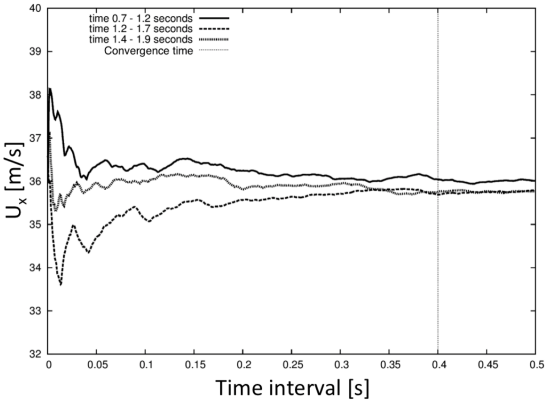

(d) Point 12

Figure 22: U_x stastistical convergence for 4 different points (see Table 18) - LES-4 case.

Curriculum Vitae

Alessio Fancello was born in Sardinia (Italy), in 1981. He studied at Liceo Classico in Nuoro. He got his Bachelor's degree in Aerospace Engineering in October 2006 at Politecnico di Torino. At the same university, he got the M.Sc. in Aerospace Engineering in 2009, specializing in Aerogasdynamics section, with a theoretical thesis in *Pressure Drops and Heat Exchange in Helicoidal Pipes*. In October 2009 he joined the airline company Eurofly, based in Malpensa Milan airport (Italy), inside the department of Maintenance Control Center. He moved to Eindhoven in 2010 to join the Combustion technology group of Technische Universiteit Eindhoven for a PhD project. His research interests mainly revolve to numerical analysis, turbulent combustion and gas turbine applications. During the past 4 years, he attended several conferences and workshops on these topics. Apart from the university services, Alessio is an active member of the gliding club Zweefvliegen Eindhovense Studentent (ZES).

Nederlandse samenvatting

Het H2-IGCC project is eind 2009 gestart met als doel technische oplossingen te genereren voor uiterst efficiënte en betrouwbare gasturbines voor de volgende generatie Integrated Gasification Combined Cycle (IGCC) fabrieken. Binnen dit project is het belangrijkste doel om een correct model op te stellen dat het ontwerp en de verbetering van het gasturbine verbrandingsproces beschrijft. De belangrijkste problemen in het verbrandingsmodel zijn stabiliteit en flexibiliteit van brandstof. Daarom wordt een compressibel CFD model gebruikt om het probleem op te lossen, in combinatie met toevoeging van waterstof aan de brandstof. Een van de aspecten van dit onderzoek is het gebruik van open source software OpenFOAM ® , wat een grote uitdaging is om in het verbrandingsmodel te verwerken.

Binnen het modelleren van verbranding is het grootste probleem de hoge computerkosten om een oplossing voor het gehele reactiesysteem te verkrijgen: de Flamelet Generated Manifold (FGM) techniek biedt een oplossing. Deze reductie-methode heeft als belangrijkste doel om het verbrandingsproces te behandelen door een klein aantal partiële transport differentiaal vergelijkingen op te lossen: dit betekent dat de vergelijking voor elke stof vervangen wordt door een verzameling van een klein aantal controle variabelen vergelijkingen. De voortgangsvariabele (de massafractie van een bepaalde stof in het mengsel) en de enthalpie zijn typische controle variabelen in een premix verbrandingsregime. Het manifold, of database, in de FGM techniek wordt verkregen door de oplossing van de eendimensionale flamelet vergelijkingen te gebruiken. Thermische eigenschappen, zoals de dichtheid, diffusiecoëfficiënt of temperatuur worden opgeslagen in de zogenaamde FGM database en kunnen opgezocht worden tijdens een CFD berekening.

Een laminaire vlam *flame in a box* is als eerste gebruikt om de FGM eigenschappen te laten zien. Een eenvoudige 2D geometrie test, genaamd vlam in een doos, is gebruikt om als validatie te dienen. De stationaire oplossingen zijn al bekend uit de literatuur en worden uitgevoerd

met stationaire incompressibele solvers. Er is echter geen bestaand werk met tijdseffecten en juist dit aspect moet als startpunt van het onderzoek genomen worden. Vervolgens is turbulente verbranding bestudeerd: aangenomen wordt dat de beta-PDF aanpak voor turbulente stromingen een redelijke keuze is als verdelingsfunctie van de subgrid chemische termen. De variantie van de voortgangsvariabele wordt op deze manier een controle variabele van het FGM systeem. Deze aanpak is geschikt voor relatief eenvoudige gassen zoals methaan, waarvoor een balans bestaat tussen moleculaire en thermische diffusie. De 3D geometrie van een jet vlam is gebruikt als validatie voor de turbulente verbranding.

Een studie naar een *single jet flame* configuratie is uitgevoerd, gebruik makend van de LES aanpak i.v.m. een turbulente verbranding, zonder adiabatische effecten. De resultaten laten een voldoend vergelijk zien met experimentele data.

Een *sudden expansion flow* configuratie is bestudeerd met behulp van RANS en LES methodes, waarbij warmteverlies effecten in de turbulente verbranding werden geïncorporeerd. De resultaten komen goed overeen met experimentele data en zijn een belangrijke verbetering ten opzichte van resultaten van voorgaand werk.

Kortom, zowel laminaire als turbulente verbranding werd bestudeerd door gebruik te maken van OpenFOAM ® en de FGM reductie methode. Dit heeft geresulteerd in gewichtige berekeningstijden in vergelijking met de gedetailleerde chemische aanpak. Bovendien resulteert de code in een goede validatie van voorgaand werk en experimentele data. De code is daarmee een veelbelovende tool voor toekomstig werk.

Sommario italiano

Negli ultimi anni l'interesse mondiale per la riduzione dell'inquinamento e delle emissioni nelle turbo macchine è cresciuto in maniera considerevole, così come la ricerca di standard migliori che assicurino una combustione efficiente. Infatti, la progettazione di nuove configurazioni di combustori è diventato un tema particolarmente sensibile sia nell'industria che nell'accademia. Sia i metodi classici utilizzati fino a questo momento che le tecniche sperimentali richiedono requisiti particolarmente impegnativi, visti gli alti costi delle strutture utilizzate.

Il progetto H2-IGCC è iniziato alla fine del 2009 con lo scopo preciso di fornire soluzioni tecniche altamente efficienti e affidabili per turbine a gas, da utilizzare negli impianti di nuova generazione, mediante il ciclo combinato di gasificazione integrata (IGCC). Il presente progetto di tesi ha lo scopo di proporre delle soluzioni tali da migliorare il processo di combustione delle turbine a gas, tenendo conto dei principali problemi relativi alla modellizzazione della combustione che riguardano sia la stabilità che la flessibilità del carburante, richiedendo di fatto l'utilizzo di un solutore numerico CFD per risolvere il problema dell'aggiunta di idrogeno nel carburante in un prossimo futuro. Al momento, la presente ricerca è concentrata sulla combustione di metano. Attenzione particolare è stata rivolta alle condizioni al contorno per la pressione, al fine di evitare i fenomeni oscillatori. Al fine di raggiungere gli obiettivi preposti, questa ricerca vede inoltre l'utilizzo del codice open source OpenFOAM ® per il quale l'implementazione del modello ha richiesto un impegno considerevole.

II metodo Flamelet Generated Manifolds (FGM) è un metodo ridotto di combustione, che si basa sul considerare il processo di combustione tramite la soluzione di un numero limitato di equazioni alle derivate parziali, in aggiunta alle classiche equazioni di conservazione, proponendo così una nuova configurazione matematica che rappresenta una risposta al problema dell'enorme costo computazione richiesto per la soluzione di una sistema dettagliato, con tutte le specie chimiche coinvolte nella reazione. Tali equazioni delle specie chimiche sono, in-

fatti, rimpiazzate da un numero limitato di equazioni relative a delle variabili di controllo. La creazione del database (manifold) nella tecnica FGM è effettuata tramite la soluzione di una equazione per la fiamma laminare monodimensionale. Queste fiamme sono create tramite un programma di chimica dettagliata denominato CHEM1D. Le proprietà della fiamma, quali la densità, il termine sorgente, la diffusività e la temperatura vengono immagazzinate nel database FGM e tabulate durante il calcolo CFD.

Il primo passo per dimostrare le capacità del FGM si basa su un approccio laminare. A tale proposito è stata utilizzata una geometria 2D chiamata *flame in a box*. In letteratura sono presenti unicamente soluzioni stazionarie riguardo a questa configurazione, non esiste dunque un lavoro precedente che racchiuda uno studio dinamico del problema. Per questo motivo, si è scelto di usare un approccio dedicato allo studio del transitorio della combustione, dando enfasi alla stabilità e alla stabilizzazione della fiamma. Durante questa ricerca, sono emersi diversi fenomeni interessanti relativi agli aspetti dinamici della combustione. La ricerca include anche gli aspetti delle perdite di calore, considerando l'entalpia come una nuova variabile di controllo, oltre alla variabile di progresso.

Nell'introdurre la turbolenza nella combustione, sistemi come le β-PDF possono essere considerati uno strumento adeguato per la descrizione dei termini di sotto griglia dal punto di vista chimico. La varianza della variabile di progresso diventa una nuova variabile di controllo e viene modellata utilizzando un modello algebrico. Questo lavoro presenta anche diverse applicazioni relative a configurazioni realistiche di combustori. Per esempio, un lavoro congiunto con Siemens AG propone una configurazione con fiamma a singolo getto e i risultati ottenuti tramite l'approccio LES-FGM sono messi a confronto con dati sperimentali. I risultati mostrano che, sebbene alcune differenze dovute nel predire le grandezze descritte, riescono a dare una sufficiente previsione del campo di moto. Le differenze che appaiono da questo lavoro sono dovute principalmente al fatto di considerare l'approccio adiabatico del sistema FGM, senza perdite di calore. Per concludere il lavoro garantendo anche un approccio più completo al problema della combustione turbolenta, si propone un'ulteriore analisi di un caso industriale, effettuata con la ditta CFD Engineering, tenendo in considerazione in questo caso anche le perdite di calore. I risultati sono raggiunti utilizzando sia modelli RANS che LES. Questi risultati mostrano che le lunghezze di fiamma e i profili stimati sono in buona corrispondenza con i dati sperimentali utilizzati come riferimento, e migliorano consistentemente alcuni risultati precedenti proposti in letteratura.

In conclusione, si presenta il modello FGM tramite l'utilizzo di OpenFOAM ® così come si studiano e si validano alcuni casi laminari e turbolenti. Il codice impiegato per raggiungere questo obiettivo dimostra notevoli risparmi in merito ai tempi computazionali, se paragonati con quelli della chimica dettagliata. Detto questo, si presume che questo codice possa essere utilizzato in futuro, soprattutto nei casi in cui avviene una combustione di gas differenti rispetto al semplice metano, come ad esempio l'idrogeno, per il quale l'interesse industriale sta crescendo considerevolmente nella situazione attuale.

Acknowledgements

Since I have started my PhD at TU/e, I met many people who contributed in different ways to the success of my life here. I don't think that there are proper words to thank them in a considerable way.

Rob, since our first interview at your office until the present moment, I have had a great time with you. I have always appreciated your comments in my research, giving me the right freedom to develop my steps, being always honest towards my work quality and proposing me the possible paths to follow. My research direction was not straightforward, but you always gave me the right motivation to keep the proper attitude.

Philip, although we didn't have time enough (as I would have liked to have with), your guidance and your words had contributed significantly to the successful conclusion of this research. Your critics and your helpful comments became always a part of my work footprint.

Jeroen, I always appreciated your help and your suggestions while developing my work. You always proposed the proper solution. Bart, your interest towards OpenFOAM became a significant support for me: you introduced me to the network and you also involved me in sharing the knowledge of this tool within the community.

During my adventure with this new open source code, I had the chance to know more people who helped me significantly: Erik & Georgios. Armin, you made my life easier with your great suggestions and constant help! Manuel and Gabriele, our frequent discussions and our conjoint work TU/e-CFD Engineering provide meaningful insights in terms of quality and results: I would like to express my deepest gratitude to your enormous help.

I would like to thank my committee members for the thesis revision, the precious comments and critical advices. With some of you I also have had such valuable conversations: prof. Anderson,

prof. Pittaluga and prof. Germano. Lukasz, it is has been a pleasure to work together with you: your competency and friendly attitude have been of great importance in my work. I would also like to thank my European sponsorship, the H2-IGCC project members, the ETN community, DLR and Siemens AG. With this regards, special thanks to O. Lammel, W. Krebs. C. Beck and S. Martin.

Andrea, you were not only a colleague: you have been a very good friend, we could discuss about everything, especially not related to job issues. I want to thank you so much for the help and the advices during my working hours. Furthermore, our life out of office has been priceless, from our business trips to our recreational times, including gliding activity. I don't think it is easy to find such a nice office mate. Francisco, your enthusiastic helps in reading and commenting on my thesis manuscript have been so precious. I also appreciated a lot your friendiness outside the office environment. Last but not least, life in and out of the office could not be better without the presence of good office buddies such as Maarten and Ulaş.

I would like to express my gratitude to all my combustion colleagues, in particular to Mayuri, Thiago, Ugur, Sudipto, Maurice, Nico, Jos, Sridhar, Akshay and Marcelo. Within my working environment, special mentions go to Marjan, Mariken and Thea. I would like to thank Elly for her Dutch language lessons, Saskia for the advices in helping me during the difficult work search and Fritz for his precious physiotherapy support.

Living in *Nederland* has been a unique experience: I am not sure if I will spend my future life here or if I have to move somewhere else. Whatever happens, I will never forget all my friends here, in particular Francesca, Chiara, Lena, Riccardo, Vanessa, Pedro, Michele, Giulia, Alberto, Luca, my godson Devis, Domenica and Julia. Last but not least, my gratitude goes to the very nice people of the Zweefvliegen Eindhovense Studentent (ZES) club: you have been like a family for me! Switching finally to Italian language, un saluto ai miei vecchi amici: Andrea P., Vito, Luca, Andrea I., Federico, Enrico, Daniele, Mimmo, Angelo, Elena, Antonio Sfuncia, Igor, Marcello P., Francesca, Carlo, Anna Maria, Francesco & Giusi, Donatella & Fabio, Antonio & Barbara. Un pensiero anche a chi, come Andrea, non è più fra noi.

Un ringraziamento particolare alla mia famiglia che mi ha sempre sostenuto nella mia vita: mamma, babbo e Valentina, mi siete sempre stati vicini e mi avete sempre aiutato, supportandomi in tutti i modi senza risparmio di energie. Grazie di cuore. Un caro saluto anche a mio padrino e alle mie due madrine.

In conclusione, dopo la protasi iniziale di questo lavoro, posso dire di aver fatto un cammino molto importante in questa mia vita olandese. Ciò non sarebbe potuto avvenire se non avessi conosciuto una persona importante come la mia musa ispiratrice, la mia cara Eleonora, alla quale questo lavoro è dedicato. Ci siamo trovati in un momento particolare di questo percorso di dottorato, mi hai sostenuto, mi hai aperto gli occhi e mi hai incoraggiato fino alla fine, senza mai stancarti, non potrò mai ringraziarti abbastanza.